Pakistan Journal of Engineering and Technology, PakJET
Multidisciplinary | Peer Reviewed | Open Access

Volume: 1, Number: 1, Pages: 1- 6, Year: 2018

Implementation and Hardware Optimization for Real Time Target Tracking

Omer Khan[*,1], Umair Tahir[1], Raheel Muzzammel[1] and Nayab Saeed[1]

[1]Electrical Engineering Department, The University of Lahore, 1-KM Defence Road, Lahore, 54000, Pakistan
Corresponding author: Omer Khan (Email: omer.khan@ee.uol.edu.pk)

Abstract— **Real time target tracking algorithms provides challenging environment in the field of computer vision. These challenges arise due to chaotic environment, irregular motion of objects, noise of both camera and video sequence, changes in target object and scene, etc. There are many optimized techniques used for target tracking, however to develop a system for real time target tracking these algorithms are to be implemented on some hardware. In this paper Fast- Normalized Cross-Correlation is carefully chosen for the purpose of real time target tracking. Usually these algorithms require enormous computations in real time which makes it hard to accomplish. To implement such algorithms high performance embedded hardware is required. In this research "TMS320DM642 evaluation module with TVP video decoders" digital signal processor embedded board is used to implement real time tracking algorithm. Digital signal processor hardware has limited recourse, so to achieve real time target tracking some hardware optimization techniques are also implemented.**

Index Terms— Normalized Cross-Correlation (NCC); Real time Tracking (RTT); Region of Interest (ROI); Sum of Squared Distance (SSD); Digital Signal Processor (DSP); Phase Alternation Line (PAL); Computational time; Frame rate; Throughput.

I. INTRODUCTION

Target tracking is used widely in both government and business organizations, such as airports, post offices, convenient stores, banks and public streets. It requires target tracking in real time to provide real time target tracking we need fast and reliable algorithm, with the help of intelligent tracking system this problem can be improved. The aim of this research is to design a target tracking algorithm that can used to detect and classify the events in real time. In most of the systems hardware optimization is also required for real time tracking for automated systems. Dedicated hardware can be designed to perform application's specific tasks but it will be much expensive to use redundant hardware. Optimizing the code will not provide same results as of hardware optimization but hardware optimization is not cost effective and fusible.

To get the optimized target tracking algorithm for TMS320DM642 Evaluation Module with TVP Video Decoders that provides output with the maximum frame rate, which is compatible with chaotic environment and deal more efficiently with the contrast of the video.

II. RELATED WORK

The phenomenon of analyzing video sequences is known as video surveillance [1]. Video surveillance is a demanding and vigorous region in the field of computer vision and has been proved vital in data storing and displaying. Automated surveillance systems are required to provide target tracking and feature extraction [2]. To provide video surveillance for a long time by a human operator is not possible [3]. Statistical method is introduced to overcome the inadequacy of the shortcomings in background subtraction using alpha methods.

In correlation based methods velocity is calculated by estimating the shifts, between two consecutive images of an image sequence. The shift describes the movement of region between images [4], [5]. Some of the existing correlation based methods include method proposed by Sutton, Walters, Peters, Anson and McNeil [6] where optical flow is estimated by iterative minimization of SSD of deformation parameter, obtained by linear deformation of local image patches. A 3x3 spatial operator is used by Kories and Zimmerman [7] to classify central pixel intensity by counting the low intensity values of the neighboring pixels. In [8], [9] Cauchy-Schwartz inequality is used to calculate NCC for medical image registration by template matching. MATLAB is used for the implementation purpose of NCC template matching.

In [10], [11] for efficient search a winner update scheme is introduced by combining multilevel adaptive partition for NCC. The literature for fast-

NCC can be studied from [6], [12] which provide significant basic knowledge of our research.

Hardware optimization is also a part of this research. Different techniques for memory optimizations are implemented [13] to enhance results. These techniques also improve; CPU utilization, reduce power consumption, etc [14]. A novel cluster-based register optimization technique called Power Islands Synthesis (PIS) is introduced by Deniz et al. [15]. Hardware optimization techniques are the main area of research these days to provide best performance for general purpose embedded hardware. Keoncheol Shin et al. devised a technique that can be used effectively to the synthesis of arithmetic circuits aiming power minimization while satisfying the timing constraint of the circuit [16], [17]. By implementing both tracking and hardware optimizations better system can be provided for the purpose of Real time target tracking.

In this research cross correlation target tracking algorithm technique is implemented. After implementation results are recorded in terms of

- Processing time
- Frame rate
- Percentage error
- Throughput
- Power consumption

Target tracking using cross correlation is then modified to Normalized Cross-Correlation (NCC) and Fast-NCC and then results are compared. Additional hardware optimization algorithm are applied which are discussed below, kernel technique is also applied to further improve the results. All techniques provide some improvement and decaying in results but kernel technique showed promising improvements in results. Results of all the hardware techniques are discuss in later sections.

III. Proposed System

The proposed system is developed by merging different techniques to provide best suited real time tracking algorithm for embedded system (TMS320DM642 evaluation module with TVP video decoders) with hardware optimization as shown in figure 1.

IV. Implementation Of Target Tracking

A standard and most commonly used approach for feature matching is correlation between two frames, some sophisticated techniques are also used but they are much expensive regarding computations and power consumption.

A. *Template Matching By Cross-Correlation*

Euclidean distance is considered as an origin for template matching using cress-correlation.

$$\boldsymbol{d^2}_{\boldsymbol{f,t}}(\boldsymbol{u},\boldsymbol{v}) = \sum_{\boldsymbol{x,y}}[\boldsymbol{f}(\boldsymbol{x},\boldsymbol{y}) - \boldsymbol{t}(\boldsymbol{x}-\boldsymbol{u},\boldsymbol{y}-\boldsymbol{v})]^{\boldsymbol{2}}) \qquad (1)$$

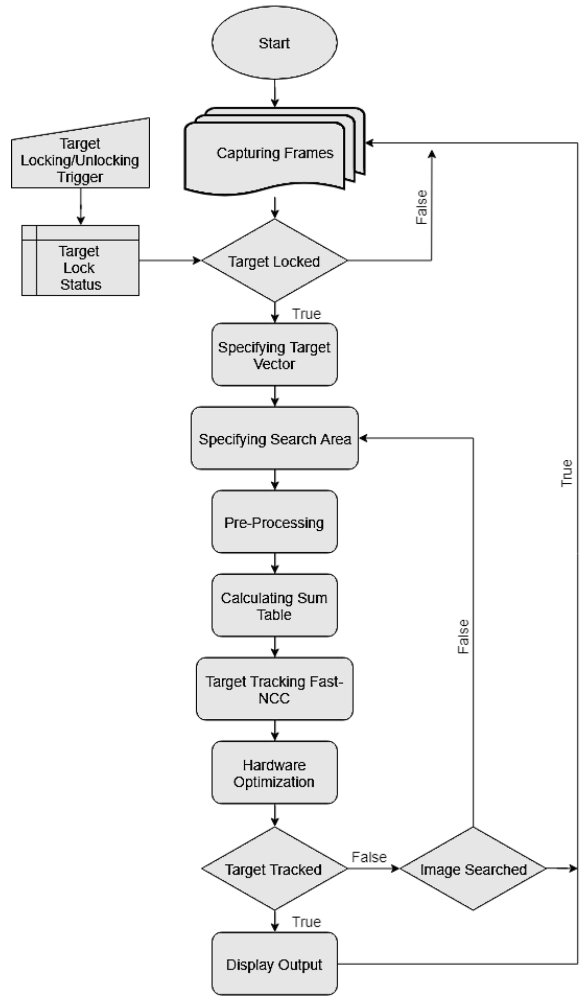

Figure 1 Flow Chat

In (1) f is the search area extracted from the video input. If sum is provided over x, y under the window containing the target vector t positioned at u, v. Expansion of equation:

$$\boldsymbol{d^2}_{\boldsymbol{f,t}}(\boldsymbol{u},\boldsymbol{v}) = \sum_{\boldsymbol{x,y}} \boldsymbol{f^2}(\boldsymbol{x},\boldsymbol{y}) - \boldsymbol{2f}(\boldsymbol{x},\boldsymbol{y})\boldsymbol{t}(\boldsymbol{x}-\boldsymbol{u}, \boldsymbol{y}-\boldsymbol{v}) + \boldsymbol{t^2}(\boldsymbol{x}-\boldsymbol{u},\boldsymbol{y}-\boldsymbol{v}) \qquad (2)$$

In above equation term $\sum t^2(x-u, y-v)$ is a constant value, the term $\sum f^2(x,y)$ is approximately constant. By considering above two terms constant we can say that above equation can be written as follows:

$$\boldsymbol{d^2}_{\boldsymbol{f,t}}(\boldsymbol{u},\boldsymbol{v}) = \sum_{\boldsymbol{x,y}} \boldsymbol{f}(\boldsymbol{x},\boldsymbol{y})\boldsymbol{t}(\boldsymbol{x}-\boldsymbol{u},\boldsymbol{y}-\boldsymbol{v}) \qquad (3)$$

Above equation represents the cross-correlation equation, it is used to measures the similarity between the search area and the target vector.

i. Correlation coefficient

Cross-correlation faces problems due to changes in amplitude of values, which is caused by changes, occur in brightness with the passage of time. These difficulties in correlation are overcome by normalizing the search area and target vectors to unit length with the help of correlation coefficient, yielding a cosine-like correlation coefficient.

B. Normalized Cross-Correlation

The problem mentioned in above section is handled by using normalized cross-correlation. To determine the location of target vector in search area of two-dimensional frame is by computing the normalized cross-correlation coefficient γ for every point of (u, v) for f and t, which has been shifted by u pixels along x direction and v pixels along y direction. Equation below represents the basic equation of normalized cross-correlation coefficient.

$$\boldsymbol{\gamma(u,v)} = \frac{\sum_{x,y}\left[\boldsymbol{f(x,y)} - \bar{\boldsymbol{f}}_{\boldsymbol{u,v}}\right]\left[\boldsymbol{t(x-u,y-v)} - \bar{\boldsymbol{t}}\right]}{\sqrt{\left\{\sum_{x,y}\left[\boldsymbol{f(x,y)} - \bar{\boldsymbol{f}}_{\boldsymbol{u,v}}\right]^2 \sum_{x,y}\left[\boldsymbol{t(x-u,y-v)} - \bar{\boldsymbol{t}}\right]\right.}} \quad (4)$$

Where $\bar{t}$ represents the mean value target vector and $\bar{f}_{u,v}$ signifies the mean value of search area $f(x, y)$ extracted from video input. The equations for determining mean of search area and target vector are below

$$\bar{\boldsymbol{f}}_{\boldsymbol{u,v}} = \frac{\mathbf{1}}{\boldsymbol{N_x N_y}} \sum_{\boldsymbol{x=u}}^{\boldsymbol{u+N_x-1}} \sum_{\boldsymbol{y=v}}^{\boldsymbol{v+N_y-1}} \boldsymbol{f(x,y)} \quad (5)$$

$$\bar{\boldsymbol{t}}_{\boldsymbol{u,v}} = \frac{\mathbf{1}}{\boldsymbol{M_x M_y}} \sum_{\boldsymbol{x=u}}^{\boldsymbol{u+M_x-1}} \sum_{\boldsymbol{y=v}}^{\boldsymbol{v+M_y-1}} \boldsymbol{t(x-u,y-v)} \quad (6)$$

Where N_x *and* N_y determine the dimensions of search area frame, M_x *and* M_y are the limits defined for the target vector.

C. FAST NORMALIZED CROSS-CORRELATION

Image function f and search area energy f^2 are processed to compute their sum tables to provide fast calculation of the normalized cross-correlation, and these are the pre-computed integrals used for Fast-NCC.

i. Calculation for Denominator

To reduce the computations of denominator of normalized cross-correlation coefficient, the procedure used is by maintaining two sun tables $s(u, v)$ and $s^2(u, v)$ for the search area $f(x, y)$ and its energy $f^2(x, y)$. The sum table can be expressed by

$$\boldsymbol{s(u,v) = f(u,v) + s(u-1,v) + s(u,v-1) - s(u-1,v-1)} \quad (7)$$

Similar recursive function for search area energy is given by

$$\boldsymbol{s^2(u,v) = f^2(u,v) + s^2(u-1,v) + s^2(u,v-1) - s^2(u-1,v-1)} \quad (8)$$

Using these sum tables mean for search area from equation 5 can be very efficiently calculated independent of the size of target vector.

ii. Calculation of Nominator

Algorithm presented in last subsection efficiently reduces the denominator equation of normalized cross-correlation, but calculation for numerator for NCC-coefficient is still comparatively high. If it is implemented in frequency domain using fast Fourier transform algorithm. Therefore, to avoid many computations nominator is to be simplified, numerator can be represented as:

$$\boldsymbol{N(u,v)} = \sum_x \sum_y \boldsymbol{f(x,y)t'(x-u,y-v)} - \bar{\boldsymbol{f}}_{\boldsymbol{u,v}} \sum_x \sum_y \boldsymbol{t'(x-u,y-v)} \quad (9)$$

Where, in above equation $t'(x-u, y-v)$ is known as zero mean template function defined by

$$\boldsymbol{t'(x-u,y-v) = t(x-u,y-v) - \bar{t}(x,y)} \quad (10)$$

Now, in above equation $\bar{t}(x, y)$ has zero mean value and thus also zero sum, the term $\bar{f}_{u,v} \sum_x \sum_y t'(x-u, y-v)$ will also approaches to zero as well. Now numerator of equation 4.6 can be expressed as:

$$\boldsymbol{N(u,v)} = \sum_{\boldsymbol{x}} \sum_{\boldsymbol{y}} \boldsymbol{f(x,y)t'(x-u,y-v)} \quad (11)$$

Where (2) provides the simplified term for nominator of normalized cross-correlation coefficient.

V. Implementation Of Hardware Optimization Techniques

Various techniques are followed by researchers to optimize their algorithm to improve hardware utilization. Some techniques are so simple and easy to implement; however, they provide enhancements in CPU utilization, power consumption, response time, and throughput of the system. There are few constraints in embedded hardware that can be referred as:

- Time: Time allowed to complete a task requires optimization of machine cycles to complete a task, in real time systems time is a major constraint.
- Computational Platform: Embedded system usually power consumption, cost, size, memory are major factors to develop a system.

A. CPU Optimization Techniques

Central processing unit (CPU) is referred as brain of any system, as all processing is done by CPU such as addition, multiplication, decision making and input/output controls. To maximize the through put one must increase the CPU utilization, but it will cause more power consumption. There are some CPU optimization techniques that increase the throughput without increasing power consumption.

- Pass object by reference instead by value
- Avoid using library functions
- Use of inline function

B. Memory Optimization Technique

In the field of embedded systems memory optimization has its own importance. Embedded systems have limited memory which provide challenging environment to provide best suited solutions for such scenarios. External memory can be interfaced with embedded systems with input/output ports but it introduces additional overhead to the systems.

- Loop unrolling
- Reuse of memory spaces
- Direct Memory Access

C. Minimization of Code

Compact code is a key to develop optimized and efficient embedded system. Line of code can be minimized by many techniques without disturbing the actual functionality of the algorithm. A very effective and efficient technique which improves performance of our system exponentially is Kernel technique.

In target tracking by cross-correlation we have to compare target vector in search area to find the desired location. Time to process a frame depends upon two things size of target vector and search area and displacement of object from its original location. It is impossible to control displacement of the object as it moves with its own free will but we can reduce the size of vectors in such a manner that efficiency of the system is not reduces. By reducing the size of vectors we actually reduced number of additions and multiplication in to process of tracking algorithm. After locating kernel, whole target vector is matched to verify whether the correct object is tracked or not.

In this research we only reduce the size of target vector to one fourth of the actual template size. By this we reduce the response time exponentially which allows the system to process more frame with respect to time, so frame rate is automatically increased.

VI. Real Time Target Tracking And Hardware Optimization Results

In order to examine our implemented real time target tracking algorithm some experiments are to be made to obtain some results. We take four set of video sequences of time interval two minutes; normal video sequence, chaotic video sequence, low contrast video sequence and dark video sequence to compute the results.

A. Experimental Parameters

Parameters selected to investigate the efficiency of this implemented algorithm are; average time to process a frame, frame rate, accuracy by percentage of throughput and error and power consumption.

i. Process Time

A hardware pin was set high when processing starts and set zero when process is done; this pin is then monitored by using logic analyzer to calculate the average time duration to process a frame.

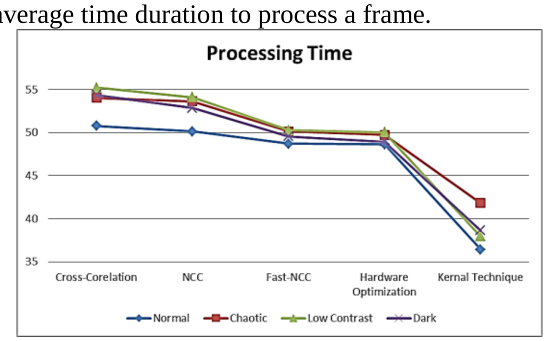

Figure 2 Comparison of Process Time in ($\boldsymbol{ms}$)

It clear from above graph that there is a small improvement in processing time between cross-correlation and NCC, but fast-NCC provides way enhanced results from both of the techniques. Hardware optimization techniques showed exponential progress in processing time especially by Kernel method.

ii. Frame Rate

IEEE standard for efficient PAL standard video sequence is 25 frames per second (FPS). As mentioned in previous sub-section we control an output pin during process, we can also calculate no. of frames processed in one second.

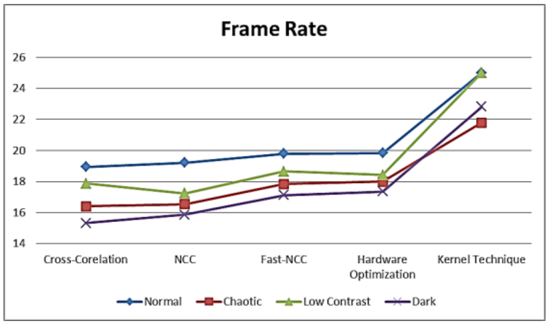

Figure 3 Comparison of Frame Rate in FPS

Comparison of frame rate is showen in figure 3, cross-correlation, NCC, fast-NCC, and hardware optimization showed liner improvement. Kernal basesed technique provide maximum frame rate, nearly equal to input frame rate.

iii. *Percentage Throughput*

Throughput can be computed for a target tracking algorithm in terms of number of frames with target object located. It can be computed by this formula.

$$Throughput\ \% = \frac{frame\ recived - target\ lost}{frame\ recived} \times 100$$

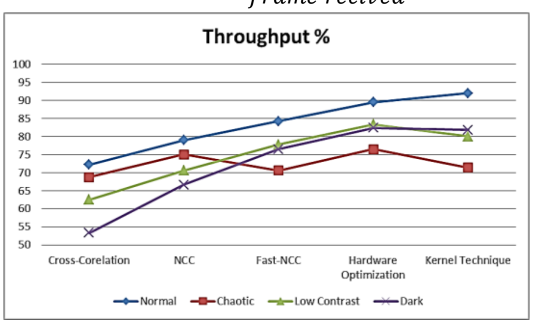

Figure 4 Comparison of Percentage Throughput

Throughputs of all the implemented techniques are liner except for the video sequence of chaotic environment. Fast-NCC and Kernel method is not best suited for chaotic scenes.

iv. *Percentage Error*

Error can be computed in terms of number of frames with target object fail. Frames with number of target object fail can further be categorized into two categories object lost and false object located. But in this research we only consider whether target is found or lost. It can be calculated by using this formula.

$$Error\ \% = \frac{frame\ recived - target\ located}{frame\ recived} \times 100$$

Below figure shows percentage error of our research. Error ratio for all the techniques are improved but results for chaotic environment does not change or improved.

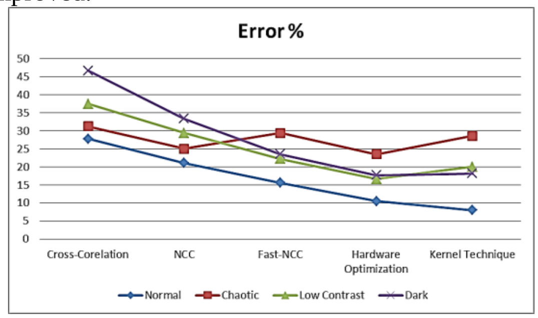

Figure 5 Comparison of Percentage Error

v. *Power Consumption*

Power consumption is one of the important parameter in the field of embedded system. In our research we are implemented our algorithm on TMS320DM642 evaluation module with TVP video decoders as it is patched hardware so it is impossible to calculate power consumption of individual modules so we calculate power consumption of the whole system. Maximum power that can be utilized by TMS320DM642 evaluation module with TVP video decoders is 25 watt.

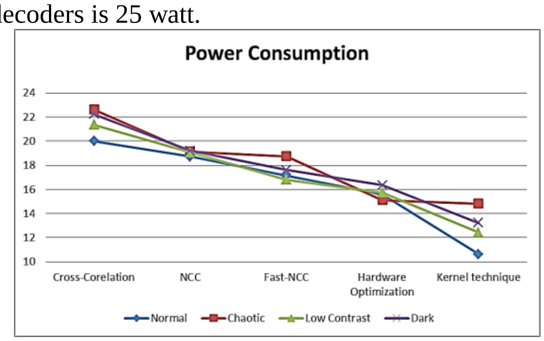

Figure 6 Comparison of Power Consumption in Watts

Power consumption is reduced in a regular manner as showed in figure 6. There are no irregular behaviors observed in this research.

VII. Conclusion And Future Work

This paper presents simple techniques to improve the results of Real Time Target Tracking by two means; optimizing target tracking algorithm, and some hardware optimization techniques. The results showed that Fast-NCC provide significant improvement in all the experimental parameters. Our proposed algorithm provides enhanced results in different complex environment; chaotic, low contrast, and dark scenes. Congregated results from fast-NCC provide satisfactory results but to further enhance the throughput of the system we use hardware optimization techniques, but kernel-based technique provides exponential improvement in all the results parameters. Results showed significant improvement in performance, and object tracking.

In future further tracking optimization can be implemented, hardware optimizations algorithm that can utilize provided resources for maximum throughput can be implemented as well. Our algorithm does not deal with situations like; target object is scaled, tilted, and object rotates from its original location.

REFERENCES

[1] R. Venkatesan, and A. B. Ganesh, "Supervised and Unsupervised Learning Approaches for Tracking Moving Vehicles", Proceedings of the 2014 International Conference on Interdisciplinary Advances in Applied Computing, article 6, Kerala, Oct., 2014.

[2] H. Sui, Z. Song, D. Gao and L. Hua, "Automatic Image Registration Based on Shape Features and Multi-scale Image Segmentation," 2017 2nd International Conference on Multimedia and Image Processing (ICMIP), Wuhan, 2017, pp. 118-122.

[3] I. S. Kim, H.S. Choi, K. M. Yi, J. Y. Choi and S.G. Kong. "Intelligent visual surveillance — A survey", International Journal of Control Automation and Systems, vol. 8, no. 5, pp. 926-939, 2010.

[4] J. L. Barron, D. J. Fleet and S. S. Beauchemin, "Performance of optical flow techniques", International Journal of Computer Vision, vol. 12, no. 1, pp. 43-77, 1994.

[5] L. Wang, X. Wang, M. Tornatore, K. J. Kim, S. M. Kim, D. U. Kim, K. E. Han and B. Mukherjee, "Scheduling with machine-learning-based flow detection for packet-switched optical data center networks," IEEE/OSA Journal of Optical Communications and Networking, vol. 10, no. 4, pp. 365-375, April, 2018.

[6] A. Bruhn and J. Weickert, "Towards Ultimate Motion Estimation: Combining Highest Accuracy with Real-Time Performance," Tenth IEEE International Conference on Computer Vision (ICCV'05), vol. 1, Beijing, pp. 749-755, 2005.

[7] P. Kruizinga, F. Mastik, J. G. Bosch, N. de Jong, G. van Soest and A. F. W. van der Steen, "High frame rate ultrasound displacement vector imaging", 2014 IEEE International Ultrasonics Symposium, Chicago, IL, 2014, pp. 707-709.

[8] J. N. Sarvaiya, S. Patnaik and S. Bombaywala, "Image Registration by Template Matching Using Normalized Cross-Correlation," 2009 International Conference on Advances in Computing, Control, and Telecommunication Technologies, Trivandrum, Kerala, 2009, pp. 819-822.

[9] F. E. T. Munsayac, L. M. B. Alonzo, D. E. G. Lindo, R. G. Baldovino and N. T. Bugtai, "Implementation of a normalized cross-correlation coefficient-based template matching algorithm in number system conversion", IEEE 9th International Conference on Humanoid, Nanotechnology, Information Technology, Communication and Control, Environment and Management (HNICEM), Manila, 2017, pp. 1-4.

[10] S. Wei and S. Lai, "Fast template matching algorithm based on normalized cross correlation with adaptive multilevel winner update‖", IEEE Transactions on Image Processing, Vol. 17, No. 11, Nov. 2008.

[11] Z. Yang, "Fast Template Matching Based on Normalized Cross Correlation with Centroid Bounding," 2010 International Conference on Measuring Technology and Mechatronics Automation, Changsha City, 2010, pp. 224-227.

[12] C. Zach, T. Pock, and H. Bischof, "A duality-based approach for real time TV-L1 optical flow", 29th DAGM conference on Pattern recognition, Heidelberg, Germany, 2007, pp. 214-223.

[13] Panda, Dutt and Nicolau, "Exploiting off-chip memory access modes in high-level synthesis," 1997 Proceedings of IEEE International Conference on Computer Aided Design (ICCAD), San Jose, CA, USA, 1997, pp. 333-340.

[14] Xiaoyong Tang, Tianyi Jiang, A. Jones and P. Banerjee, "Compiler optimizations in the PACT HDL behavioral synthesis tool for ASICs and FPGAs", IEEE International Systems-on-Chip SOC Conference, Portland, OR, USA, 2003, pp. 189-192.

[15] D. Dal and N. Mansouri, "Power Optimization with Power Islands Synthesis", IEEE Transactions on Computer-Aided Design of Integrated Circuits and Systems, vol. 28, no. 7, pp. 1025-1037, July 2009.

[16] K. Shin and T. Kim. "Leakage power minimization for the synthesis of parallel multiplier circuits", Proceedings of the 14th ACM Great Lakes symposium on VLSI (GLSVLSI 04), Boston, 2004, pp. 166-169.

[17] C. Wang, X. Chang, Y. Zhang, L. Zhang and X. Chen, "Failure Analysis of Composite Structures Based on Digital Image Correlation Method", International Conference on Sensing, Diagnostics, Prognostics, and Control (SDPC), Shanghai, 2017, pp. 473-476

Pakistan Journal of Engineering and Technology, PakJET
Multidisciplinary | Peer Reviewed | Open Access

Volume: 1, Number: 1, Pages: 7- 16, Year: 2018

Improving the Transient and Steady State Response of Combustion Process in Jet Engines

Umair Tahir[*,1], Raheel Muzzammel[1], Omer Khan[1] and Nayab Saeed[1]

[1]Electrical Engineering Department, The University of Lahore, 1-KM Defence Road, Lahore, 54000, Pakistan
Corresponding author: Umair Tahir (Email: umair.tahir@ee.uol.edu.pk)

***Abstract*— Acoustic ways are generated during combustion process in jet engines. These waves create a lot of noise which cause mechanical disturbance and sometimes can lead to mechanical failure as well. Active controllers are designed to reduce the effect of acoustic waves. Microphone is normally used to read the sound waves and loudspeaker is used as an actuator to reduce the effect by generating opposing pressure waves. Different techniques of control theory such as root locus, phase lead and lag compensation, proportional integral compensation, proportional derivative compensation, proportional integral derivative controller and controller-Observer controller are applied to reduce the acoustic waves generated in combustion chamber. Improvement in transients and steady state response is achieved up to a certain level by using control techniques and results of used techniques are discussed in this paper.**

Index Terms*— *transfer functions; lead and lag compensators; PI and PD compensators; PID controller; Controller and Observer; Matlab / SISO Tools

I. INTRODUCTION

When a combustion process is carried out in gas turbines and jet engines waves are generated which are commonly known as acoustic waves. The whole assembly can be explained a simplified diagram as:

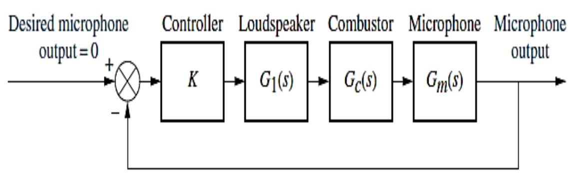

Fig 1. Feedback system of combustor [1]

The forward transfer function of the plant as described in [1] is:

$$G(s) = KG_1(s)G_c(s)G_m(s)$$
$$= \frac{K\left(s+z_f\right)\left(s^2+2\zeta_2\omega_2 s+\omega_2^2\right)}{\left(s+p_f\right)\left(s^2-2\zeta_1\omega_1 s+\omega_1^2\right)\left(s^2+2\zeta_2\omega_2 s+\omega_2^2\right)}$$

For three different configurations, the values are given in Table 1 [1].

For each configuration root locus is plotted and if the configuration is stable, then the transient response and steady state response using lead/Lag compensators, PID controllers, observer and canonical controllers are improved.

	A	B	C
z_f	1500	1500	1500
p_f	1000	1000	1000
ζ_z	0.45	0.45	−0.45
ω_z	4500	4500	4500
ζ_1	0.5	−0.5	−0.5
ω_1	995	995	995
ζ_2	0.3	0.3	0.3
ω_2	3500	3500	3500

TABLE 1: Values for transfer function

II. OPERATING PRINCIPLE AND RESULTS

Root Locus: A root locus is the locus of the close loop pole. Closed loop poles are graphically represented by root locus by which we analyze and design the stability and response of the system [2].By using root locus, percentage overshoot and transient responses are analyzed by changing the value of gain correspondingly for the change in values of the variables which are of closed loop.

Poles of the Open loop transfer function are plotted on the real axis and then after introducing the gain K, the closed loop transfer function poles are analyzed [3]. As gain is increased, the odd poles are moved to the left and even poles are moved to the right. For the specific value of the gain for a system, the poles meet at a point where the system is critically damped and by further increasing the gain, the poles collide with each other and split away at 90 degrees giving complex poles for which the system is under damped. After breaking out, the poles move toward the zeros of the system or the zero at the infinity and die out [4].

The damping ratio (ζ) and natural frequency (ω_n) of a system with a feedback path can also be designed using root locus. By adjusting the value of gain K, the required dominant poles are calculated for which the required settling time and peak time is required. Not only this, root locus also defines the angle of departure and arrival of poles thus giving the complete information about the stability or un-stability of the system [5].

1. The root locus for configuration (a) is:

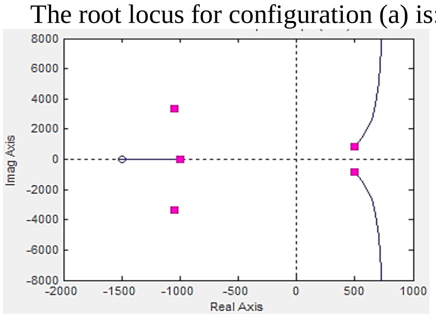

Fig. 2: Root locus for configuration (a)

From the root locus it can be seen that the system is unstable because two poles lie in the right half side of the plane.

2. The root locus for configuration (b) is:

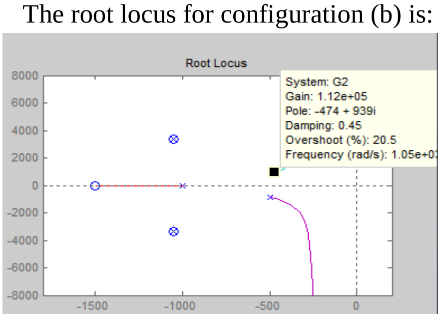

Fig. 3: Root locus for configuration (b)

$$\%O.S = e^{-\left(\frac{\zeta\pi}{\sqrt{1-\zeta^2}}\right)} = 20.5 \qquad \text{(i)}$$

3. The root locus for configuration (c) is:

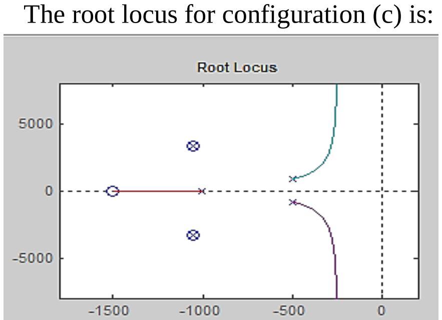

Fig. 4: Root locus for configuration (c)

From (i) the required percentage overshoot of the system is: %O.S= 362.96.

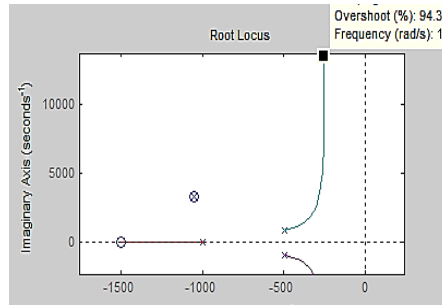

Fig. 5: Root locus for configuration c (zoom view)

Since this system cannot provide us the required percentage overshoot, so this system is not discussed further.

Compensation Techniques: Sometimes the required settling and peak time defined by the percentage overshoot does not lie on the root locus. At these situations the desired point cannot be achieved by simply adjusting the gain. The required characteristics can be achieved by replacing the original system with a system whose root locus provides the desired results but the replacement is expensive, time consuming and is avoided.

So, to achieve the desired results, the original system is compensated with additional zeros and poles at low power end of the system [6]. This addition of zeroes and poles are realized using compensators which are implemented using ideal or passive networks. The steady state error is improved or reduced to zero and system transient and steady state response is increased.

Proportional Integral (PI) Compensator: System that integrates the error and feeds that integrated error forward towards the plant is known as proportional integral compensators. In ideal PI compensation which is realized using op-amps, steady state error is improved without affecting the transient response by placing pole at the origin [7]. Steady state error is reduced by increasing the system type by the addition of integration in the system but increasing the system type by adding a pole at the origin disturbs the angular contribution which no longer remains 180 degrees and this problem is solved by adding a zero near the pole, so, the angular contribution of the additional pole and zero is cancelled out.

The compensators which have pole placed at the origin and a zero placed close to that pole are called ideal integral compensators. The Ideal PI Compensator is explained by following figures. Here an uncompensated is shown first. Then the effect of adding pole at origin is shown. After adding a pole at origin, the required pole does not lie on the root locus, so, the required pole is made to lie at root locus by adding a zero with the pole.

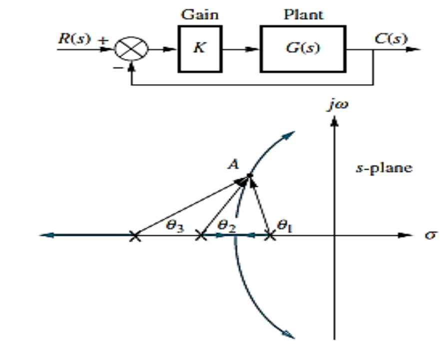

$$-\theta_1-\theta_2-\theta_3=(2k+1)180°$$

Fig. 6**:** Uncompensated system [1]

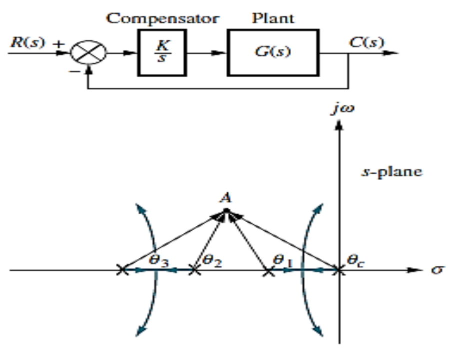

$$-\theta_1-\theta_2-\theta_3-\theta_c\neq(2k+1)180°$$

Fig. 7**:** Effect of compensator pole [1]

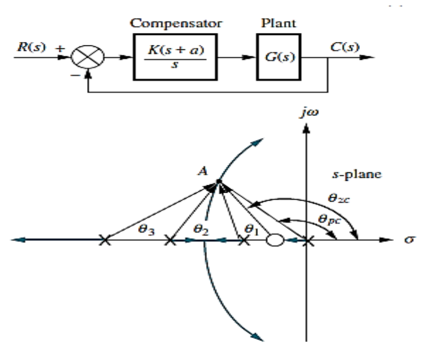

$$-\theta_1-\theta_2-\theta_3-\theta_{pc}+\theta_{zc}\cong(2k+1)180°$$

Fig. 8**:** Effect of compensated pole and zero [1]

The uncompensated and compensated response of system is explained by following figure:

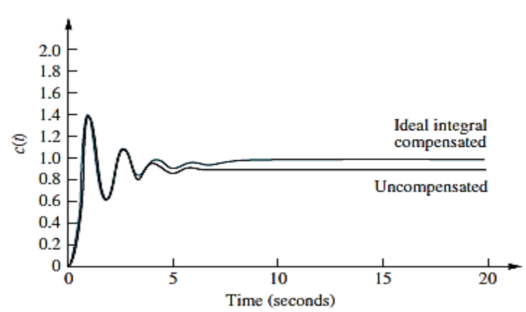

Fig. 9**:** Difference between step response of uncompensated and ideal compensated system [1]

Now, apply this technique on original system which is configuration (b).

The root locus of original system with %O.S= 20.5:

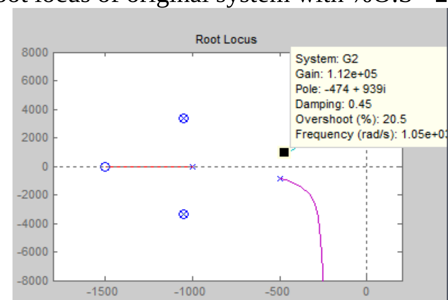

Fig. 10**:** Root locus of original system

Now the root locus of PI compensated system is where the pole is introduced at origin and a zero at -0.1.

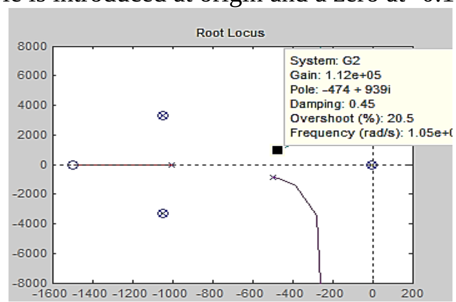

Fig. 11**:** Root locus of PI compensated system

The difference between uncompensated and PI compensated system can be explained by the following parameters:

	Uncompensated	Compensated
System Type	0	1
% O.S	20.5	20.5
Gain (K)	1.12 e^05	1.12 e^05
Static error constant (K_p)	0.1697	∞
Steady state error e(∞)	0.8549	0

TABLE 2: Comparison between compensated and uncompensated system

Lag Compensation: Ideal integral compensation add pole at the origin but it requires an active integrator. When the passive networks are used then the pole is not placed on the origin but the poles and zeros are moved to the left side of the origin. This addition of poles and zeros close to the left of the origin is known as lag compensation [8]. Neither this increase the system type nor reduce the steady state error to zero as in the case of ideal proportional integral compensation, but stills it yields a remarkable improvement in the steady state error without effecting the transient response. Lag compensator improve the steady state constant by a factor equal to Z_c / p_c.

The following figure shows uncompensated system and its root locus:

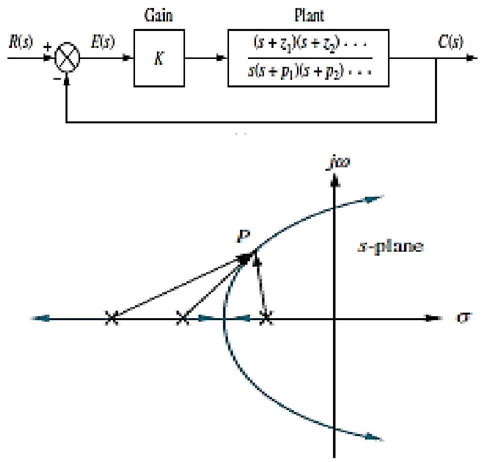

Fig. 12**:** Root locus of general uncompensated system [1]

The following figure shows compensated system and its root locus:

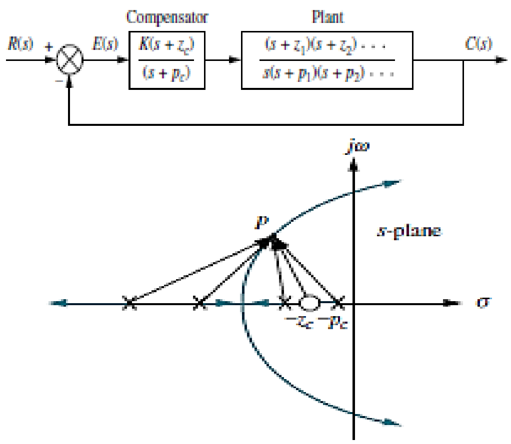

Fig.13**:** Root locus of lag compensated system [1]

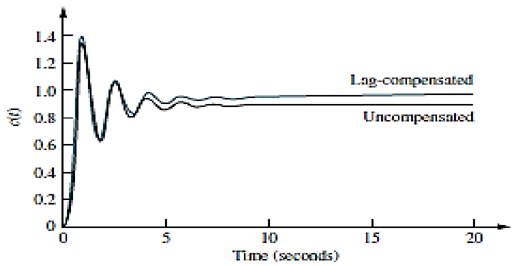

Fig.14**:** Difference between step responses of lag-compensated and uncompensated system [1]

Now, apply this technique on our original system. The root locus of original system with %O.S= 20.5:

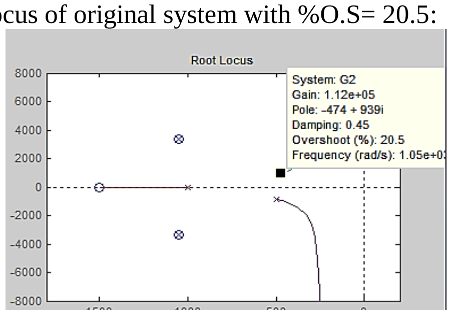

Fig. 15**:** Root locus of original system

Here the steady state error was 0.8549. Now improving this error by say 10 times, the new steady state error becomes

$$e(\infty)\text{new} = 0.08549$$

$$so, k_p(new) = \frac{1-0.08549}{0.08549} = 10.697$$

So, for compensated system the ratio of compensated zero to compensated pole is:

$$\frac{z_c}{p_c} = \frac{k_p(new)}{k_p} = \frac{10.697}{0.1697} = 63.03$$

Now, arbitrary selecting compensation pole (p_c) at 0.01, the location of compensation zero becomes

$$z_c = 63.03 p_c = 0.6308$$

Now the root locus of Lag compensated system is where pole is introduced at -0.01 and a zero at -0.6308.

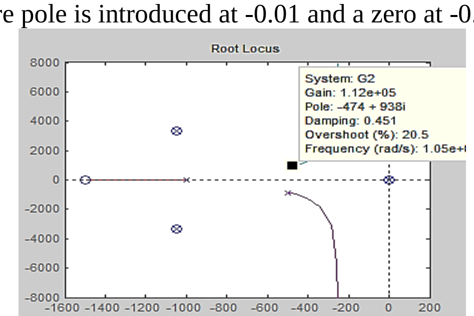

Fig.16**:** Root locus of lag compensated system

	Uncompensated	Lag Compensated
System Type	0	1
% O.S	20.5	20.5
Gain (K)	1.12 e^05	1.12 e^05
Static error constant (K_p)	0.1697	10.697
Steady state error e(∞)	0.8549	0.08549

TABLE 3: Comparison between compensated and uncompensated system

Proportional Derivative (PD) Compensation: System that takes derivative of the error and feeds it forward to the plant is called proportional derivative compensators [9]. The ideal PD compensators are designed using op-amps. The ideal derivative speeds up the response of the system by adding a zero to the forward path. Proper position of zero in compensated system speeds up the response over the uncompensated system. Percentage overshoot remain the same in both the compensated and uncompensated systems but in the compensated system the dominant closed loop poles have more negative real part and larger imaginary parts thus reducing the settling and peak time of the system. The change after adding a differentiator can be seen in settling time, peak time where there is at least a doubling of speed.

The zero which is added by an ideal PD Controller tends to remove the number of branches of the root locus that cross in to the right half plane. By using ideal PD controller, zero can be introduced at any required position where the transient response fulfills our requirements [10]. This method can be explained by following general examples where a zero is introduced at different positions and corresponding settling and peak time is improved. The following figure (a) shows uncompensated system:

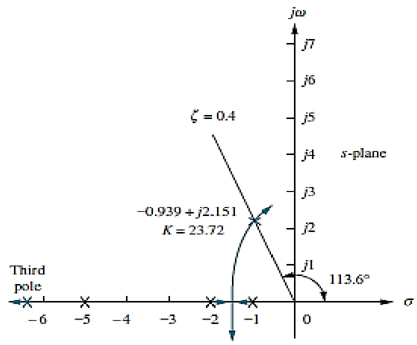

Fig.17**:** Root locus of general compensated system [1]

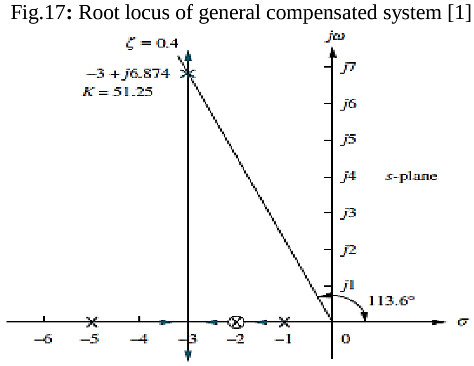

Fig.18**:** Compensated system with zero at -2 [1]

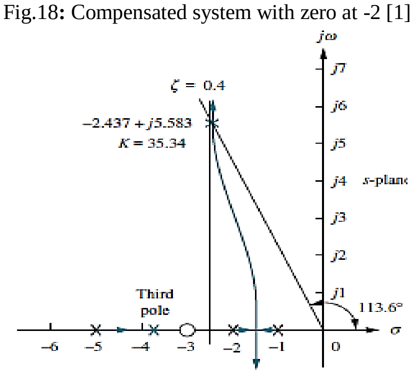

Fig.19**:** Compensated system with zero at -3 [1]

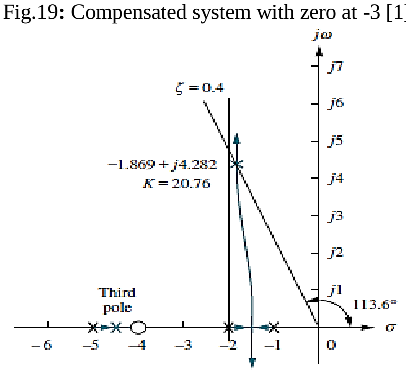

Fig.20: Compensated system with zero at –4 [1]

Parameters	Un-compensated	Compensated b	Compensate c	Compensated d
Plant & Compensator	$\frac{K}{(s+1)(S+2)(S+3)}$	$\frac{K(S+2)}{(s+1)(S+2)(S+3)}$	$\frac{K(s+3)}{(s+1)(S+2)(S+3)}$	$\frac{K(s+4)}{(s+1)(S+2)(S+3)}$
Dominant Poles	-0.939±j2.151	-3±j6.874	-2.437±j5.583	-1.87±j.4.282
K	23.72	51.25	35.34	20.76
ξ	0.4	0.4	0.4	0.4
ωs	2.347	7.5	6.091	4.673
% O.S	25.38	25.38	25.38	25.38
Ts	4.26	1.33	1.64	2.14
Tp	1.46	0.46	0.56	0.733
Kp	2.372	10.25	10.6	8.304
e (∞)	0.297	0.089	0.086	0.107

TABLE 4:Parameters of Uncompensated & Compensated Systems

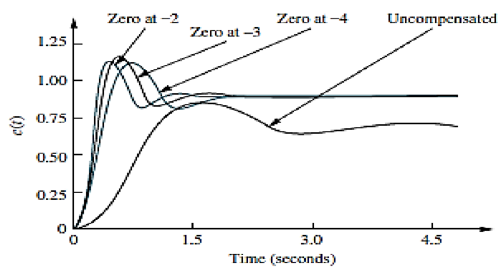

Fig.21**:** Difference between responses of each compensated systems [1]

Now, for the original system the root locus is:

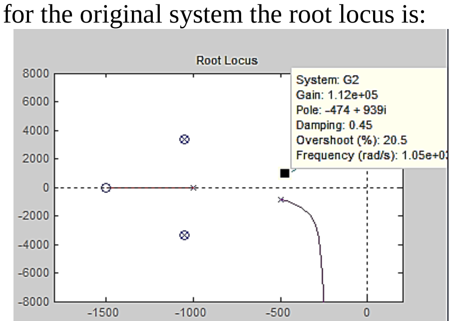

Fig. 22**:** Root locus of original system

And after placing a zero by PD Compensation Method at -2100, the root locus becomes:

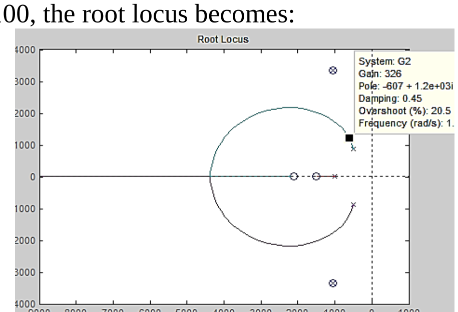

Fig. 23**:** Root locus of PD compensated system

By placing a zero at -2100, the value of gain has much reduced as compared to the original ones and also the dominant pole has more negative real and imaginary parts which considerably show reduced settling and peak time.

	Uncompensated	PD Compensated
System Type	0	0
% O.S	20.5	20.5
Gain (K)	1.12 e^05	326
Settling Time (T_s)	8.4399 e^-3	6.5897 e^-3
Peak Time (T_p)	3.3456 e^-3	2.6179 e^-3
Static error constant (K_p)	0.1697	1.0372
Steady state error e(∞)	0.8549	0.49

TABLE 5: Comparison between PD compensated and uncompensated system

Now again after placing zero at 3000, the root locus intersects the percentage overshoot line at two points with different gain values. It entirely depends on us which point we are going to use by judging the gain and dominant poles location.

Root locus showing first point of intersection:

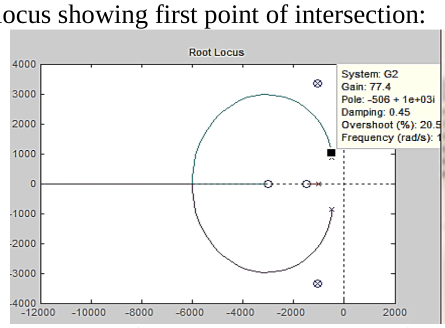

Fig. 24**:** Root locus of PD compensated system with first point of intersection

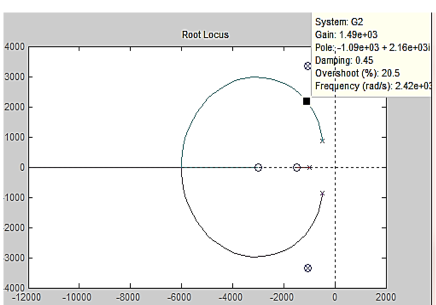

Fig. 25: Root locus of PD compensated system with second point of intersection

At first point of intersection the value of gain is just 77.4 and

$$\text{Settling time } (T_s) = \frac{4}{506} = 7.905e^{-3} \text{ sec}$$

$$\text{Peak time } (T_p) = \frac{\pi}{1000} = 3.14e^{-3} \text{ sec}$$

At second point of intersection the value of gain is much high as compared to first point of intersection which is 1490 and

$$\text{Settling time } (T_s) = \frac{4}{1090} = 3.669e^{-3} \text{ sec}$$

$$\text{Peak time } (T_p) = \frac{\pi}{2160} = 1.4544e^{-3} \text{ sec}$$

Since the settling and peak time has low values but practically the system with low gain adjustment values is preferred.

***Lead Compensator**:* An active ideal derivative compensator can be approximated with a passive lead compensator. When passive networks are used, a single zero cannot be produced; rather, a compensator zero and a pole result. However, if the pole is farther from the imaginary axis than the zero, the angular contribution of the compensator is still positive and thus approximates an equivalent single zero [11]. In other words, the angular contribution of the compensator pole subtracts from the angular contribution of the zero, the net angular contribution is positive, just as for a single PD controller zero. The addition of pole using lead compensator does not reduce the number of branches of the root locus that cross the imaginary axis in to the right half plane. This entire phenomenon and the insertion of zero and pole are shown below.

The root locus of original system is:

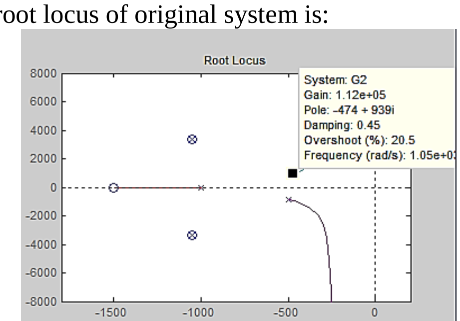

Fig. 26**:** Root locus of original system

Now say we want to reduce the settling time by half. So, original T_s = 8.4388 e^-3. By reducing it half the new settling time becomes

T_s (new) = 4.2194 e^-3.

From this new settling time the real part of new dominant pole becomes -948. And the value of imaginary part of new dominant is calculated as:

$$-948 * \tan^{-1}(180 - \cos^{-1} 0.45) = 1881.3$$

So the new dominant pole becomes -948+1881.3ί. By inserting a zero at -100 arbitrary, the angular contribution which must be required of the new poles is calculated as:

$$180 - (-114.2635 - 73.6475 + 113.867 + 99.335 + 88.4167) = 66.4446$$

Angular contribution of the new added pole must be 66.446º. The position of new compensated pole is calculated as:

$$\frac{1881.3}{\tan 66.4446} + 948 = 1768.17$$

The decrease the settling time the new zero is inserted at -100 and new pole at 1768.17. The root locus of the new system becomes:

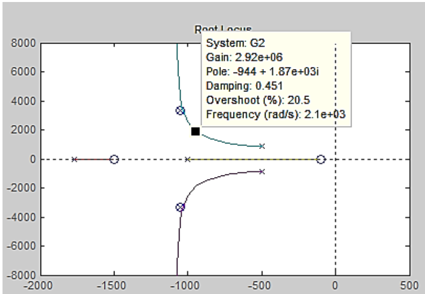

Fig. 27: Lead compensated system for -100

Now after inserting a zero at -5 and corresponding pole at 1683.37373, the root locus becomes:

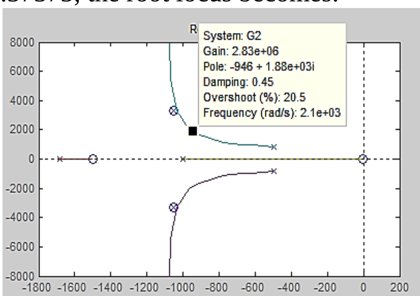

Fig. 28**:** Lead compensated system for -5

The Root locus of the system by inserting compensation zero at -250 and compensation pole at -1932.1988

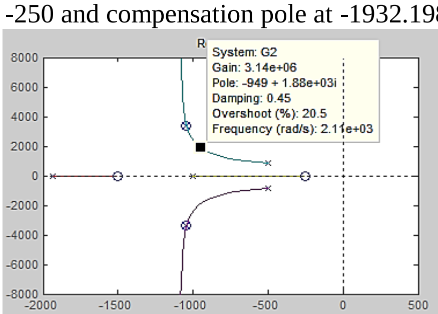

Fig. 29**:** Root locus of lead compensated system with zero at -250 and compensation pole at -1932.1988

PID Controller: When both ideal PD and ideal PI controllers are merged together, then resultant controller is proportional integral derivative controller. As name signifies, this controller improves both transient responses and steady state errors [12].

The following diagram explains the construction of a simple PID Controller.

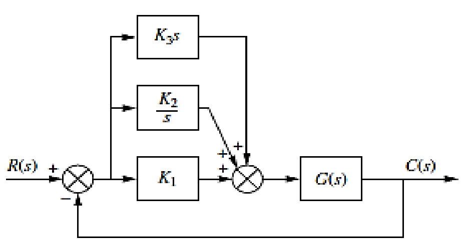

Fig. 30: block diagram of PID Controller [1]

The transfer function of the PID controller is:

$$G_c(s) = K_1 + \frac{K_2}{s} + K_3 s = \frac{K_3(s^2 + \frac{K_1}{K_3}s + \frac{K_2}{K_3})}{s}$$

As from the transfer function it can be realized that the controller has two zeros and one pole. One pole and one zero are tuned to realize the PI controller in such a way that the pole in inserted at origin and the zero is placed near the pole. The other remaining zero is simply placed at desired point to improve the transient response just like and ideal PD compensator [13]. The difference in response of any uncompensated system, PD Compensated system and PID controller compensated system can be visualized by the following diagram.

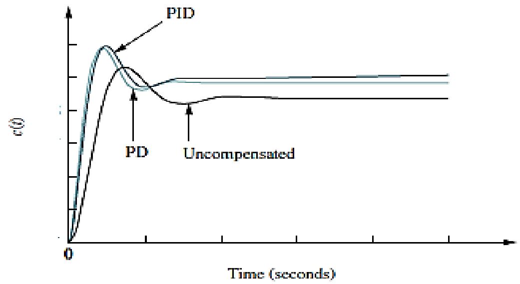

Fig. 31**:** difference between step responses of PID, PD and un-compensated system [1]

Now apply this technique on the original system which is under consideration now. The step response of the original system is:

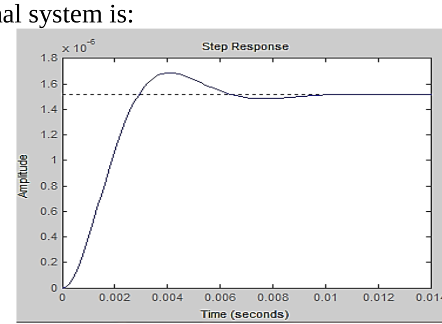

Fig. 32: Step response of original system

After placing a pole at origin and a zero at -0.01 to improve the steady state error and a zero at -2100 to improve the transient responses, the root locus of the PID Compensated system is:

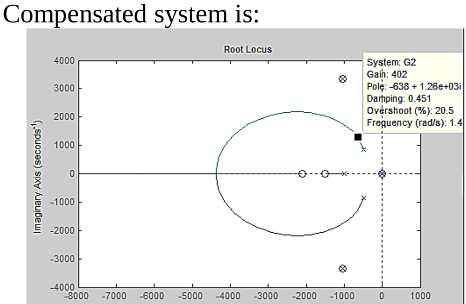

Fig. 33: Root locus of PID compensated system

Also, the step response of the PID Compensated system is:

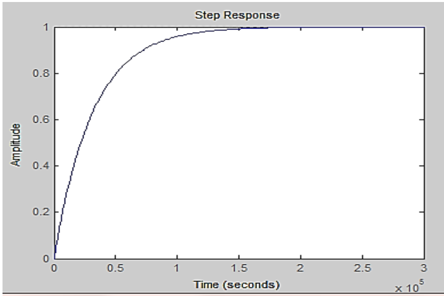

Fig. 34**:** Step response of PID compensated system

	Uncompensated	PID Compensated
System Type	0	1
% O.S	20.5	20.5
Gain (K)	1.12 e^05	402
Dominant poles	-474+939i	-638+1260i
Settling Time (T_s)	8.4399 e^-3	6.2696 e^-3
Peak Time (T_p)	3.3456 e^-3	2.4933 e^-3
Static error constant (K_p)	0.1697	∞
Steady state error e(∞)	0.8549	0

TABLE 6: Comparison between PID compensated and uncompensated system

Controller Design: The original system can be represented in phase variables form as:

$$\dot{\mathbf{x}} = \mathbf{Ax} + \mathbf{Bu} \qquad \text{(ii)}$$
$$y = \mathbf{Cx} \qquad \text{(iii)}$$

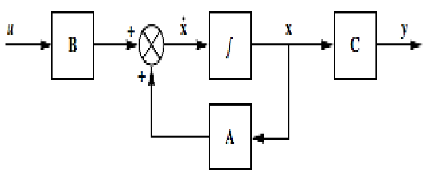

Fig. 35: State space representation [1]

Where **A, B** and **C** matrices for general system are:

$$\mathbf{A} = \begin{bmatrix} 0 & 1 & 0 & 0 & 0 \\ 0 & 0 & 1 & 0 & 0 \\ 0 & 0 & 0 & 1 & 0 \\ 0 & 0 & 0 & 0 & 1 \\ -a_0 & -a_1 & -a_2 & -a_3 & -a_4 \end{bmatrix}$$
$$\mathbf{B} = [0 \quad 0 \quad 0 \quad 0 \quad 1]^T$$
$$\mathbf{C} = [c_1 \quad c_2 \quad c_3 \quad c_4 \quad c_5]$$

Instead of feed backing the output to the summing junction just like in ordinary controllers, in controller design the feedback is taken from the state variables with adjustable gains, k in their path, so that the desired output can be achieved by simply adjusting the gains [14]. The whole concept is explained with the help of the block diagram of with state variable feedback as:

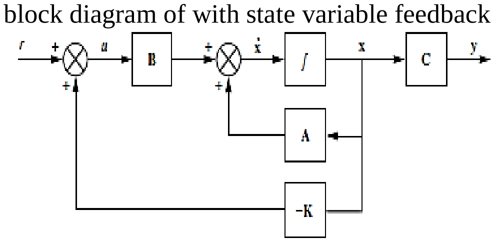

Fig. 36: Plant with state-variable feedback

The equations for closed loop controller design with feedback state variables are:

$$\dot{x} = (A - BK)\,x + Br \qquad \text{(iv)}$$
$$y = Cx \qquad \text{(iii)}$$

The det (s**I**-(**A** - **BK**)) is calculated and co-efficient are compared with desired characteristics equation to evaluate the gain **K**'s variables.

Arbitrary choosing that this controller decreases the settling time half as compared to the original system. So, the new settling time is 4.2190 e^-3. From this, the real part of new dominant pole is -947.285. Since, ζ is 0.45, so, the new ω_n becomes 2105.08

The other three poles will be placed exactly at zeros of original transfer function to nullify their effect.

So, the desired new characteristics equation becomes:

$$s^5 + 5494.57s^4 + 26651899.0418s^3 + 63504569798.6632s^2 + 103056313841870s + 103056313841870 \qquad \text{(v)}$$

Here **(A - BK)** is:

$$\begin{bmatrix} 0 & 1 & 0 & 0 & 0 \\ 0 & 0 & 1 & 0 & 0 \\ 0 & 0 & 0 & 1 & 0 \\ 0 & 0 & 0 & 0 & 1 \\ -a_0-k_1 & -a_1-k_2 & -a_2-k_3 & -a_3-k_4 & -a_4-k_5 \end{bmatrix}$$

Now, after calculating det (s**I**-(**A** - **BK**)) the results are:

$$s^5 + (4095 + k_5)s^4 + (18424525 + k_4)s^3 + (29597327500 + k_3)s^2 + (26395608750000 + k_2)s + (12127806250000000 + k_1) \qquad \text{(vi)}$$

By comparing the equation (1) with equation (2), the values of variables K's are determined and are:

$$\begin{bmatrix} -1202474994 * 10^7 \\ 76660705090000 \\ 33907242300 \\ 8227374.042 \\ 1399.57 \end{bmatrix}$$

Here **(A - BK)** is:

$$\begin{bmatrix} 0 & 0 & 0 & 0 & -1.0305631e\text{^}14 \\ 1 & 0 & 0 & 0 & -1.030563138e\text{^}14 \\ 0 & 1 & 0 & 0 & -6.35045698e\text{^}10 \\ 0 & 0 & 1 & 0 & 26651899.04 \\ 0 & 0 & 0 & 1 & -5494.57 \end{bmatrix}^T$$
$$\mathbf{B} = [0 \quad 0 \quad 0 \quad 0 \quad 1]^T$$
$$\mathbf{C} = [18375000000 \quad 15400000 \quad 3600 \quad 1 \quad 0]$$

And the transfer function of the new system becomes:

$$\frac{-1.894e24\, s\text{^}3 - 1.587e21\, s\text{^}2 + 1.408e19\, s + 2.959e22}{s\text{^}5 + 5495\, s\text{^}4 + 2.665e07\, s\text{^}3 + 6.35e10\, s\text{^}2 + 1.031e14\, s + 1.031e14}$$

Observer Design: In observer design, instead of actual, the estimated outputs are fed back to yield the quick response. In observer design, the state variables are fed back to achieve the required response of the system [15].

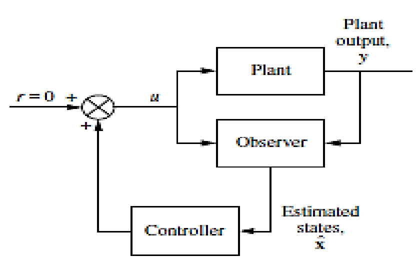

Fig. 37: Block diagram of closed loop observer [1]

The feedback with adjustable gain provides the arrangement so that the state variable estimated error is reduced [16].

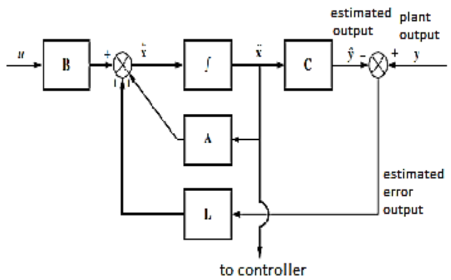

Fig. 38: Block diagram of observer design with feedback adjustable gain arrangement [1]

In following procedure, the observer controller is being designed for our original system to yield fast response. In observer design, the procedure is carried out using and by comparing with the required characteristic equation.

The observer canonical for any system is;

$$\dot{\mathbf{x}} = \mathbf{Ax} + \mathbf{Bu} \qquad \text{(ii)}$$

$$y = \mathbf{Cx} \qquad \text{(iii)}$$

Where general matrices A, B and C are:

$$\mathbf{A} = \begin{bmatrix} -a_4 & 1 & 0 & 0 & 0 \\ -a_3 & 0 & 1 & 0 & 0 \\ -a_2 & 0 & 0 & 1 & 0 \\ -a_1 & 0 & 0 & 0 & 1 \\ -a_0 & 0 & 0 & 0 & 0 \end{bmatrix}$$

$$\mathbf{B} = [b_1 \quad b_2 \quad b_3 \quad b_4 \quad b_5]^{\mathrm{T}}$$

$$\mathbf{C} = [1 \quad 0 \quad 0 \quad 0 \quad 0]$$

In observer controller, the equations for error between the actual and estimated state vectors are given by:

$$\dot{\mathbf{e}}_{\mathbf{x}} = (\mathbf{A} - \mathbf{LC})\, \mathbf{e}_{\mathbf{x}}\, \mathbf{Bu} \qquad \text{(iii)}$$

$$y - \hat{y} = \mathbf{Ce}_{\mathbf{x}} \qquad \text{(iv)}$$

So, for the observer design the (**A – LC) matrix** is:

$$\begin{bmatrix} -a_4+l_1 & 1 & 0 & 0 & 0 \\ -a_3+l_2 & 0 & 1 & 0 & 0 \\ -a_2+l_3 & 0 & 0 & 1 & 0 \\ -a_1+l_4 & 0 & 0 & 0 & 1 \\ -a_0+l_5 & 0 & 0 & 0 & 0 \end{bmatrix}$$

For the original system the dominant poles are:

-497.5 + 861.695276765517i

For the observer design for ten times fast response the new dominant poles become: Original dominant poles*10 = -4975 + 8616.95276765517i

Likewise, 3rd pole become 100 times the real part of original dominant pole, 4th and 5th pole becomes 1000 and 10000 times the real part of original dominant pole. So, the new characteristic equation from these new poles becomes:

$$s^5 + 5532200s^4 + 2802364764952.30s^3 + 151016903448478000s^2 + 149717823116442000000s + 121906035408223000000000000 \text{ --- } (3)$$

Now, after calculating det (s**I-(A - LC)**) the results are:

$$s^5 + (4095 - l_1)s^4 + (-18424525 + l_2)s^3 + (29597327500 - l_3)s^2 + (26395608750000 + l_4)s + (-12127806250000000 + l_5) \text{ ---- } (4)$$

By comparing the equation (3) with equation (4), the values of variables L's are determined and are:

$$\begin{bmatrix} -5528105 \\ 2.802383189\text{e}^{\wedge}12 \\ -1.510168739\ \text{e}^{\wedge}17 \\ 1.497178205\ \text{e}^{\wedge}21 \\ 1.212060355\ \text{e}^{\wedge}25 \end{bmatrix}$$

So, the closed loop representation of the new system in phase variable form becomes:

A – LC=

$$\begin{bmatrix} -5532201 & 1 & 0 & 0 & 0 \\ 2802364764475 & 0 & 1 & 0 & 0 \\ -1.51016903497327\text{e}^{\wedge}17 & 0 & 0 & 1 & 0 \\ -26395608749998.5 & 0 & 0 & 0 & 1 \\ 1.21206035378722\text{e}^{\wedge}25 & 0 & 0 & 0 & 0 \end{bmatrix}$$

$$\mathbf{B} = [0 \quad 1 \quad 3600 \quad 15400000 \quad 18375000000]^{\mathrm{T}}$$

$$\mathbf{C} = [1 \quad 0 \quad 0 \quad 0 \quad 0]$$

And so, the required transfer function is:

$$\frac{1\,s^3 + 3600\,s^2 + 1.54\text{e}^{\wedge}7\,s + 1.837\text{e}^{\wedge}10}{s^5 + 5.532\text{e}^6 s^4 - 2.802\text{e}^{12} s^3 + 1.51\text{e}^{17} s^2 + 2.643^{13} s - 1.212\text{e}^{\wedge}25}$$

III. CONCLUSION

Any compensation technique can be adopted according to the required requirement. The PI compensation eliminates the steady state error but it requires active system. The lag compensation reduces the steady state error but not reduces it to zero. Lag compensation requires passive network which is its advantage over PI compensation. The ideal PD compensation helps achieving the desired transient responses but ideal PD compensation is only possible with active system. The lead compensation also improves the desired transient response but due to passive network it produces pole. The ideal PID compensation not only provides the desired transient responses but also eliminates the steady state error. The controller design also helps in achieving the desired responses but in this system the values of adjustable gain are very high so, practically it is not favorable for this system**.** The observer design provides much quick response due to more negative real and imaginary parts but it is also not practically favorable due to higher value of adjustable gains. The most efficient controller for this system is PID controller because it eliminates the steady state error and provides any desired transient response with small values of adjustable system. Among all compensation techniques, PID controllers are best suited for this system as they are cheap, efficient and provide small gain parameters which are practically favorable.

REFERENCES

[1] N.S. Nise, Norman, Control systems Engineering, 6th ed. Reading, Wiley, 2011.

[2] Jatinder Kaur, Kamaljeet Kaur, Gurpreet Singh Brar and Monika Bharti, “Analysis of a Control system through Root locus Technique”, International Journal of Innovative Research in Science, Engineering and Technology, Vol. 2, Issue 9, Sept., 2013.

[3] B. Osman and H. Zhu, “Design of milling machine control system based on root locus method”, 3rd IEEE International Conference on Control Science and Systems Engineering (ICCSSE), Beijing, 2017, pp. 141-144.

[4] T.R. Kurfess and M.L. Nagurka, “Understanding the root locus using gain plots”, IEEE Control Systems, Volume 11, Issue 5, Aug., pp. 37–40, 1991.

[5] O. V. Prokhorova and S. P. Orlov, "Parametric optimization of control systems by the Etalon Control System assign using the root locus method or the poles and zeros location", IEEE II International Conference on Control in Technical Systems (CTS), St. Petersburg, 2017, pp. 16-19.

[6] R. Zanasia, S.Cuoghia and L. Ntogramatzidis, “Analytical and graphical design of lead–lag compensators”, International Journal of Control, Vol. 84, No. 11, Nov., pp 1830–1846, 2011.

[7] J. C. Basilio and S. R. Matos, “Design of PI and PID Controllers with Transient Performance Specification”, IEEE Transactions on Education, Vol. 45, No. 4, Nov., pp 364-371, 2002.

[8] A. Madady, H. Reza and R. Alikhani, “First-Order Controllers Design Employing Dominant Pole Placement”, IEEE 19th Mediterranean Conference on Control and Automation, Aquis Corfu Holiday Palace, Corfu, Greece June 20-23, 2011, pp 1498-1503.

[9] Derek Atherton, “PI-PD, an Extension of Proportional–Integral–Derivative Control”, Journal of Measurement and Control, Vol. 49, Issue 5, pp 161–165, 2016.

[10] J. A. Jaleel and N. Thanvy, “A Comparative Study between PI, PD, PID and Lead-Lag controllers for Power System Stabilizer”, IEEE International Conference on Circuits, Power and Computing Technologies, 2013, pp 456-460.

[11] A. Nassirharand and S. R. M. Firdeh, “Design of Nonlinear Lead and/or Lag Compensators”, International Journal of Control, Automation and Systems, vol. 6, no. 3, pp. 394-400, Jun., 2008.

[12] H. Wu, W. Su, Z. Liu, “PID controllers: design and tuning methods”, IEEE 9th Conference on Industrial Electronics and Applications (ICIEA),2014, pp 808-813.

[13] Y. Liao, T. Kinoshita, K. Koiwai and T. Yamamoto, "Design of a performance-driven PID controller for a nonlinear system," 6th International Symposium on Advanced Control of Industrial Processes (AdCONIP), Taipei, 2017, pp. 529-534.

[14] K. Tian and H. Yu, "Robust H∞fault-tolerant control based on state-observer," Proceeding of the 11th World Congress on Intelligent Control and Automation, Shenyang, 2014, pp. 5911-5914.

[15] G. Fan, Z. Liu and H. Chen, “Controller and Observer Design for a Class of Discrete-Time Nonlinear Switching Systems”, International Journal of Control, Automation, and Systems, Vol. 10, Issue 6, 2012, Pages1193-1203.

[16] J. Daafouz, P. Riedinger and C. Iung, “Observer-based switched control design with pole placement for discrete-time switched systems”, International Systems of Hybrid Systems, 2003, pp 263-282.

Pakistan Journal of Engineering and Technology, PakJET
Multidisciplinary | Peer Reviewed | Open Access

Volume: 1, Number: 1, Pages: 17- 20, Year: 2018

SVD Based Optimal Massive MIMO Transmission and Capacity

Zeeshan Raza[*,1] and Ishtiaq Ahmad[1]

[1]Electrical Engineering Department, The University of Lahore, 1-KM Defence Road, Lahore, 54000, Pakistan
[*]Corresponding author: Zeeshan Raza (Email: zeeshanraza.nfc@gmail.com)

***Abstract*— Spatial multiplexing of channel is the core of diversity in Multiple Input Multiple Output (MIMO) and massive MIMO. The array of antennas on a base station is the key to success for upcoming 5G multimedia communication network. Massive MIMO due to its substantial number of antennas produces high data rate. when an UEs transmit a signal towards base stations, large number of parallel streams produce high capacity. Channel interference and small-scale fading is minimized. In this paper we will analyze the massive MIMO model for single antenna MS transmit signal towards BS having hundreds of antennas. We will examine the behavior of this uplink scenario using matrix theory. We will develop SVD based massive MIMO system and investigate how SVD based system provides interactive feature of spatial multiplexing and decoupling of channels. Our hypothesis will prove minimization of interference and fading. We will examine the total capacity of parallel stream. This performance analysis will prove an optimal SVD based massive MIMO model**

***Index Terms*—Channel Estimation, MIMO, Spatial Multiplexing, SVD, ZF Receiver.**

I. INTRODUCTION

Massive MIMO multimedia communication network design is described as a base station (BS) with hundreds of antennas instantaneously serve a set of single-antenna MSs and the multiplexing gain can be shared by all MSs. The cheap antennas are supposed to be used in massive MIMO instead of costly antenna system. Due to its diversity nature, the massive MIMO is less sensitive to the propagation environment than in the conventional MIMO case [2]. Massive MIMO has become an essential part of Wireless communications standards, such as 802.11 (WiFi), 802.16 (WiMAX), LTE. The illustration of massive MIMO network is given in Fig1. [1]

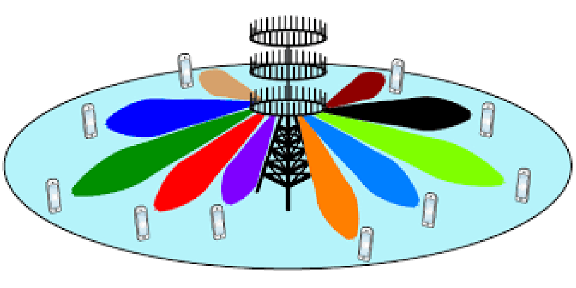

Figure 1: illustration of massive MIMO wireless network [4].

It is observed that, as the number of antennas increase the effects of uncorrelated noise and small-scale fading eliminate [3]. The concept of deep fading is finished in massive MIMO due to its parallel stream and LOS is maintained. The number of users is said to be independent of the size of cell. The antenna structure in massive MIMO supports the low energy consumption and negligible channel interference due to decoupling of channels. the received signal is approximately same as transmitted. [2]

The linear receivers like Maximum Ratio Combining (MRC), Zero Forcing (ZF), Minimum Mean Square Error (MMSE) produce excellent results unlike conventional MIMO performance which is only proportional to high SNR. signal processing approaches, such as matched- filter (MF) precoding/detection, is used in massive MIMO systems [6][8]. The assumption for MF based massive MIMO network is shown. [1][3] that under realistic propagation 17 Mb/s data rate could be achieved for each of 40 users in a 20 MHz channel with an average throughput of 730 Mb/s per cell and an overall spectral efficiency of 26.5 bps/Hz. Since the number of antennas at the BS assumed to be significantly larger [2] [11] [22].

In massive MIMO number of antennas on base station are larger than mobile station (MS) antennas that is why the channel matrix is not invertible like square matrix so instead of simple decomposition methods some complex methods are used like, Jacobi and Gauss-Seidel methods etc. [3] [13] In our proposed work, we will analyze the SVD based massive MIMO. The singular Value Decomposition (SVD) method produce simple decomposition in to parallel stream in case of linear receivers. The spatial multiplexing performs a tremendous role in massive MIMO and decoupling of channel decreases the channel interference. This paper is distributed in following section. in Section II we will discuss system model of our prescribed scenario of massive MIMO wireless communication network. section III will explain singular value Decomposition (SVD)method. We will analyze SVD based Massive MIMO system and compute total capacity in Section IV. In Section V, Conclusions will be drawn. [6]

Notations: In this paper, upper/lowercase boldface letters denote matrices/ vectors. X_i, h_{ji}, and y 1,2…..m denote the input signal, channel matrix and output signals respectively the {h} h and{t} shows the Hermitian and transpose . Ex, Ex^2, Rx^2 describe the expected value , variance and covariance. I represent identity matrix, M describe the large number of antennas placed on BS and K shows the single MS antenna. The acronym i.i.d denote independent and identically distributed, respectively.

II. SYSTEM MODEL

we will discuss our proposed scenario which is an uplink massive MIMO network model given in Fig 2, where the BS contain M antennas Where $j_1, j_2 \dots . j_m$ m are serving on BS and K are the mobile stations antennas describe as $i_1, i_2 \dots \dots . i_k$. Each MS contain single antenna. The scenario is considered in our study which can be designed as M >>K Here N ≤ K, is likely pilot design approach. We also consider Rayleigh communication fading model $f_{A(a)} = 2\text{ae}-^{2}$ [6]

Figure 2: massive MIMO wireless network model

Our proposed scenario is a single antenna I from K set of mobile station antennas is transmitting a symbol x_i which is received by M number of antennas placed on BS which are $M = j_1, j_2 \dots j_m$ the output signals will be received on BS which would be $y_1, y_2, y_3 .. y_m$ .The basic equation can be expressed as

$$Y = HX + N \quad (1)$$

"Y" term as received signal and "X" is transmitted signal where "H" denotes the channel Coefficient and "N" is additive white Gaussian noise (AWGN). Now putting the values in (1). The output signal Y can be expressed as

$$Y = \{h_{j_{1_i}}, h_{j_{2_i}} \dots . . h_{j_{m_i}}\}^T\{x_i\} + \{n_{j_1}, n_{j_2} \dots . n_{j_m}\}^T \quad (2)$$

The signal is transmitted in a time instant "t "as we have considered time domain, so the output signal can be expressed as,

$$Y = \sum_{j=1}^{m} h_{ji}x_i + n_j \quad (3)$$

This is clearly shown that a signal is transmitting from a mobile station and a large number of antennas are receiving this signal. [8] [16] Zero forcing (ZF) receivers are supposed to be used on base station and transmitting signal is precoding before transmitting [7] [16]. we are going to decompose the channel matrix using singular value decomposition method for our given scenario. We have discussed that a single antenna is transmitting a signal and large number of antennas on base station are receiving that signal. We will analyze the performance of SVD based massive MIMO. We will prove how spatial multiplexing produce independent stream with help of matrix theory. We will compute the expression for total capacity of our prescribed scenario of massive MIMO multimedia network [5][20][14]

III. SVD

Singular value decomposition is very useful method for characterization of channels and it is popular in analyzing the behavior of MIMO and massive MIMO wireless communication. It produces the decomposition of channel matrix. Let us consider channel matrix as given above r × t which is stated as r > t the SVD is described as given bellow [1] [14] [16],

$$H = U\Sigma V^H \quad (4)$$

Here U is r×t matrix having t column and Σ is diagonal matrix containing singular value. It is t×t matrix and V is unitary matrix also t × t matrix as well. SVD is implied only if the properties of SVD are followed which are given bellow [4] [16].

$$u_1^h u_2 = \begin{cases} 1 & if\ i = j \\ 0 & if\ i \neq j \end{cases} \quad (5)$$

The column should be orthonormal. It concluded that

$$U^H U = I_{t\times t} \quad (6)$$

Second property regarding V matrix which is stated as:

$$V^H V = VV^H = I_{t\times t} \quad (7)$$

This matrix v is known as unitary matrix Third property for singular value matrix which is stated as

$$\sigma_1, \sigma_2, \dots\dots..\sigma_n > 0 \quad (8)$$

$$\sigma_1 > \sigma_2 > \cdots \dots .>.\sigma_n \quad (9)$$

Singular values are non-negative and are arranged in decreasing order number of nonzero singular value denote the rank of matrix in next Section, we will analyze the performance of our prescribed scenario using singular value decomposition methods and drive the expression for SVD and find out output signal Y. We will compute and analyze the expression for total capacity for parallel stream of channel [3-5].

IV. PERFORMANCE ANALYSIS

Let us start to find out the expression. We will substitute the value in SVD according to our scenario and the equation can write as [12-13],

$$U\Sigma V^H = \{1\}^H \quad (10)$$

U vector is normalized as unit norm and singular value matrix is t × t matrix and V matrix is also in same formation now we can see that all the properties of SVD is followed for the substitution of values in $U^H U - I$ and Σ matrix is non-zero matrix. It shows that the expression of our prescribed scenario is valid for SVD decomposition although if the expression does not follow all the properties then using row matrix [6][16]19] operation we must convert the expression so that it follows the properties of SVD. The massive MIMO channel matrix has derived as $H = U\Sigma V^h$ using singular value decomposition method we know the system modal equation as given Eq[1].which can be write as

$$\overline{Y} = U^H\overline{x} + \overline{n} \quad (11)$$

At the receiver, we multiply U^H which can be written as

$$U^H\overline{Y} = U^H(U^H\overline{x} + \overline{n}) \quad (12)$$

$U^H\overline{Y}$ can be demoted as Y the above equation can be rewritten as

$$\tilde{Y} = \Sigma V^h x + U^H\bar{n} \quad (13)$$

The value of $U^H\bar{n}$ can be replaced some modified noise vector which is term as n this effective noise vector Now some manipulation on the transmitter as called precoding It must be done before transmission $\bar{x}$= Vx here is transmit vector it effects on our system as given in equation [21-22]

$$\widetilde{Y} = \Sigma\tilde{x} + \tilde{n} \quad (14)$$

However, we know Σ is diagonal matrix Here if we elaborate our equation and observe that it looks as given bellow in Eq[15]. We are observing in this scenario there is no interference between symbol. This transform domain is also called decoupling of massive MIMO channel and known as parallelization of massive MIMO system [4] the equation can be expanded as

$$\widetilde{y_1} = \sigma\widetilde{x_\iota} + \widetilde{n_1}$$
$$\widetilde{y_2} = \sigma\widetilde{x_\iota} + \widetilde{n_2}$$
$$\widetilde{y_m} = \sigma\widetilde{x_\iota} + \widetilde{n_m} \quad (15)$$

This is the collection of parallel channels this is possible due to singular value decomposition system in which A symbol is added with the signal on transmitter end to increase SNR. This transformation of signal is called beamforming and precoding schemes are applied on receivers for getting original signal. A symbol is transmitted through parallel channel which termed as spatial multiplexing, stated as in same time same frequency [3] [12] [14]. It can be written as,

$$\tilde{n} = U^H n$$
$$E\{\widetilde{n\, n^h}\} = E\{U\, \widetilde{n\, n^h} U^h\}$$
$$= \sigma_n^2 I \quad (16)$$

It is shown that noise power is uncorrelated in different antennas as shown (17), which mean power of noise before beam forming and after beamforming now we can compute SNR of these parallel channel. Let us see the SNR of one channel as jth,

$$SNR = \{\sigma_j^2 p_j)/(\sigma_n^2\} \quad (17)$$

Now we can investigate the SNR of parallel channel it can be understand with the diagram given bellow,

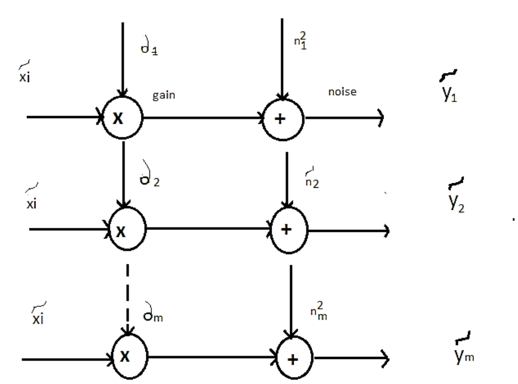

Figure 3: stream of parallel decoupled channel

The parallel channel which is shown the schematic diagram the independent stream of symbol transmitted through parallel channel which is spatial multiplexing [6, 16]. Now t we will see the Shannon capacity for maximum rate which is given by [5, 11].

$$C = Blog_2(1 + SNR) \quad (18)$$

Putting the value of SNR of jth channel

$$C = Blog_2\left(1 + \sigma_j^2 p_j/\sigma_n^2\right) \quad (19)$$

$$C = B\sum_{j=1}^{m} log_2\left(1 + \sigma_j^2 p_j/\sigma_n^2\right) \quad (20)$$

The sum of individual capacity of each parallel stream shows that noise factor and interference decreases as the number of parallel stream increases this is leads to increase the net capacity of wireless communication network. This is one of the motivation behind the recognition of massive MIMO as supposed to be core technology of upcoming 5G multimedia communication network.

V. CONCLUSION

SVD based massive MIMO offers the optimal transmission and maximum channel capacity near about 10 time of conventional capacity. Our hypothesis also proved that SVD based system provides interactive feature of spatial multiplexing and decoupling of channel which clearly shows the negligible interference and fading. in short, the SVD produces simple and interactive decomposition and optimal performance for massive MIMO. The massive MIMO would be the key for the upcoming 5G wireless communication network.

REFERENCES

1. Lee M. Garth and Peter J. Smith, “Exact Symbol Error Probabilities for SVD Transmission of BPSK Data over Fading Channels” In EEE Trans, vol 10, P 271-280 , 2008.
2. F. Rusek , D. Persson , B. K. Lau , E. G. Larsson , Scaling up MIMO: Opportunities and challenges with very large arrays. In IEEE Signal Process, vol 30, P 718-725 ,Jan , 2013.
3. W. Liu , S. X. Ng , Multicell Cooperation Based SVD Assisted Multi-User MIMO Transmission. In IEEE Signal Process, vol 19, P 611-620 ,sep , 2009.
4. H. Q. Ngo, E. G. Larsson, T. L. Marzetta, Energy and spectral efficiency of very large multiuser MIMO systems In IEEE Trans. Commun, Vol 61, P 1436-1449, Apr,2013.
5. Gilberto Berardinelli , Troels B.Srensen , SVD-based vs. Release 8 codebooks for Single User MIMO LTE-A Uplink. In E E E V T S Vehicular Technology Conference. Proceedings, 2010.
6. Pitarokoilis, S. K. Mohammed, E. G. Larsson. On the optimality of single carrier transmission in largecale antenna systems. in IEEE Wireless Commun. Lett,Vol 01, no 04, p 276-279, Aug 2012.
7. Y. Chen, S. Zhang, S. Xu, Fundamental trade-offs on green wireless networks . In IEEE Commun. Mag. Vol 49, no 06, p 30-37, Apr 2011.Tombaz, A. Vstberg, J. Zander, Energy- and cost-efficient ultra highcapacity wireless access. In IEEE Wireless Commun. Mag. Vol 18, no 05, p 18-24, Jan 2011.
8. T. L. Marzetta, B. M. Hochwald, Capacity of a mobile multiple antenna communication link in Rayleigh flat fading . In IEEE Trans. Inform. Theory. Vol 45, p 139-157, Mar 2011.
9. F. Fernandes, A. Ashikhmin, T. L. Marzetta, Inter-cell interference in noncooperative TDD large scale antenna systems . In EEE J. Sel. Areas Commun. Vol 31,no 2, p 19-31, Jan 2013.
10. Bjrnson, P. Zetterberg, ”Capacity limits and multiplexing gains of MIMO channels with transceiver impairments”, ” IEEE Commun. Lett”, 2013, Vol, 17, no,1, pp, 91-94.
11. F. Rusek , D. Persson , B. K. Lau , E. G. Larsson , t”Scaling up MIMO: Opportunities and challenges with very large arrays”, ”IEEE Signal Process. Mag”, vol 30, no, 2, pp,40-60, Jan,2013.
12. H. Q. Ngo, E. G. Larsson, T. L. Marzetta, ”Energy and spectral efficiency of very large multiuser MIMO systems ”, ”IEEE Trans. Commun”, Vol, 61, pp, 1436-1449, Apr,2013.
13. A. Pitarokoilis, S. K. Mohammed, E. G. Larsson, ”On the optimality of single carrier transmission in large-scale antenna systems ”, ”IEEE Wireless Commun Lett”, Vol, 01, No,.04, pp, 276-279, Aug,2012.
14. Y. Chen, S. Zhang, S. Xu, ”Fundamental trade-offs on green wireless networks ”, ”IEEE Commun. Mag”, Vol,49, No,.06, pp, 30-37, Apr,2011.
15. S. Tombaz, A. Vstberg, J. Zander, ”Energy- and cost-efficient ultrahighcapacity wireless access ”, ”IEEE Wireless Commun. Mag”, Vol,18, No,5, pp,18-24, Jan,2012.
16. T. L. Marzetta, B. M. Hochwald, ”Capacity of a mobile multiple antenna communication link in Rayleigh flat fading ”, ”IEEE Trans. Inform. Theory”, Vol, 45, pp,139-147, Jan,1999.
17. F. Fernandes, A. Ashikhmin, T. L. Marzetta, ”Inter-cell interference in noncooperative TDD large scale antenna systems”, ”IEEE J. Sel. Areas Commun”, Vol, 31, no,2, pp,19-23, Jan,2013.
18. T. L. Marzetta, ”Non cooperative cellular wireless with unlimited numbers of base station antennas ”, ”IEEE Trans. Wireless Commun”, Vol, 9, No,11, pp,3590-3500, Nov,2010.
19. Neha Mehrotra, Ashutosh Kr, ”Pilot Contamination Effect in Massive MIMO and Analysis of Mitigation Techniques ”, ”International Journal of New Technology and Research ”, Vol, 3, no,2. pp,19-23, Feb,2017.
20. J. K. Tugnai, ”Self-contamination for detection of pilot contamination attack in multiple antenna systems”, ” IEEE Wireless Communications Letters ”, Vol, 4, No, 5, pp,525-529, 2015.
21. X. Gao, O. Edfors, ”Linear pre-coding performance in measured very-large MIMO channels”, ”in Proc. IEEE VTC ”, Vol, 4, No,2, pp,25-29, 2011.

Pakistan Journal of Engineering and Technology, PakJET
Multidisciplinary | Peer Reviewed | Open Access

Volume: 1, Number: 1, Pages: 21- 28, Year: 2018

Estimating Dynamics of Switching Converter Using System identification Technique

Nasir Abbas[1] and Ghulam Abbas[*,1]

[1]Electrical Engineering Department, The University of Lahore, 1-KM Defence Road, Lahore, 54000, Pakistan
Corresponding author: Ghulam Abbas (Email: ghulam.abbas@ee.uol.edu.pk)

***Abstract*—The switching converters are widely used in power electronics. These converters convert low input DC voltage to higher DC output voltage by switching the source voltage. These converters are nonlinear in nature. This paper deals with the estimation of dynamics of converters. Applying system identification technique, one can estimate the transfer function of switching converters which can be used for the controller design. Although many identification techniques such as cross correlation and circular correlation-based and state space averaging have been used to estimate converter dynamics but they require heavy mathematical computations. In the proposed research, frequency response-based data from duty cycle to output voltage estimation have been employed to estimate converter dynamics. In this method, frequency response data (FRD) are collected by injecting the sine stream signal having frequency from few hertz to many kilo hertz at duty cycle input which excite the system at different frequencies and varying output response is obtained. The transfer functions of converters such as buck-boost, boost and buck are estimated using such a system identification technique. Well- estimation of the converter transfer functions is validated through MATLAB/Simulink based simulation results.**

***Index Terms*—Bode plot, frequency response data, identified transfer function, switching converters, system identification, MATLAB/Simulink.**

I. INTRODUCTION

In modern era, all the services depend upon continuous functioning of different electronics devices and systems which require energy for their reliable operation. The energy is treated by switching converters for reliable operation which is prime importance for their quality. These are used to convert one DC voltage level to other one by switching the source voltage. Due to their switching behavior, they are nonlinear in nature. Determining their dynamics through well-established techniques is a difficult task. Because the lengthy derivation and complicated calculation is compulsory to obtain desired results. Firstly, one has to linearize, then average the circuit over a complete cycle to get approximated dynamics. To overcome past complications, we will use frequency response technique to achieve the intended objectives. By using this technique, we will be able to find the transfer function of any system as it does not require haddock mathematical derivation.

The dynamics of switching converters can be characterized by transfer function. In this paper, the transfer function of the switching converter is estimated using the system identification techniques. In one of the techniques, the transfer function is determined from frequency response data with the help of Sine Sweep Method (SSM) [1]. In this method, frequency response is obtained by injecting the sinusoidal signal having frequency from few hertz to many kilo hertz into the input of the converter. The estimated transfer function will be helpful to find the controlling parameters of the switching converter to regulate the output. Three converters, namely buck, boost and buck-boost are considered and have been identified. MATLAB/Simulink will be used for simulation purposes.

Besides, it is possible to create arbitrary excitation waveform with a broad band spectrum to collect all spectral information in one measurement. There are ten signals used in [2] to estimate transfer function of switching converters by frequency response data. It used Maximum length binary sequence (MLBS) to estimate the transfer function. The MLBS is used to evaluate transfer function of any linear system and now also being used in field of acoustic [3], impedance spectroscopy of single living cells [4], sensors for gas, odor and or aroma analysis [5], sonar system for zooplankton survey [6]. The method is equally employed for power converters [7]-[11]. But this method is not feasible to measure all transfer functions of power converters. So, we will use sine sweep method to estimate transfer function of purposed switching converters. Linear systems can also be identified by extensively studied method called cross correlation in system identification tools [12]. But this method, working on the basis of cross-correlating the system input and output, causes errors in results when we deal with finite signal length. Another familiar method Autoregressive with Exogenous Terms (ARX) is used in system identification to estimate the frequency response of model. This method creates disturbances which are also part of the system dynamics.

In the proposed method named Sine Sweep Method (SSM), a change in amplitude and phase of sinusoidal output with respect to input signal, on the application of a sinusoidal signal of known frequency to a linear system input, is observed. The frequency response data estimation is best technique to find the dynamics of a switching converters.

The paper is constructed in the following way. Operation of switching converters is described in Section II. Dynamics of the converters using system identification technique are estimated in Section III. In Section IV, additional simulation results are presented to further validate the estimated transfer functions. Section V contains conclusion.

II. Switching Converters Fundamentals

Switching converters are electronic systems which alter one DC level to another DC level by switching action. Switching converters are DC to DC voltage converters which provide high efficiency as compared to linear power supplies. The main trend of using switching converters is their smaller size, flexibility, not having transformer and provides efficiency of 75% to 98%. Therefore, they are used extensively in solar battery charging system, UPS system, medical electronics, communication, computer peripherals and personal computers [13]. Modern electronic instruments need light weight, high quality and efficient power supplies. The operation of buck converter, boost converter and busk boost converter is discussed here. The input and output of switching converters are shown in Fig. 1. Here duty cycle is input to switching converters and voltage is the output.

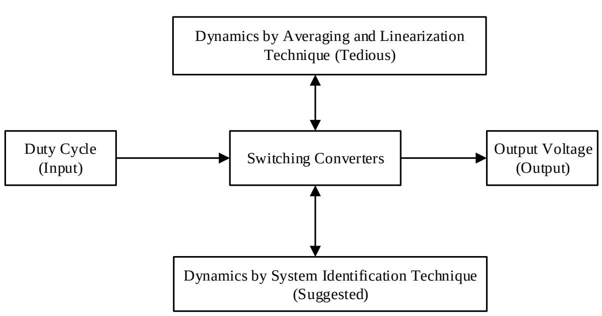

Input-output representation of switching converter.

A. Buck Converter

The buck converter circuit consists of a switching transistor along with flywheel circuit containing capacitor, inductor and diode. When transistor is on, the current starts to flow through the energy storing element called inductor and stores energy in the form of magnetic field. The inductor opposes the abrupt change in current. In this way the output of switching transistor output is prevented from increasing suddenly to its peek value because inductor stores energy taken from the increasing output. The stored energy in the form of magnetic field is delivered to the circuit when transistor is switched off. The basic buck converter circuit is shown in Fig. 2.

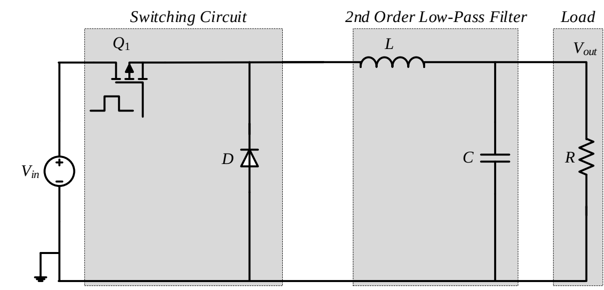

Fig. 1. Basic buck converter circuit.

The duty ratio k relating input voltage V_{in} and output voltage V_{out} of the of buck converter is given in (1)

$$\frac{V_{out}}{V_{in}} = k \tag{1}$$

B. Boost Converter

Boost converter is the DC to DC converter which converts low DC voltage level to another DC voltage level higher than input. The boost converter consists of a MOSFET switch, energy storing elements inductor and capacitor, diode, power supply and load as shown in Fig 3. The input voltage V_{in} and the output voltage V_{out}, in case of boost converter, are related as [14]

$$V_{out} = \frac{V_{in}}{(1-k)} \tag{2}$$

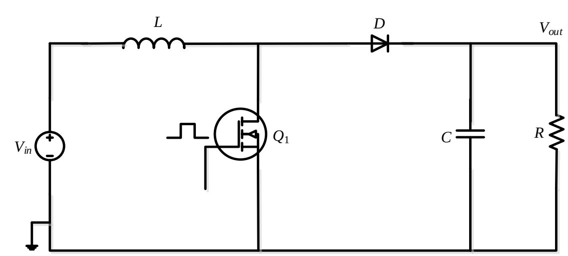

Fig. 2. Basic boost converter circuit.

C. Buck-Boost Converter

Buck-boost converter (see Fig. 4) like other switched mode power supplies converts one DC level to another DC level and is the combination of principles of both buck and boost converters in single circuit due to switching action of MOSFET.

When switch is turned on, the input energy is supplied to inductor and it gets magnetized. The current flows from positive polarity to negative polarity via inductor. The diode is reverse biased and current passes through load and charges the capacitor. The load is supplied by the capacitor that was charged in previous cycle. When MOSFET is turned off, the inductor and input is disconnected. During off state the inductor is the main source of energy. Now diode is forward biased and circuit current flows through load and capacitor is discharged. In this way the output voltage is at least equal to or greater than source voltage.The output voltage V_{out} and the input voltage V_{in} are related as

$$\frac{V_{out}}{V_{in}} = -\frac{k}{1-k} \tag{3}$$

Where, k *is* duty cycle of buck-boost converter

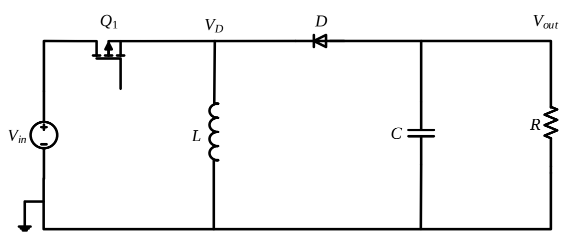

Fig. 3. Basic buck-boost converter circuit.

III. System Identification Technique

System identification refers to making the mathematical models of dynamic system with the help of measured data. System identification is divided into parametric and nonparametric techniques [15], [16]. In parametric identification a system model is assumed and model parameters are estimated. But in nonparametric no assumption is made about the model under test and identification is used to directly compute the frequency response of system. Nonparametric method includes correlation analysis, transient response analysis, frequency response, Fourier, and spectral analysis. In this research, we focus on nonparametric identification. We have used frequency response estimation to find the dynamics of converter.

Frequency response estimation requires input signal at input linearization point which excites the model at desired frequencies, like sine stream or chirp signal. We have used sine stream signal as shown in Fig. 5, which is a series of sinusoids. Output response is achieved at output linearization point (see Fig. 6).

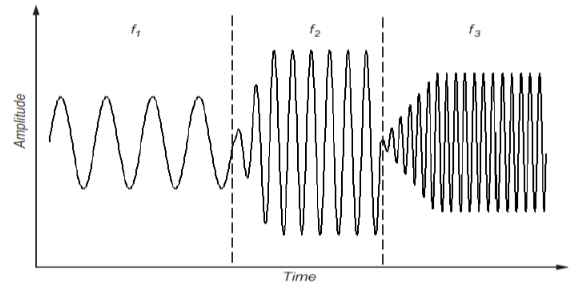

Fig. 4. Sinestream having different frequencies.

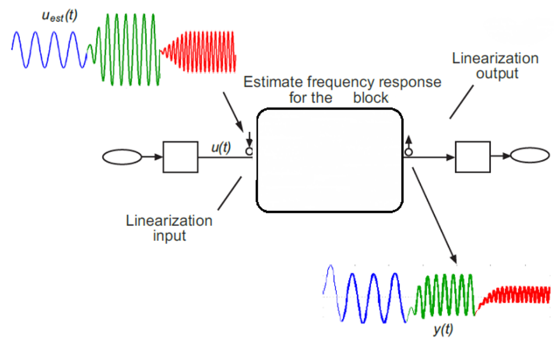

Fig. 5. Sinestream injected at point of linearization.

The complete algorithm is illustrated in flow chart shown in Fig 7.

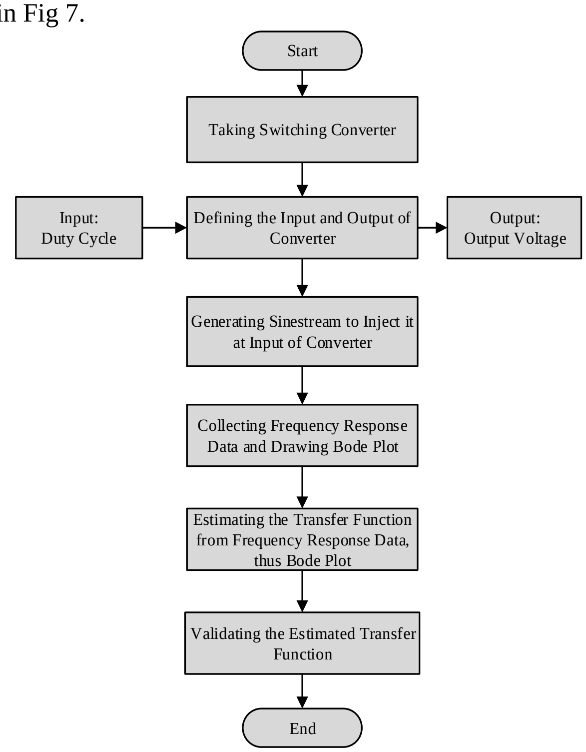

Fig. 6. Flow chart describing identification technique mechanism

TABLE I

CONVERTER SPECIFICATIONS

Converter	Switching Frequency	Input Voltage	Output Voltage	Duty Ratio
Buck	10 kHz	200 V	150 V	75 %
Boost	100 kHz	24 V	48 V	50 %
Buck-Boost as Inverting Buck	10 kHz	12 V	-5 V	29.4 %
Buck-Boost as Inverting Boost	10 kHz	12 V	-28 V	70 %

The input and output, duty ratio and switching frequencies for the three converters, namely buck, boost and buck-boost have been summarized in Table I.

A. Buck Converter Transfer Function Estimation

Buck converter (stepping down 200 V to 150 V by duty ratio of 0.75) to be estimated is illustrated in Fig. 8. The open loop response is obtained by introducing the sinusoidal signal having frequency variation from few 100 kHz to 20 kHz at the 'duty cycle input'. Resultantly, a plot of gain and phase variation with respect to frequency sweep is shown in the form of Bode plot in Fig. 9.

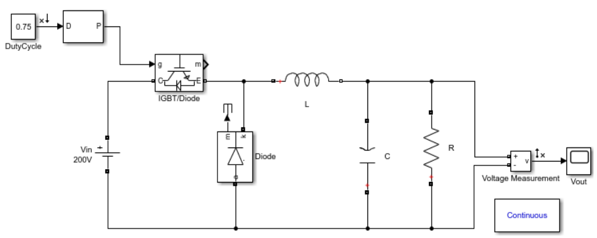

Fig. 7. Buck converter Simulink model.

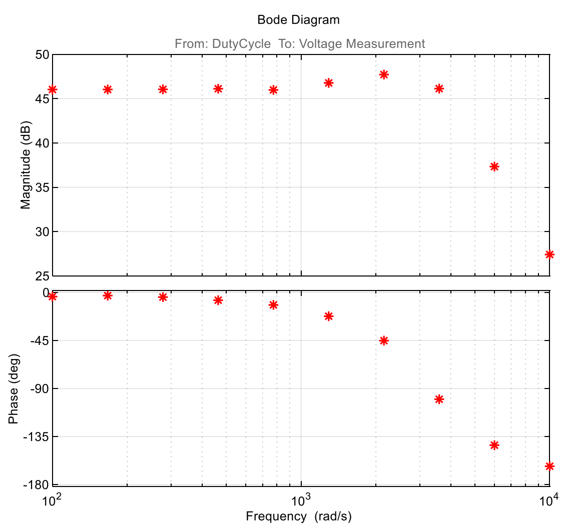

Fig. 8. Frequency response Bode plot of buck converter Simulink model.

The filtered steady state time response along with its FFT of the circuit is shown in Fig. 10.

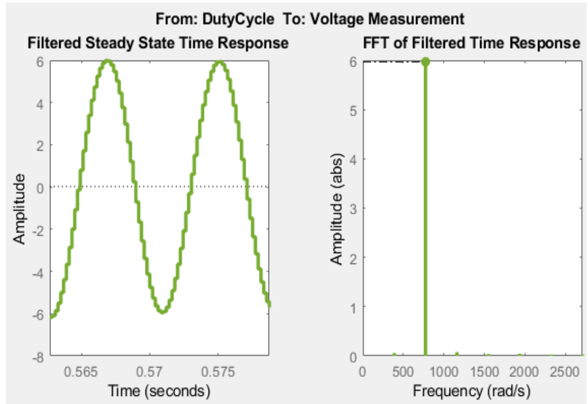

Fig. 9. Output response of buck converter against sinestream.

Once the Bode plot is achieved from the frequency response data, transfer function of the converter can be easily extracted from the Bode plot. The estimated transfer function of the buck converter, thus, is

$$G_{Buck}(s) = \frac{2.198\times10^{9}}{s^{2}+2975\,s+1.105\times10^{7}} \tag{4}$$

The Bode plot of the estimated transfer function of the buck converter matches exactly to the one obtained through frequency response data (see Fig. 11). This confirms the well-mapping of FRD into the transfer function.

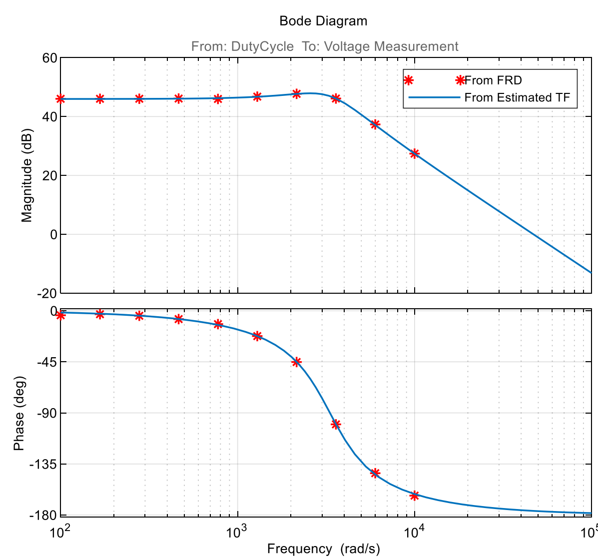

Fig. 10. Bode plot of FRD (blue line) and estimated transfer function (asterick red line).

B. Boost Converter Transfer Function Estimation

The boost converter steps up 24 V to 48 V. The sine stream input signal is a series of sinusoids with frequency range 100 kHz to 20 kHz. The proposed model configuration is shown in Fig. 12. The frequency response data is collected and then used to get the Bode plot. The Frequency Response Bode Plot (FRBP) is illustrated in Fig. 13.

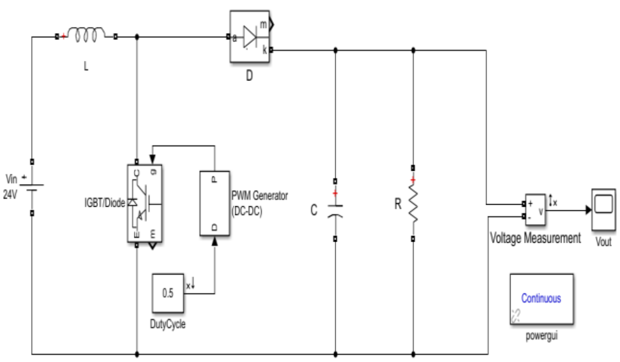

Fig. 11. Boost converter Simulink model.

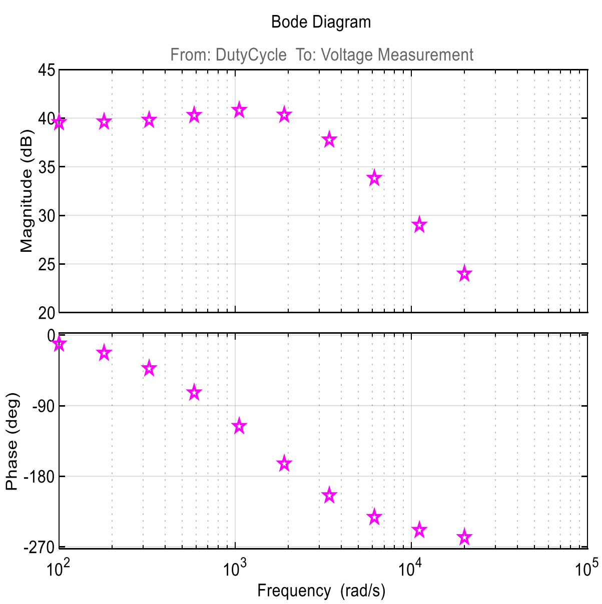

Fig. 12. Frequency response Bode plot of boost converter Simulink model.

The transfer function of boost converter stepping up voltage from 24 V to 48 V is estimated using frequency response data and is expressed as

$$G_{Boost}(s) = \frac{-3.151\times10^5 s + 2.637\times10^8}{s^2 + 3282\ s + 2.789\times10^6} \tag{5}$$

The Bode plot of the estimated transfer function of the boost converter matches exactly to the one obtained through frequency response data (see Fig. 14). This confirms the well-mapping of the frequency response data into the transfer function.

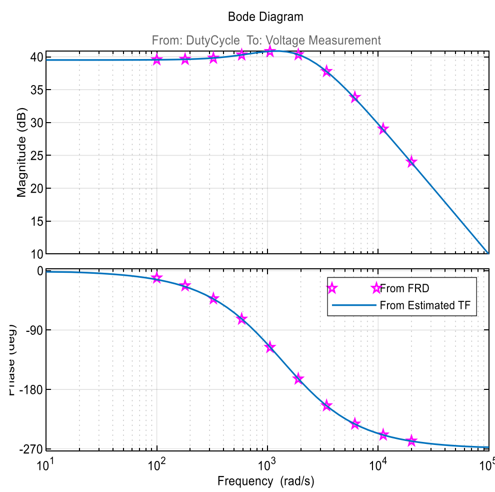

Fig. 13. Bode plot of the FRD (blue line) and estimated transfer function (asterick red line).

C. Buck-Boost Converter Transfer Function Estimation

The buck-boost converter is constructed by amalgamating the principle of both buck and boost converter. The proposed technique is very simple and can be used to linearize all types of plant.

1) Buck-Boost as an Inverting Buck

The Simulink model is illustrated in Fig. 15. The frequency response Bode plot of buck-boost converter is shown in Fig. 16 against the sine stream applied at the duty cycle input.

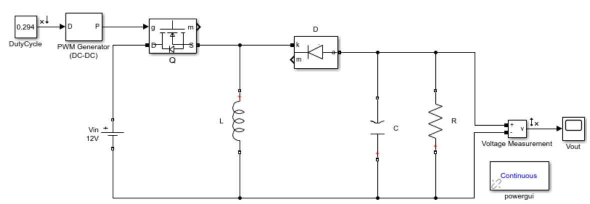

Fig. 14. Buck-boost Simulink model.

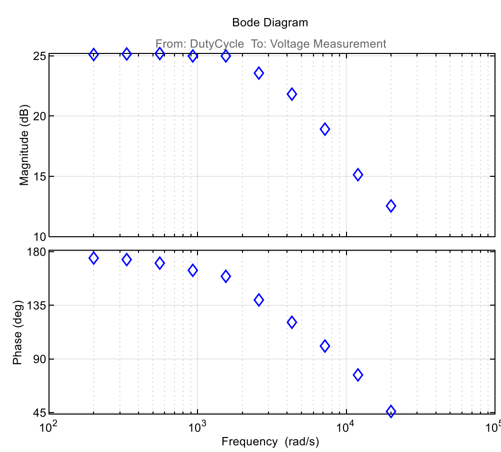

Fig. 15. Frequency response Bode plot of buck-boost Simulink model.

When buck-boost converter acts as buck converter then its duty cycle should be less than 50%. The considered buck-boost converter converts 12 V to -5V using duty cycle of 29.4%. The output displayed by the converter against the sine stream is shown in Fig. 17.

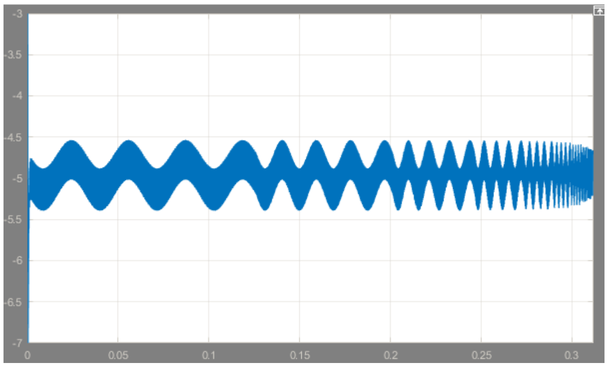

Fig. 16. Output response of buck-boost converter acting as inverting buck.

The estimated transfer function of the buck-boost converter, in case of inverting buck, from FRD is expressed by

$$G_{Buck-Boost}(s) = \frac{1.019\times10^{5}s - 3.64\times10^{9}}{s^{2} + 5.304\times10^{4}s + 2\times10^{8}} \qquad (6)$$

The Bode plot of the estimated transfer function of the buck-boost converter matches exactly to the one obtained through frequency response data (see Fig. 18). This confirms the well-mapping of the frequency response data into the transfer function.

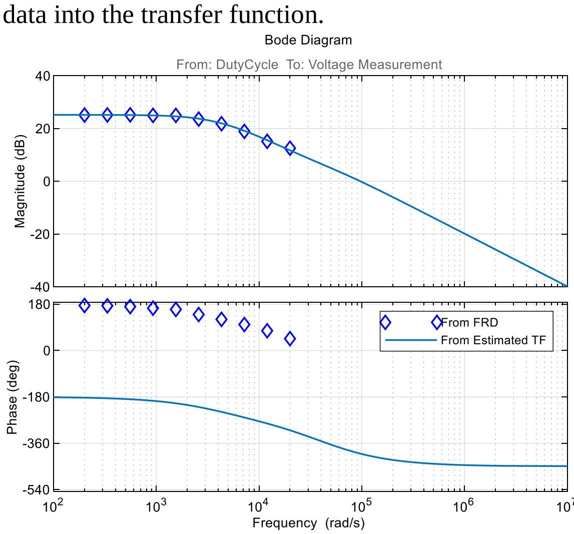

Fig. 17. Bode plot of FRD (blue line) and estimated transfer function (asterick red line).

2) Buck-Boost as an Inverting Boost

The buck-boost converter acts as an inverting boost converter when duty cycle lies between 0.5 and unity (in our case it is 0.7). The Bode plot obtained by FRD is shown in Fig. 19 whereas the output against the sine stream is shown in Fig. 20.

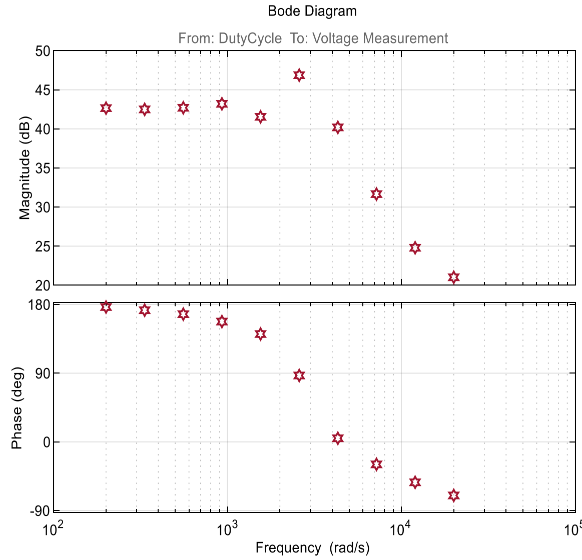

Fig. 18. Bode plot of frequency response data.

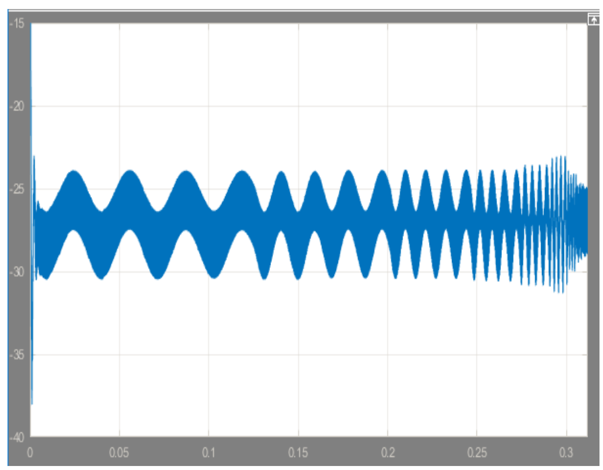

Fig. 19. Output response of buck-boost converter acting as inverting boost.

The estimated transfer function of the buck-boost converter, in case of inverting boost, from FRD is expressed by

$$G_{Buck-Boost}(s) = \frac{1.851\times10^{5}s - 1.081\times10^{9}}{s^{2} + 1985s + 8.747\times10^{6}} \qquad (7)$$

The Bode plot of the estimated transfer function of the buck-boost converter matches exactly to the one obtained through frequency response data (see Fig. 21). This confirms the well-mapping of the frequency response data into the transfer function.

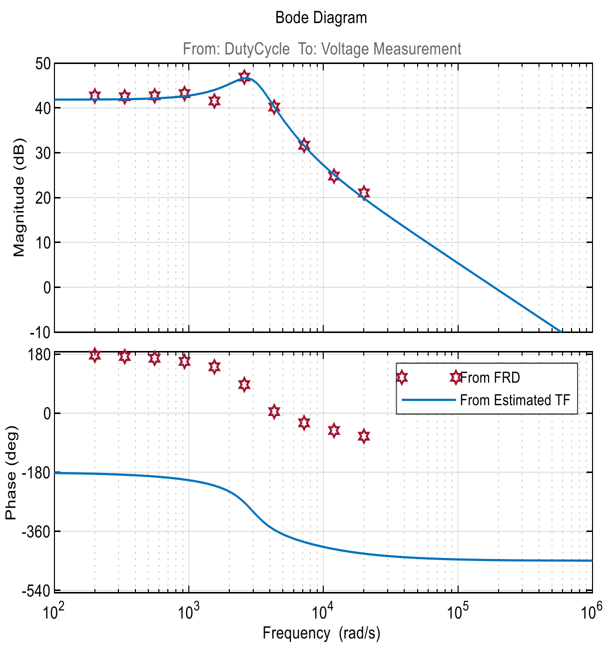

Fig. 20. Bode plot of FRD (blue line) and estimated transfer function (asterick red line).

In summary, the estimated transfer functions of three converters named buck, boost and buck-boost are tabulated in Table II.

TABLE II
ESTIMATED TRANSFER FUNCTIONS OF SWITCHING CONVERTERS

Converter	Estimated Transfer Function
Buck	$G_{Buck}(s)=\dfrac{2.198\times10^{9}}{s^{2}+2975\,s+1.105\times10^{7}}$
Boost	$G_{Boost}(s)=\dfrac{-3.151\times10^{5}s+2.637\times10^{8}}{s^{2}+\ 3282\ s+2.789\times10^{6}}$
Buck-Boost as Inverting Buck	$G_{Buck-Boost}(s)=\dfrac{1.019\times10^{5}s-3.64\times10^{9}}{s^{2}+5.303\times10^{4}s+2\times10^{8}}$
Buck-Boost as Inverting Boost	$G_{Buck-Boost}(s)=\dfrac{1.851\times10^{5}s-1.081\times10^{9}}{s^{2}+1985\,s+8.747\times10^{6}}$

IV. ADDITIONAL SIMULATION RESULTS

For the sake of validating the transfer functions of the converters estimated through proposed identification technique, additional MATLAB/Simulink based simulation results are presented. Open-loop response for the circuits and their estimated transfer functions is observed. From Figs. 22 to 27, it can be observed that the estimated transfer functions show the same step response as that of their circuits from which they are derived. This further validates that the estimated transfer functions well-model the circuits.

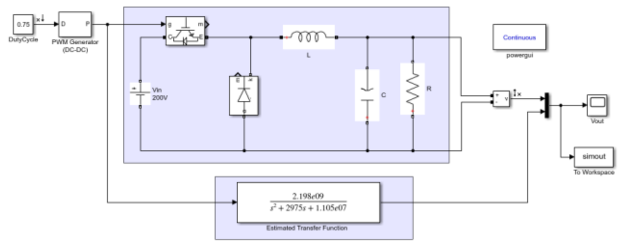

Fig. 21. Simulink model containing buck converter circuit and its estimated transfer function.

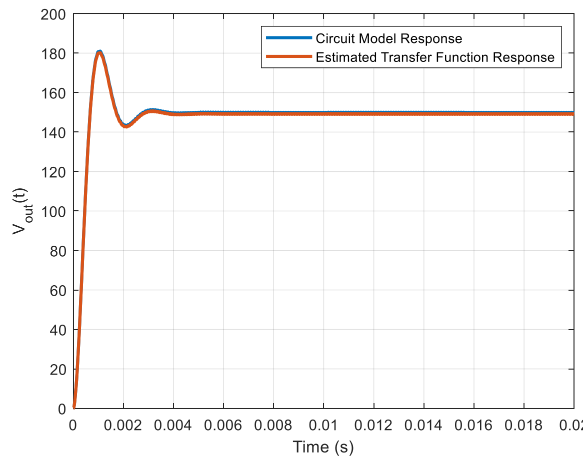

Fig. 22. Response shown by buck converter circuit and its estimated transfer function.

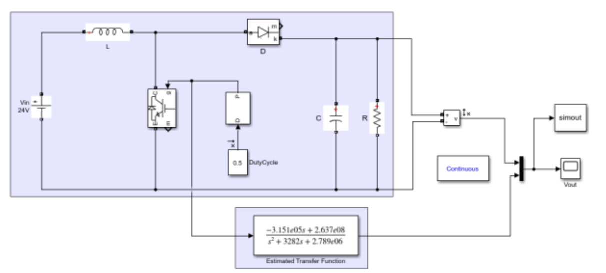

Fig. 23. Simulink model containing boost converter circuit and its estimated transfer function.

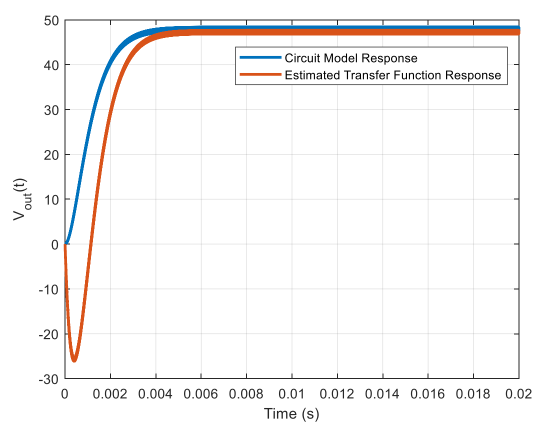

Fig. 24. Response shown by boost converter circuit and its estimated transfer function.

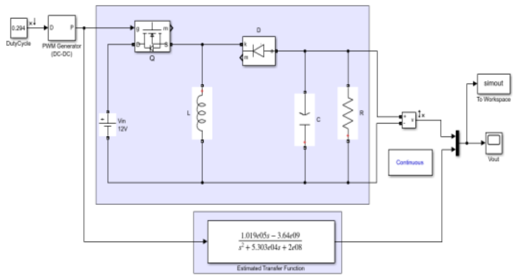

Fig. 25. Simulink model containing buck-boost converter circuit and its estimated transfer function.

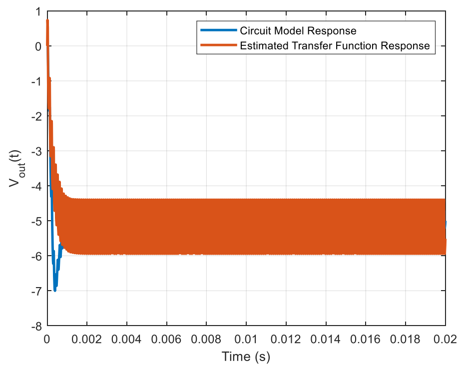

Fig. 26. Response shown by buck-boost converter circuit and its estimated transfer function.

V. Conclusions

In past the non-parametric identification of switching converter has not been discussed in detail. It is due to lack of knowledge about potential of fast frequency response measurement and analysis. Besides this, frequency response measurement requires modern knowledge regarding identification and restriction of practical implementation. Here we have used Sine Sweep Method (SSM) by means of which proposed converters from frequency response data has been identified accurately. Using frequency response estimation technique, the transfer functions of all converters have been identified successfully. The proposed technique is numerically verified and validated in MATLAB Simulink Environment. Cross Correlation method has been used in past to identify the switching converters but it causes error to identification results especially when considering finite length of signal. Now Sine Sweep Method is introduced in this research to nullify the inaccuracies on frequency response measurement. The proposed method can be applied both in development phase and production of switching converters. Here the main critical thing is to select the suitable range of amplitude an applying too much greater value can cause non-linear distortions. In future the controller can be designed to find suitable excitation amplitude about the converter under experiment.

References

[1] Vilkko, Matti, and Tomi Roinila. "Designing maximum length sequence signal for frequency response measurement of switched mode converters." In Nordic Workshop on Power and Industrial Electronics (NORPIE/2008), June 9-11, 2008, Espoo, Finland. Helsinki University of Technology, 2008.

[2] R. M. H. M. Rathnayake, R. Dutta, J. E. Fletcher and D. Xiao, "Torque ripple minimization of an IPMSG with fractional-slot, concentrated-winding using uncontrolled rectifier-connected boost converter control," 2017 20th International Conference on Electrical Machines and Systems (ICEMS), Sydney, Australia, 2017, pp. 1-6.

[3] Schoukens, Johan, Rik Pintelon, Edwin Van Der Ouderaa, and Jean Renneboog. "Survey of excitation signals for FFT based signal analyzers." IEEE Transactions on Instrumentation and Measurement 37, no. 3 (1988): 342-352.

[4] Miao,Botao, Regan Zane, and Dragan Maksimovic. "Practical on-line identification of power converter dynamic responses." In Applied Power Electronics Conference and Exposition, 2005. APEC 2005. Twentieth Annual IEEE, vol. 1, pp. 57-62. IEEE, 2005.

[5] Vanderkooy, John. "Aspects of MLS measuring systems." Journal of the Audio Engineering Society 42, no. 4 (1994): 219-231.

[6] Gawad, Shady, Tao Sun, Nicolas G. Green, and Hywel Morgan. "Impedance spectroscopy using maximum length sequences: Application to single cell analysis." Review of Scientific Instruments 78, no. 5 (2007): 054301.

[7] Xiang, Ning, and Dezhang Chu. "Fast M-sequence transform for quasi-backscatter sonar in fisheries and zooplankton survey applications." In Signal Processing, 2004. Proceedings. ICSP'04. 2004 7th International Conference on, vol. 3, pp. 2433-2436. IEEE, 2004.

[8] Armani, M. E. H., R. M. Dowd swell, P. A. Payne, and K. C. Persaud. "Pseudo-random binary sequence interrogation technique for gas sensors." Sensors and Actuators B: Chemical47, no. 1 (1998): 118-124.

[9] Barkley, Adam, and Enrico Santi. "Improved online identification of switching converters using digital network analyzer techniques." In Power Electronics Specialists Conference, 2008. PESC 2008. IEEE, pp. 891-896. IEEE, 2008.

[10] Miao, Botao, Regan Zane, and Dragan Maksimovic. "System identification of power converters with digital control through cross-correlation methods." IEEE Transactions on Power Electronics 20, no. 5 (2005): 1093-1099.

[11] Miao, B., Zane, R. and Maksimovic, D., 2005. System identification of power converters with digital control through cross-correlation methods. IEEE Transactions on Power Electronics, 20(5), pp.1093-1099.

[12] Miao, Botao, Regan Zane, and Dragan Maksimovic. "Practical on-line identification of power converter dynamic responses." In Applied Power Electronics Conference and Exposition, 2005. APEC 2005. Twentieth Annual IEEE, vol. 1, pp. 57-62. IEEE, 2005.

[13] M. K. Kazimierczuk, “Pulse-Width Modulated DC-DC Power Converters”, Willey, 2nd edition 2015.

[14] Ljung, Lennart. "System identification." In Signal analysis and prediction, pp. 163-173. Birkhäuser, Boston, MA, 1998.

[15] Ljung, L. "System Identification-Theory for the User 2nd edition PTR Prentice-Hall." Upper Saddle River,USA (1999).

[16] Franklin, Gene F., J. David Powell, and Michael L. Workman. Digital control of dynamic systems. Vol. 3. Menlo Park, CA: Addison- wesley, 1998

Pakistan Journal of Engineering and Technology, PakJET
Multidisciplinary | Peer Reviewed | Open Access

Volume: 1, Number: 1, Pages: 29- 34, Year: 2018

Design and Development of a Potato Seed Cutter Machine

Ahmad Shafi*,1, Muhammad Saleem Shuja[1], Hassan Farid Khan[1] and Tauqeer Ahmad Khan[1]

[1]Mechanical Engineering Department, The University of Lahore, 1-KM Defence Road, Lahore, 54000, Pakistan
*Corresponding author: Ahmad Shafi (email: ahmad.shafi@me.uol.edu.pk)

***Abstract*— Potato growers in Pakistan obtain disease free seed from Holland, plant it as spring crop, cutting tubers into few pieces for seed multiplication using manual labor. Keeping in view of extensive labor involved in cutting of potato seeds manually for planting, a simple, efficient and easy to operate mechanical cutter machine powered by 1/2 hp electric motor using eight cam driven reciprocating cutting plungers was designed, fabricated and tested for quantitative as well as qualitative performance. Foreign makes of the seed cutters costs are too high to be purchased. The working capacity of locally made developed fixed cam machine varies between 410-490 kg/hr. For smooth operation, speed reduction of motor from 1450 to 406 rev/min was further reduced to 9.0 rev/min using worm and worm gear assembly. A novel idea to use a fixed cylindrical mild steel cam enhanced the cut pieces tuber seeds production. Machine cutting and manual cutting of potato tubers resulted in 5.0 % and 2.5 % seed damages respectively. A cost comparison of machine cutting versus manual cutting indicated that manual labor for cutting potato tubers is 6.0 times costlier than the mechanical cutter.**

***Index Terms*— Cylindrical Cam; Potato Seed cutter; Seed damage; Worm and worm gear assembly.**

I. INTRODUCTION

Potato by virtue of its inherent potential for tonnage production, remunerative income and food values, has been highly esteemed as a food as well as cash crop. Potato has been an important food crop for growers and consumers not only in Pakistan but all over the globe. It is a crop that can generate high production and more income with more nourishing value. It attained its high rank among the most important crops due to its high volume of production and benefits. Its high returns attract the farmer to cultivate more and more. Globally it is playing a key role in food security and rising as a big source against hunger. It is assuming that one day it will be a leading crop and the hunger from the earth will be eaten by it [1].

Last decade has a two fold increase in area under potato cultivation in Pakistan. Total area for spring, autumn and spring crops amount to 179.30 thousand hectares with a total production of 3,849.5 thousand tons in Pakistan [2]. Potato has played a significant role in human diet as supplement to Wheat and Rice and it has found to produce more food per unit area than the cereals [3]. Being a short duration and high yielding crop, potato can feed more people per unit area and significantly help improving the food situation in Pakistan. The present per hectare yield of 10.50 tons is considerably low against 25-40 tons obtained in the main potato growing countries [4]. A low production per unit area in Pakistan can be attributed to the non-availability of disease free and certified seed of high yielding potato varieties and poor agronomic practices.

Buchele's second law of machine [5] stated that mechanization of any process of production results in surplus. Thus, if more production of any item is desired, the process of its production should me mechanized.

Presently, farmers in Pakistan are growing three crops, namely spring and autumn crop in plains and a summer crop in hilly areas. Growers obtain diseases free seed from Holland, plant it as spring crop, cutting tubers into few pieces manually for seed multiplication. Seed rate of potato planting ranges from 2.0 tons/hectare to 3.5 ton/hectare. For spring crop 60-80 gram potato is cut into two pieces, 80-100 grams is cut into three pieces and 100 grams and above is cut into four pieces. Small size is planted without cutting. It should be noted carefully, that each cut Generally 25-30 potato crates, 50 kg each are required for planting a hectare [4], (see figure 1). Each crate takes 1-2 man hours to be cut into desirable pieces. Thus seed for a hectare requires up to 60 man hours for cutting it. Labor problem aggravates further and assumes alarming dimensions as the area to be planted per day increases. In view of extensive manual labor involved in cutting of potato seed, there was a dire need to design and develop a machine that could efficiently cut potato seed and reduce the manual labor involved in potato planting [6].

Figure 1 Potato crates of imported hybrid seed

The present study was planned to design and develop a machine (see figure 2) using local materials and workmanship for mechanical cutting of potato tubers into desirable pieces and to test the machine for its performance.

Figure 2 Potato seed cutter machine

II. Design and Development of Machine Cutter

In the light of literature reviewed, the seed cutter machine was conceived. This machine was powered through a small electric motor of 1450 rev/min. For reducing speed of motor (M) to about 9.0 rev/min at the shaft S, a two-step reduction was planned viz; using pulleys (P1), (P2) and worm and worm gear mechanism W&W (see figure 3).

The shaft passes through plates D, J, L and cam C. The plate D would hold pockets to accommodate potatoes to be cut. The plates J & L would hold plungers restricting their movement in the horizontal plane. The cylindrical cam C is stationary, whereas plates J, L and D would rotate with the shaft at approximately 9.0 rev/min. The plungers would move up and down cutting potatoes at the bottom dead center position of the stroke (see figure 3).

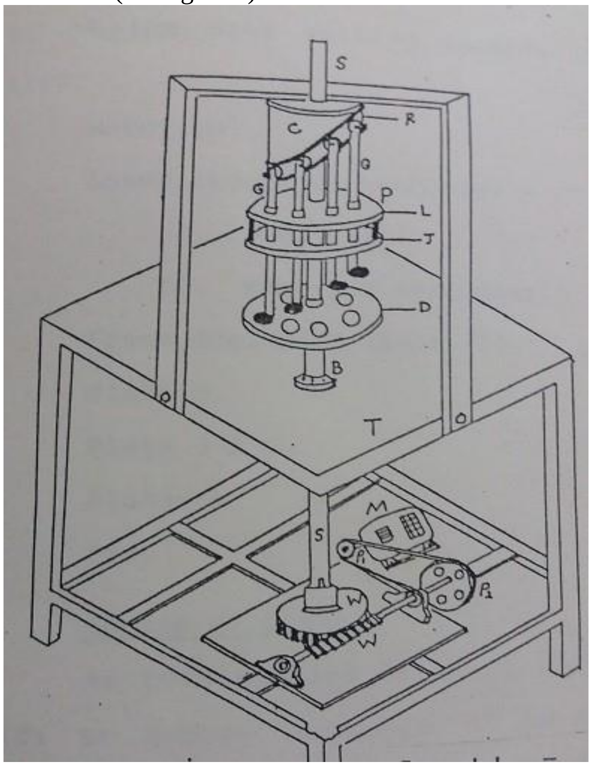

Figure 3 Isometric view of Potato seed cutter

Where P = Plungers, C= Cylindrical Cam, M = Motor P1 & P2 = Motor and Worm pullies, W&W = Worm and worm gear, T = Feeding/ Discharge table,
D = Pocket plate, S = shaft, J & L= Plungers holding plates.

III. Development of Different Parts of Potato Seed Cutting Machine

A. Source of Power

As this machine is to be operated in agricultural field at remote locations of farms, tractor would be an appropriate source of power for the machine. However, for villages where electricity is available a laboratory model, a single phase 1450 rev/min, ½ hp AC motor was considered appropriate.

B. Pulleys and V-belt selection for seed cutter

A single, heavy duty A-size, V-belt for minimum small sheave motor pulley dia. of 2.75 inch was appropriate. A 10.0 inches large sheave pulley was selected to transmit motor power to run worm shaft of 1.50 inch. The length measured of outer periphery of belt was 53.0 inches. Specifications of pulleys and belt are shown in figure 4.

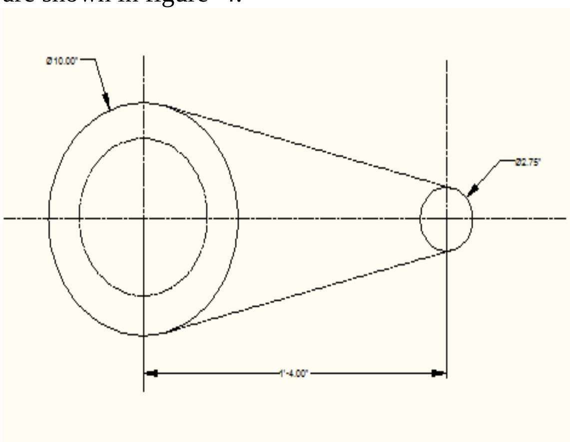

Figure 4 Specifications of machine small and large sheave pulleys.

C. Design of speed reduction mechanism

The speed of 1450 rev/min motor powering the unit was reduced in two steps. Firstly the ratio of the diameters of pulleys were so selected to cut down the speed to 406 rev/min.

$$N_m D_m = N_w D_w \qquad [7]$$

Where:

N_m = Motor speed, (1450 rev/min)

D_m = Dia. of motor pulley (2.75 in)

N_w = Speed of worm, rev/min

D_w = Dia. of worm pulley (10 in)

$$N_w = \frac{1450 \times 2.75}{10.0} = 406 \text{ rev/min}$$

This speed of 406 rev/min was further reduced by selection of worm and worm gear assembly. If speed reduction is 48:1, then it was found that output speed of worm gear was about 9.0 rev/min. Single threaded worm with 50 worm gear teeth was developed for better performance giving speed of worm shaft equal to 8.45 rev/min as shown in figure 5.

D. Fabrication of Main Frame

Development of the Main frame consisted of the reduction mechanism at lower end and feeding, cutting and discharging mechanism at the top, is a table of (30 in x 36 in x 32 in) made of hollow rectangular square section pipes of (1 in x1.82 in) dimensions. This table has sufficient stiffness to carry machine load and rotating parts. A rectangular steel plate of thickness 1/16 in is screwed at the top of the table for feeding and discharging access.

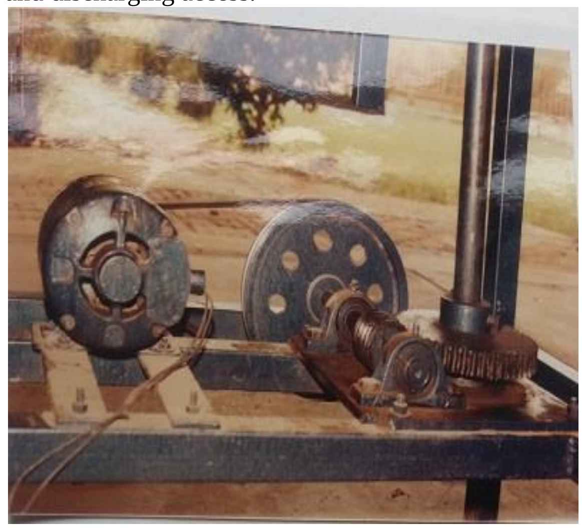

Figure 5 Worm and worm gear assembly

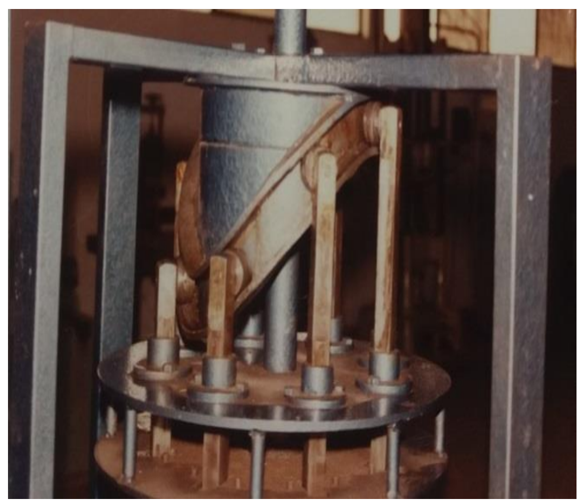

Figure 6 Cylindrical cam holding cutting plungers in vertical plane

E. Design of Cylindrical Cam

The most challenging feature of the machine was the design and fabrication of a cam required to bring about reciprocating motion of cutting plungers in the vertical plane (see figure 6). Several cam motions were studied. In any mechanism, usually a cam is a part which rotates and follower (plunger) is a part which reciprocates doing useful work. However, the nature of the work here was, cutting and discharging of cut seeds should be done at the same time. In this machine the cam is fixed but plungers move up and down 6.0 inches and rotate simultaneously. This problem was solved with the selection of cylindrical cam having groove in the outer periphery of the cam. Another

problem while designing cam was solved by careful consideration, it was decided that for some portion of the cam there should be no up and down motion of the plungers i.e. dwell. This dwell time of rotation was safely used as hand feeding time, at the point when fall of plungers is completed smoothly after the seeds has been cut. The groove shown in the unwrapped cylinder will give the roller follower the proper rise of 6 inches when cut into the actual cylinder.
Plungers are to be moved upward 6 inches up to 90 degrees, dwell for 180 degrees and then falls 6 inches with Simple harmonic motion (S.H.M). Front view of developed cam and plungers is shown in figure 7.
Initially mild steel cutting blades were used. Cutting action was not fine rather crushing due to larger thickness of the blades. Surface pitting and rusting of mild steel blades was observed. Therefore mild steel blades were replaced with 1/32 inch thick stainless steel blades. Due to smaller thickness and desirable materials, cutting of seeds was accomplished without visible sign of crushing. Similarly pitting and rusting of blades became obsolete. In order to overcome crushing of the cut pieces, rubber disks each ¼ inch thick were glued to the lower ends of ½ inch disks. Grooves were also arranged in the rubber disks. The grooves of both the steel and rubber disks were aligned properly.

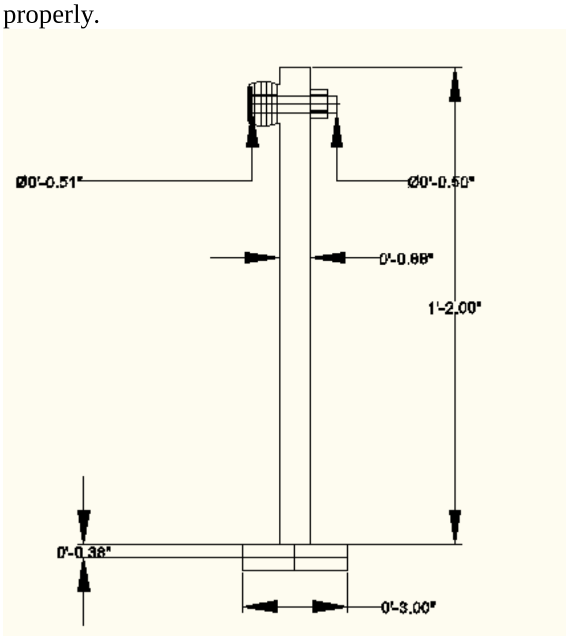

Figure 7 Cam and plunger assembly cutting blades

F. Feeding System of potatoes tubers

In the model conceived the potatoes are manually fed into pockets at a point where plunger is at the top dead center position. As the 1.5 inch round center shaft moves at 9.0 rev/min with 8.0 plungers moving up and down and rotating simultaneously in the cam groove, the number of potatoes to be fed manually stand 72.0 per minute. The top of the table is used as feeding platform. The height of the table is so selected that it is comfortable for standing person. Potatoes cut into pieces during operation are delivered under the bottom dead center position of plungers on the table.

G. Materials used for fabrication of different parts of machine

Following materials and working summary for fabrication of potato seed cutter were used for different parts (see table 1). After the development and fabrication of the machine, it was decided to undertake testing for quantitative as well as qualitative performance of the machine as whole and /or its parts individually.

Table 1 Summary of potato seed cutter Materials specifications and working details

No.	Parts	Materials	Working details
1	Pulleys	Cast Iron	Driven by A-size V-belt
2	Center shaft	1.50 inch Mild steel	clockwise Rotation
3	Worm and worm wheel	Carbon steel	Speed reduction ratio of Worm and worm gear, 48:1
4	Plunger Rods	Mild steel ¾ inch square bars	Eight cam driven cutting plungers with rotary and reciprocating operation
6	Main Frame	Pressed steel rectangular hollow X-section	Welded and screwed
7	Cylindrical Cam	Mild steel	plate of 1/8 inch thickness configured to the cylindrical shape for 6 in. rise and fall
8	Roller and thrust Bearings	High carbon steel	Universal type to withstand radial as well as axial thrust
9	Capacity		0.5 tons cut seeds/hr.
10	Motor	NEEMA standard	Single phase, 50 cycles, 0.5 hp,

			1425 rev/min, 220-240 V and 2.7 amp.
11	Cutting		Continuous
12	Feeding, Discharge		Manual semi-automatic

H. Testing and Working capacity of the machine

An important feature of the machine is its output capacity that was the weight of the cut pieces discharged per unit time. In order to determine output capacity of machine, it was operated for three complete revolutions by feeding potato tubers in each cup and the output of cut pieces at the discharge end was weighed. This was repeated 10.0 times. As the machine was moving at a speed of 8.75 rev/min totaling into 525 rev/hr., thus the discharge (kilograms of cut pieces) at the end of each 3 revolutions was multiplied with 175 to provide machine's output in kg/hr as given in figure 8.

The mean capacity of machine approximated 450kg/h with a standard deviation (STDEV) of 12.38. This suggests that the machine capacity would be 438-462, 425-475 and 413-487 kg/h for 66 %, 95% and 99 % of the times, respectively. It can be generalized that the capacity varied 410-490 kg/h approximately. A larger variation in the capacity resulted from variation in the sizes of the tubers.

In order to properly conceive the variations in machine's capacity potato size distribution was also studied. Potatoes were randomly picked from the lot, weighed and their volumes determined in a graduated cylinder having water. The data are given (figure. 9).

It is obvious from the mean/volume and their standard deviation (STDEV) that the variation in size of tubers is considerable. A wide variation in size of potatoes explains the variation in machine capacity. This variation also suggests that single size pockets may not be desirable to accommodate all sizes of potatoes.

Thirty pieces of cut pieces were randomly picked from each of the lots cut by machine and manual labor. All the pieces were weighed individually. Unpaired T-test was employed to test significant differences in the two means. The results revealed that the difference between the means was insignificant cleared suggested that the machine and manual cutting operations were similar as regards the uniformity of cut pieces. This reflects well on the precision of machine operation, that is, the distribution of sizes of cut pieces is same both in machine and manual cutting being viable. These losses are chances occurrences which can be seen even in the manual cut lot where the damage was up to 2.5 %.

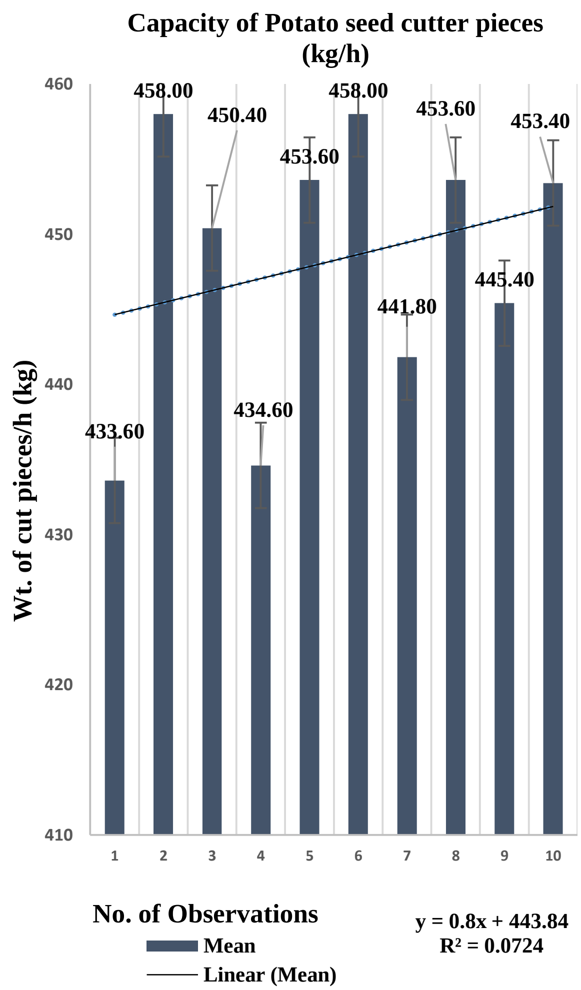

Figure 8 Working Capacity of Machine

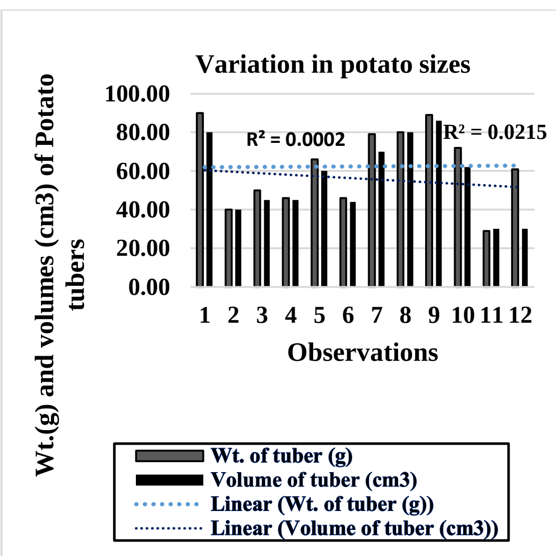

Figure 9 Variation in potatoes sizes

IV. RESULTS AND DISCUSSION

Cost of manual cutting, 450 kg potatoes = Rs. 680/hr.

$$\text{Cost ratio} = \frac{\text{Cost of manual cutting}}{\text{Cost of machine cutting}} = \frac{818.00}{131.79} = 6.206$$

It is clear from the cost of operation/h calculations that the manual cutting is approximately 6.0 times costlier compared with machine cutting of potato seeds. Naturally the initial investment of Rs. 1, 00,000 on the machine is a discouraging factor for the farmer. However, it may be remembered he will be saving about Rs.3650/acre if he will be using the machine. The farmer may recover the cost of machine after planting 60.0 acres. In addition to the considerable cost savings, the farmer using the machine may avoid the management and supervision of labor. Above all he can avoid delayed planting which generally results in poor yield. Thus the machine/mechanical cutting of potato seeds brings with it fringe benefits.

Table 2 Cost analysis of machine

Cost Analysis of Machine			
Sr. No.	First Cost of Machine	Rs. 1,000,00	Cost (Rs.)/h
1.	Salvage value (10% of first cost for most of agricultural machines [8] [9] [10]	Rs. 10,000	
2.	Life in years	10 Years	
3.	Expected hours of operation/year	500 hrs.	
4.	Total life of machine	5000 hrs.	
5.	Working capacity of machine	450kg/hr.	
6.	Lubricants/year	7.0 L	2.0
7.	Taxes, insurance and shelter expenses	Negligible for the seed cutter	Nil
8.	Depreciation	$= \frac{\text{First cost-salvage}}{\text{Life in hrs.}}$ $\frac{1,000,00-10000}{500}$	180.0
9.	Repair and maintenance cost	10 % of first cost $= \frac{10,00,00 \times 10}{5000 \times 100}$	2.0
10.	Interest rate	(14% of first cost/year) $\frac{1,000,00 \times 14}{500 \times 100}$	28.0
11	Labor cost	Rs. 500/labor / day $= \frac{500}{8}$	62.50
12.	Energy cost 1/2 hp motor	= (0.373 kW x 1.0 hr.) 0.373 kWh x 16	5.968
13	Overhead cost	(50% of labor) = 62.50/2	31.25
14.	Total cost of operation per hour for cutting 450 kg potato seed	= Sum of serial Nos.(6+9+10+11+12+13)	131.718

REFERENCES

[1] N. A. Memon, "*Potato: An important food crop in Pakistan*," 2017.

[2] "Pakistan Economic Survey, Ministry of Finance, Government of Pakistan," 2016-17.

[3] M. Akhtar, "*Vegetables of Punjab*" Department of Agriculture, Government of Punjab, 1987.

[4] H. A. Chaudhry, "*Potato Planting in Punjab*" Department of Agriculture, Punjab Agriculture Bureau, Lahore, 1988.

[5] W. F. Buchele, "*Lecture notes on Creativity*" Department of Agricultural Engineering, Iowa State University, Ames Iowa, 1985.

[6] W. F. Talburt, O. Smith, "*Potato Processing*" 3(4): pp. 67-127. The AVI. Publishing Company, Inc., Westport, Connecticut, 2013.

[7] D.W. Dudley, "*Handbook of practical gear design*" Dudley Engineering Co. McGraw-Hill Book Company, New York, 1984.

[8] R.A. Kepner, R. Bainer and E.L. Barger, "*Principles of Farm Machinery*" 3rd Edition. Avi. Publishing Company, INC. West port, Connecticut, 1978.

[9] D. Hunt, "*Farm Power and Machinery Management*" 8th Edition, Iowa State University Press, Ames, Iowa, 1983.

[10] M. F. Finner and R. J. Straub, "*Farm Machinery Fundamentals*" 2nd Edition. American Publishing Co. 2909, Syene Road Madison, Wisconsin 53713, 1985.

Pakistan Journal of Engineering and Technology, PakJET
Multidisciplinary | Peer Reviewed | Open Access

Volume: 1, Number: 1, Pages: 35- 39, Year: 2018

The Role of Value Stream Mapping (VSM) as an Integrated Approach in Lean Manufacturing

Muhammad Zeeshan Rafique[*,1], Atif Ilyas[1], Khazar Hayat[1] and Iqbal Hussain[1]

[1]Mechanical Engineering Department, The University of Lahore, 1-KM Raiwind Road, Lahore, 54000, Pakistan
*Corresponding author: Muhammad Zeeshan Rafique (email: zeeshan.rafique@me.uol.edu.pk)

***Abstract*— Leanness in Lean Manufacturing mainly leads to the elimination of non-value added activities named as wastes and there are many strategies available to tackle these wastes. Lean implementation is one of the renowned strategy which utilizes lean implementation tools (to detect and reduce wastes) like Value Stream Mapping (VSM) which is one of the most common tool. It has been observed that VSM has many different types and each type is specific to attain some certain wastes affecting but most of the time the utilization of traditional VSM has been observed regardless of studying its different types and their specific utilization. In order to fulfill this gap, the aim of this research is to study different types of VSM and their utilization for specific wastes. A state of art literature review based methodology has been utilized and the results attained clearly states that, the most common types of VSM available for lean manufacturing are process activity mapping, Production Variety Funnel, Quality Filter Mapping, Demand Amplification Mapping, Decision Point Analysis, Supply Chain Response Matrix and Physical Structure Mapping which are feasible to handle wastes like over transportation, over processing, over defects, over inventory, over production and over waiting based on their tool origin respectively. Moreover, it has been observed that the type physical structure mapping is not carrying ability to tackle wastes but helpful to improve physical structure. The contribution of this research is the development of integrated approach regarding types of VSM in relation with wastes affecting manufacturing sector**

Index Terms*— *Lean Manufacturing; Wastes; Value Stream Mapping (VSM); VSM Types: VSM integration

I. INTRODUCTION

Lean manufacturing is an important technique in industrial firms due to its capability to decrease wastes and to improve operations of any manufacturing industry [1]. Japanese initially used Lean after the World War II, when their economy was severely collapsed because of business decline. Consequently, car production was badly affected even of Toyota, which is a top car manufacturing company. This bad condition of economy prevailed when a large number of unsold cars have to be kept in inventory and furthermore there was a huge drop in the demand of cars [2]. Company was unable to launch its new-modelled cars in market under these conditions caused by financial limitations as well as space limitations because of already present a large number of unsold cars in stock [3],[4]. Under these circumstances, Toyota production manager, Taichii Ohno decided to take up an initiative and made a new production plan for the company termed as "Toyota Production System (TPS)". This TPS system has been further adopted by the United States (US) manufacturing industries and production plan was able enough to emphasis on what is the demand instead of producing cars on massive scale [5]. Afterwards, the introduction about the wastes affecting system has been introduced by Taichii Ohno [6],[7].

Afterwards, when the book named as the "The Machine that Changed the World" written by Womack and Jones [8] has further stairs the manufacturing industries of United States (US) to adopt TPM ideology in their manufacturing operations. They further called this ideology as Lean Manufacturing (LM). Subsequently, the Krafcik [9] in their investigations and study during their research explained the term lean as an effort to minimize to produce less (according to order) than mass production. Nevertheless, the final and perfect definition of lean is still not finalized because of its extreme vast scope [10] but it has been observed that the lean concept has been speeded drastically when the US has adopted this ideology in their manufacturing operations and originated the requirement of study of lean tools for lean implementation.

II. LITERATURE REVIEW

i. Wastes Affecting Lean Manufacturing (LM)

Waste is something, which is not adding value to any operations [11]. The agenda of lean implementation is the waste reduction to attain value added operations for the customers [12]. Keeping in view of internal and external customers, the value added activities are the positive activities for any operation and worth paying for both type of customers [13]. Regarding this perspective of adding values in ongoing operations, many researchers have followed different ideologies to reduce wastes [8] [14] [15] [16] [17] [18] but Taiichi Ohno has considered as the forger in this matter who had primarily noticed and explicated the wastes to the industry and the research world. [14].

It has been observed that the origination of wastes is utterly dependent on the manufacturing process involved in any system and its application on the required regime, but the Taiichi Ohno, who is one of the Lean Guru has been successful to generalize the wastes into seven different types as mentioned below [12] [14] [19] [20].

1) Over motion
2) Over production
3) Over inventory
4) Over defects
5) Over processing
6) Over waiting
7) Over transportation

ii. Lean Implementation Tool Types

In accordance to previous researches regarding the lean tools clearly states that the lean tools are highly beneficial and adoptable [21] because of their abilities like detection and minimization of wastes affecting any manufacturing system. Moreover, it has been observed that there is one tool named as Value Stream Mapping (VSM) whose benefits and ways to adoption has been introduced by many researchers but the credit goes to Rother and Shook [22], as they had clearly explained the way to how to utilize a lot of lean tools in one combination.

Subsequently, Bhuiyan, et al. [23] and Melton [24] in their research studies have emphasized some of the other lean implementation tools like Kanban, visual control, mistake proofing, 5S and Poka yoke and afterwards, There are some tools like Total Preventive Maintenance (TPM), Business Process Reengineering (BPR), Taguchi, Kaizen, agile manufacturing, Single Minute Exchange of Dies (SMED), Poka Yoke and Just In Time (JIT) which have been utilized and explained by Ahmad and Benson [25]. The most common types of lean implementation tools are:-

1) Value Stream Mapping (VSM)
2) 5s Just in Time
3) Visual management
4) 5s
5) Kanban
6) One-piece flow
7) Single minute exchange of dies
8) Kaizen
9) Cellular manufacturing
10) Total productive maintenance(TPM)
11) Poka yoke
12) Line balancing

It has been observed that all of the mentioned tools are not only helpful to implement lean but also helpful to improve operations in any manufacturing industry [26]. Moreover, some of the researchers Pavnaskar, et al. [27], Karim and Arif-Uz-Zaman [28] and Elnadi [29] has given an observation that the selection of tools is entirely dependent on the type of cause effecting the system and there is no clear methodology regarding the tools selection.

Pavnaskar, et al. [27] and Amin and Karim [33] in their research study has clearly confirmed that, as the dimensions and the orientations of each tools is entirely dependent on its ability and capability to how to minimize wastes and the problems affecting in manufacturing industry. Hence, there seems to be no certain exact technique to link lean implementation tools in one loop and mold them to utilize in a group. Srichuachom [34] in his research study has tried to utilize some of these tools in combination.

In order to understand the flow of any process, according to Esfandyari, et al. [30] and Esfandyari [26], VSM is considered as one of the excellent and the most basic tools, because, it carries the abilities to detect issues and problems in any ongoing operations by drawing the flow process. Moreover, since, the VSM has also the capability to utilize combination of tools like Kanban, Kaizen, cellular manufacturing, Takt time, JIT and many more during the formation of future state map, so this ability of VSM further increases its worth among the other tools available [22]. Subsequently, it has been observed that Anand and Kodali [31] in their research study have developed a list of lean tools which they have further subdivided into different groups, Eswaramoorthi, et al. [32] in

Table I
VSM tool types

Sr. No	Name of Tools	Tool Description
1	Decision Point Analysis	Moderate to tackle over production, over waiting & over inventory and low capable for over processing
2	Supply Chain Response Matrix	Highly helpful to tackle over waiting and over inventory. Moderate to tackle over production and low capable for over motion
3	Quality Filter Mapping	Moderate to tackle over defects and low capable for over production and processing
4	Demand Amplification Mapping	Highly helpful to tackle over inventory. Moderate to tackle over production and over waiting
5	Production Variety Funnel	Moderate to tackle over processing and inventory and low capable for over waiting
6	Process Activity Mapping	Highly helpful to tackle over transportation, over waiting, over motion, over processing. Moderate to tackle unnecessary motion and low capable for over production
7	Physical Structure Mapping	Highly capable to improve physical structure and low capability for waste detection

their study recommended 36 different lean tools as per their application in machinery tool industry.

Source: Hines and Rich [20], Ramesh and Kodali [41] and Rafique [11]

III. METHODOLOGY

A literature review based methodology has been utilized in this section to get an idea about requirement of selection of Value Stream Mapping (VSM) as a selected Tool. VSM is a concept of drawing or mapping things from raw material to customer in the form of material and information flow. VSM is helpful to differentiate between non-value added and added activates and to understand the flow of any process [3] [35].

Rother and Shook [22] mentioned in their book that VSM is inclusive of current and future state map to explain and improve the complete process of manufacturing and carries a common language inclusive of icons and symbols that is helpful to understand among experts related to VSM [36]. Moreover, Serrano Lasa, et al. [37] states and considered future state map as an complete package for lean implementation which involves lean implementation tools like kaizen, pull system, pace-maker process and Takt time and marks the VSM as a top leading tool and contributor regarding lean implementation among manufacturing processes. Moreover, Abdulmalek and Rajgopal [38] also seconds this ideology.

So, authors of this research study have no doubt to say about VSM as an excellent approach which not only emphases on the wastes elimination but also an modelling tool to study current and future situation on any manufacturing industry [26].

IV. RESULTS & DISCUSSION

VSM is an approach, which involves the study of current manufacturing operations and the formation of future state map to improve the current situation by reducing wastes affecting system and ongoing process improvements. VSM is inclusive of different types (as mentioned in Table 1) named as decision point analysis, process activity mapping, product variety funnel, supply chain response matrix, quality filter mapping, physical structure mapping and demand amplification mapping, and demand amplification mapping based on the mode of application regime and origin of tools [20] [41] [42].

Hines and Rich [20] further explained that the none of the VSM type carries the ability to tackle all types of wastes involved in process. In fact, out of seven different types of VSM available and as mentioned in Table 1, each VSM tool can cope each certain wastes and some of the other wastes involved in the system but not all types of tools as motioned in previously. Moreover, Pude, et al. [43] and Ramesh and Kodali [41] have mentioned in their studies that for the case of manufacturing, out of these seven tools, the best tool that serves the need in term of process flow is the process activity mapping as compared to the basic VSM.

However, basic VSM involves the generation of flow of material and time, which is highly feasible to study deep down ongoing operations and helpful to detect the unknown wastes affecting the system. Ramesh and Kodali [38], Vinodh, et al. [44] and Mostafa, et al. [45] and some of the other researchers have seconds that the basic VSM is more feasible and preferable for the formation of wastes detection and current state map. However, the types of VSM like process activity mapping, Production Variety Funnel, Quality Filter Mapping, Demand Amplification Mapping, Decision Point Analysis, Supply Chain Response Matrix and Physical Structure Mapping, which are feasible to handle wastes like over transportation, over processing, over defects, over inventory, over production and over waiting based on their tool origin respectively.

Moreover, it has been observed that the type physical structure mapping is not carrying ability to tackle wastes but helpful to improve physical structure. But for the cases where the wastes need to be detected and the ongoing plant operational study is required for problem detection, then in such cases the basic VSM study is the most appropriate option.

V. CONCLUSION

The research clearly concludes that VSM is one of the very powerful tool for lean implementation. And it has been observed that in order to handle wastes like over transportation, over processing, over defects, over inventory, over production and over waiting, the type of VSM tools like process activity mapping, Production Variety Funnel, Quality Filter Mapping, Demand Amplification Mapping, Decision Point Analysis, Supply Chain Response Matrix and Physical Structure Mapping are helpful to handle respectively. Additionally, it has been observed that among these different types of VSM, there is one type named as Physical Structure Mapping which is not feasible to tackle wastes and in fact, more feasible to improve physical strengths. In last, the strength of this research is the conceptualization of tactic through previous literature, which will help the future researchers to understand the integration between the wastes types and types of VSM with a limitation of reliability on the previous research.

REFERENCE

[1] J. Moyano-Fuentes and M. Sacristan-Diaz, "Learning on lean: a review of thinking and research," *International Journal of Operations & Production Management*, vol. 32, pp. 551-582, 2012.

[2] M. Holweg, "The genealogy of lean production," *Journal of operations management*, vol. 25, pp. 420-437, 2007.

[3] J. P. Womack and D. T. Jones, *Lean thinking: banish waste and create wealth in your corporation*: Simon and Schuster, 2010.

[4] J. M. Nicholas, *Competitive manufacturing management: continuous improvement, lean production, customer-focused quality*: McGraw-Hill/Irwin, 1998.

[5] L. H. Forbes and S. M. Ahmed, *Modern construction: lean project delivery and integrated practices*: CRC Press, 2010.

[6] S. Bertelsen, "Lean Construction: Where are we and how to proceed," *Lean Construction Journal*, vol. 1, pp. 46-69, 2004.

[7 P. Fewings, *Construction project management: An integrated approach:* Routledge, 2013.

[8] J. P. Womack and D. T. Jones andDanielRoos, The Machine that Changed the World, ed: New York, NY: Macmillan Publishing Company, 1990.

[9] J. F. Krafcik, "Triumph of the lean production system," *MIT Sloan Management Review*, vol. 30, p. 41, 1988.

[10] M. Bayou and A. De Korvin, "Measuring the leanness of manufacturing systems—a case study of Ford Motor Company and General Motors," *Journal of Engineering and Technology Management*, vol. 25, pp. 287-304, 2008.

[11] M. Z. Rafique, "A framework for RFID technology combined lean implementation in automotive parts manufacturing industry," PhD Thesis, mechanical, UKM, Bangi, 2017.

[12] S. Taj, "Lean manufacturing performance in China: assessment of 65 manufacturing plants," *Journal of Manufacturing Technology Management*, vol. 19, pp. 217-234, 2008.

[13] C. Karlsson and P. Ahlstrom, "Assessing changes towards lean production," *International Journal of Operations & Production Management*, vol. 16, pp. 24-41, 1996.

[14] T. Ono, *Toyota production system: beyond large-scale production.* Productivity press, 1988.

[15] J. Liker, *The Toyota way: 14 management principles from the world's greatest manufacturer,* McGraw-Hill. Retrieved November, vol. 6, p. 2011, 2004.

[16] B. Singh, S. Garg, S. Sharma, and C. Grewal, "Lean implementation and its benefits to production industry," *International journal of lean six sigma*, vol. 1, pp. 157-168, 2010.

[17] R. Sawhney, K. Subburaman, C. Sonntag, P. Rao Venkateswara Rao, and C. Capizzi, "A modified FMEA approach to enhance reliability of lean systems," *International Journal of Quality & Reliability Management*, vol. 27, pp. 832-855, 2010.

[18] R. Victor B. de Souza and L. Cesar R. Carpinetti, "A FMEA-based approach to prioritize waste reduction in lean implementation," *International Journal of Quality & Reliability Management*, vol. 31, pp. 346-366, 2014.

[19] R. G. Askin and J. B. Goldberg, *Design and analysis of lean production systems*, John Wiley & Sons, 2007.

[20] P. Hines and N. Rich, "The seven value stream mapping tools," *International journal of operations & production management*, vol. 17, pp. 46-64, 1997.

[21] O. Alaskari, M. M. Ahmad, and R. Pinedo-Cuenca, "Development of a methodology to assist manufacturing SMEs in the selection of appropriate lean tools," *International Journal of Lean Six Sigma*, vol. 7, pp. 62-84, 2016.

[2 2] M. Rother and J. Shook, *Learning to see: value stream mapping to add value and eliminate muda*: Lean Enterprise Institute, 2003.

[23] N. Bhuiyan, A. Baghel, and J. Wilson, "A sustainable continuous improvement methodology at an aerospace company," *International Journal of Productivity and Performance Management*, vol. 55, pp. 671-687, 2006.

[24] T. Melton, "The benefits of lean manufacturing: what lean thinking has to offer the process industries," *Chemical Engineering Research and Design*, vol. 83, pp. 662-673, 2005.

[25] M. Ahmad and R. Benson, Benchmarking in the process industries: IChemE, 1999.

[26] A. Esfandyari, "Reducing production lead time through value stream mapping," MS.c Thesis, Universiti Putra Malaysia, Malaysia, 2008.

[27] S. Pavnaskar, J. Gershenson, and A. Jambekar, "Classification scheme for lean manufacturing tools," *International Journal of Production Research*, vol. 41, pp. 3075-3090, 2003.

[28] A. Karim and K. Arif-Uz-Zaman, "A methodology for effective implementation of lean strategies and its performance evaluation in manufacturing organizations," *Business Process Management Journal*, vol. 19, pp. 169-196, 2013.

[29] M. Elnadi, "An innovative framework for implementing lean principles in product-service system," PhD Thesis, Cranfield, UK,2015.

[30] A. Esfandyari, M. R. Osman, N. Ismail, and F. Tahriri, "Application of value stream mapping using simulation to decrease production lead time: a Malaysian manufacturing case," *International Journal of Industrial and Systems Engineering*, vol. 8, pp. 230-250, 2011.

[31] G. Anand and R. Kodali, "Selection of lean manufacturing systems using the analytic network process-a case study," *Journal of Manufacturing Technology Management*, vol. 20, pp. 258-289, 2009.

[32] M. Eswaramoorthi, G. Kathiresan, P. Prasad, and P. Mohanram, "A survey on lean practices in Indian machine tool industries," *The International Journal of Advanced Manufacturing Technology*, vol. 52, pp. 1091-1101, 2011.
[33] M. A. Amin and M. Karim, "A time-based quantitative approach for selecting lean strategies for manufacturing organisations," *International Journal of Production Research*, vol. 51, pp. 1146-1167, 2013.
[34] U. Srichuachom, "The impact of lean approaches to support quality developments in Thailand: an investigation of a claim of universality of lean thinking," University of Southampton, 2015.
[35] D. Seth and V. Gupta, "Application of value stream mapping for lean operations and cycle time reduction: an Indian case study," *Production Planning & Control*, vol. 16, pp. 44-59, 2005.
[36] I. M. Belova and Z. Yansong, *Value stream mapping for waste reduction in playing system components flow*, Jonkoping International Business School, 2008.
[37] I. Serrano Lasa, R. d. Castro, and C. O. Laburu, "Extent of the use of Lean concepts proposed for a value stream mapping application," *Production Planning & Control*, vol. 20, pp. 82-98, 2009.
[38] F. A. Abdulmalek and J. Rajgopal, "Analyzing the benefits of lean manufacturing and value stream mapping via simulation: A process sector case study," *International Journal of production economics*, vol. 107, pp. 223-236, 2007.
[39] D. Tapping and T. Shuker, *Value Stream Management for the Lean Office: Eight Steps to Planning, Mapping, & Sustaining Lean Improvements in Administrative Areas*, CRC Press, 2003.
[40] R. Sundar, A. Balaji, and R. S. Kumar, "A Review on Lean Manufacturing Implementation Techniques," Procedia Engineering, vol. 97, pp. 1875-1885, 2014.
[41] V. Ramesh and R. Kodali, "A decision framework for maximising lean manufacturing performance," *International Journal of Production Research*, vol. 50, pp. 2234-2251, 2012.
[42] N. M. Yusof, M. Z. M. Saman, and N. K. Kasava, " A conceptual sustainable domain value stream mapping framework for manufacturing," 11 Global Conference on sustainable Manufacturig,09, 2013 pp. 54-59.
[43] G. Pude, G. Naik, and P. Naik, "Application of Process Activity Mapping for Waster Reduction: A Case Study in Foundry Industry," *International Journal of Modern Engineering Research*, vol. 2, pp. 3482-3496, 2012.
[44] S. Vinodh, S. Gautham, and A. Ramiya R, "Implementing lean sigma framework in an Indian automotive valves manufacturing organisation: a case study," *Production Planning & Control*, vol. 22, pp. 708-722, 2011.
[45] S. Mostafa, J. Dumrak, and H. Soltan, "A framework for lean manufacturing implementation," *Production & Manufacturing Research*, vol. 1, pp. 44-64, 2013.

Pakistan Journal of Engineering and Technology, PakJET
Multidisciplinary | Peer Reviewed | Open Access

Volume: 1, Number: 1, Pages: 40- 44, Year: 2018

Thermal Effect Characterization of a Hand-operated Plastic Injection Molding Machine

Khazar Hayat[*,1], Semi Javed[1], Muhammad Zeeshan Rafique[1], Aamir Shahzad[1] and Iqbal Hussain[1]

[1]Mechanical Engineering Department, The University of Lahore, 1-KM Defence Road, Lahore, 54000, Pakistan
*Corresponding author: Khazar Hayat (email: khazar.hayat@me.uol.edu.pk)

***Abstract*— Thermal conditions play a pivotal role during the injection molding of plastic products. This work aims at characterizing the thermal effects on the plastic injection molding process in order to produce dimensionally and structurally consistent products. For this purpose, six temperature sensors were installed at various locations appropriately selected on the barrel of a hand-operated in-house designed and fabricated plastic injection molding machine and on the product mold of a hoisting hook. The temperature data from the sensors was recorded during the injection molding of a commercially known ABS plastic to manufacture the product samples. The analysis of the measured data was then carried out to identify different phases of the injection molding process and to evaluate the temperature influence on the product quality. Also, a parametric study is conducted to find out the optimal temperature conditions for the barrel of injection molding machine and the product mold to manufacture a better quality ABS plastic product.**

***Index Terms*— ABS plastic; Hoisting hook; Injection Molding; Temperature sensors; Thermal effect.**

I. INTRODUCTION

Plastic injection molding is considered as a well-established manufacturing process by the plastic industry worldwide. According to an estimate, it is the most commonly used process of manufacturing plastic products after extrusion process. It also exhibits more benefits over traditional compression and transfer molding processes. Moreover, lower labor cost, improved dimensional stability of the products and short cycle time make it a suitable manufacturing process [1] [2] [3] [4] [5] [6].

An injection molding process comprises the injection of melting polymers into the mold cavities. Due to its suitability for mass production, the plastic injection molding has witnessed a perpetual growth since its early development. Apparently, it seems to attain the status of a standardized technology, however, with advancement in the plastic materials and the product requirements, the injection molding process is still being investigated, improved and optimized [7] [8].

The plastic injection molding process can be divided into several phases like melting, injection, cooling and finally the product ejection. The time consumed to complete a full injection process is called cycle time, and typically one-half to two-third of the cycle time involves the part cooling which is crucial to achieve a quality product but costly from mass production point of view [2] [3] [4]. It should be noted that a significant lower cycle time for the product cooling phase may result in undesired distortion leading to compromise the product quality [9]. Several attempts have been made by the researchers to lower the cycle time related to the product cooling phase as the cycle time for the rest of process phases is already reached its lowest possible levels and cannot be further reduced. Generally, the cooling channels (CC) that follow the shape of cavities of the mold have been used to shorten the product cooling time [9] [10] [11] [12]. However, the implementation of such cooling channels inside the mold is cumbersome and expensive and may only be feasible for large complicate plastic products.

For small plastic products made from manual injection molding machines, the mold cooling at the room temperature is the only feasible solution. However, considering the lower cost involved in manual injection molding, the process is generally neglected and solemnly left over the experience and judgment of the operators. In this paper, the thermal investigation of a hand operated injection molding machine is carried out in order to produce dimensionally and structurally consistent products while lowering the cycle time. The temperatures at various locations on the machine barrel and the mold are monitored and analyzed during injection molding of plastic products. It should be noted that the mold is kept at room temperature in order to lower the manufacturing as well as production cost.

The paper begins with a brief description of the problem statement followed by the methodology section where installation of temperature sensors and development of a cost effect data acquisition is discussed, and, finally, the result and discussion section is presented before the conclusion section.

II. PROBLEM STATEMENT

Figure 1 shows an in-house built hand-operated plastic injection molding machine to be investigated to characterize the thermal effects on the molding process. The machine comprised injection plunger, barrel, hopper, handle, nozzle and a band heater. The injection plunger and barrel were made of medium carbon steel, while, mild steel was used for hopper, handle and nozzle components. The band heater of 300W capacity wound over the barrel was used for uniformly heating the barrel to melt the polymer deposited inside. The length of injection stroke was 400 mm long. The maximum temperature of barrel achieved was 320 ºC that can be maintained by an AC power supply of 110V/60 Hz.

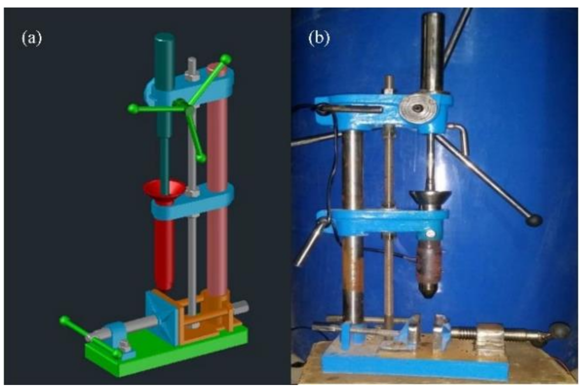

Figure 1 Plastic injection molding machine: (a) CAD model, (b) built model.

Table 1 Dimensions of injection molding machine parts.

Description	Dimensions (mm)
Injection plunger	$\phi 22 \times 900$
Barrel	$\phi 45 \times 470$
Nozzle	R10
Hopper	$90 \times 92 \times 115$
Handle	$\phi 124 \times 260$
Mold	$80 \times 60 \times 24$

The whole machine weighed approximately 48 kg. The product mold, consisting of two halves, was made of Aluminum material and was designed to mold a plastic hoisting hook. The plastic used was a commercially known ABS plastic to manufacture the samples of hoisting hook. ABS plastic was selected as it belongs the family of thermoplastics and is used for a wide range of everyday plastic products. It has the specific gravity of 1.06 and a glass transition temperature of 105 ºC [13]. Moreover, the dimensions of injection molding machine components and the mold are listed in table 1.

III. METHODOLOGY

In order to investigate the injection molding process, six different location were identified at the barrel of injection molding machine and at the product mold, as shown in figure 2. Considering the space constraints and installation difficulties, the two temperature sensors at the barrel nozzle were mounted at a distance of 10 mm, 12 mm and 25 mm from barrel bottom surface. In case of the product mold, one temperature sensor was mounted near the inlet port and while the remaining two temperature sensors were mounted close to the ends of the hoisting hook. The temperature sensors used were LM35 precision centigrade temperature sensors. This kind of sensor has an operating range of -55 ºC to 250 ºC and with a resolution of 0.5 ºC [14].

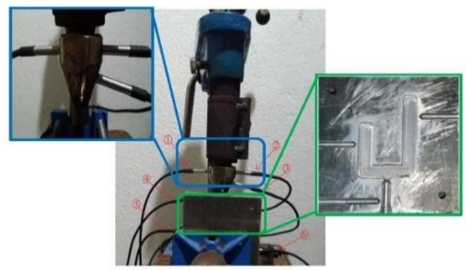

Figure 2 Temperature sensors installation on the injection molding machine and plastic hoist mold.

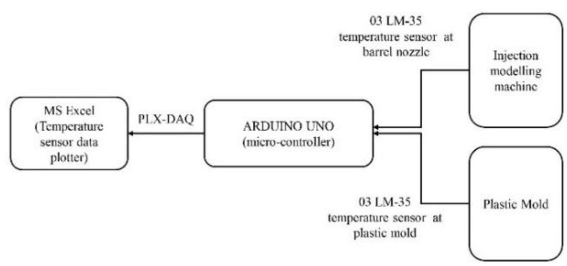

Figure 3 Schematic of temperature monitoring of plastic injection molding machine and plastic mold.

To monitor the temperature distribution along the barrel and the product mold a low cost data acquisition scheme as developed, as shown in figure 3. The analog temperature sensor data was collected using Arduino UNO, an open-source microcontroller board. It should be noted that a single Arduino UNO board can process up to fourteen digital inputs and six analog inputs by using C programming language, for further details see [15]. Since, Arduino UNO possess limited data analyzing and displaying capacities, therefore, it was interfaced with Microsoft Excel using Parallax Data

Acquisition tool (PLX-DAQ) a free software add-in which can support up to 26 data channels [16].

IV. Results and discussion

Figure 4a-b shows the temperature distributions at the barrel of injection molding machine and the mold during running empty and injection molding. In case of the empty run, it takes approximately 27 minutes by the band heater to heat the barrel until it reaches the saturation temperature (see figure 4a). On reaching the saturation temperature, a thermal equilibrium is established between the barrel and the surrounding environment as consequence the temperatures at various locations of barrel do not rise further. Moreover, there exists a temperature gradient along the barrel as can be seen by the temperature measurements from sensors 1, 2 and 3.

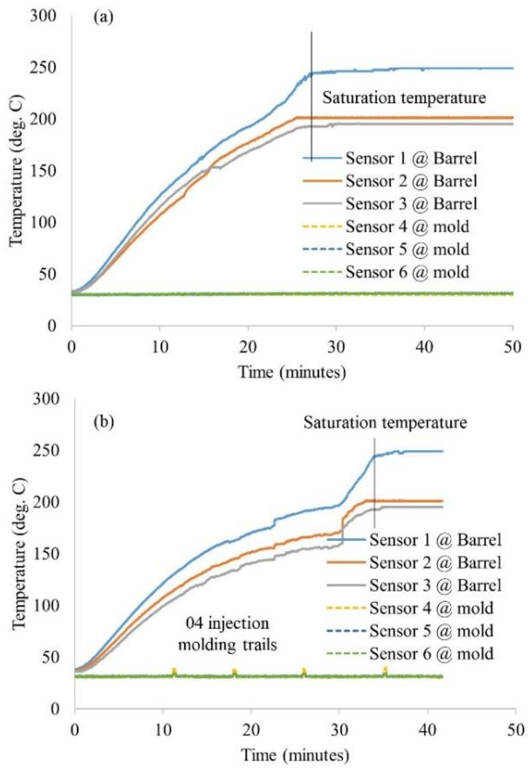

Figure 5 Temperature monitoring of the barrel of injection molding machine and the mold: (a) while running empty, (b) during injection molding.

For example, beyond the saturation limit, the measured temperature of senor 1, 2 and 3 is 250 ^{o}C, 201 ^{o}C and 194.4 ^{o}C, respectively, showing that the barrel is non-uniformly heated. On the other hand, the temperature of mold is approximately 30 ^{o}C which was consist with the environment as no molten polymer is being injected yet. In case of injection molding run, the time to reach the saturation temperature is increased to 35 minutes as more heat is required to heat the barrel and to melt the ABS plastic polymer (see figure 4b). Also, the presence of four spikes in the mold sensor data represents the four trial sets of injection molding of the hoist hook products.

Figure 5 shows the temperature distributions of the product mold during injection molding. The temperature data was collected at various locations of the mold, nevertheless, the measured data from all sensors is overlapping, depicting that the mold temperature during the injection molding is well distributed as the mold is made of Aluminum material which exhibits a good thermal conductivity.

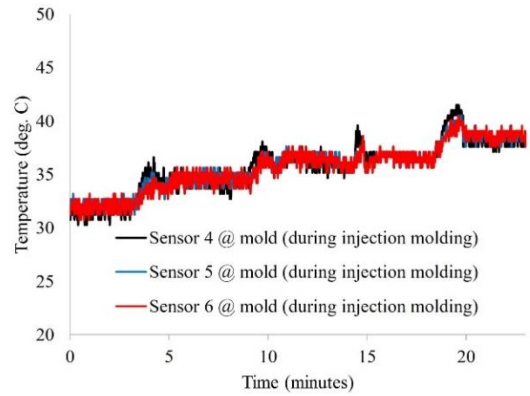

Figure 5 Mold temperature distribution

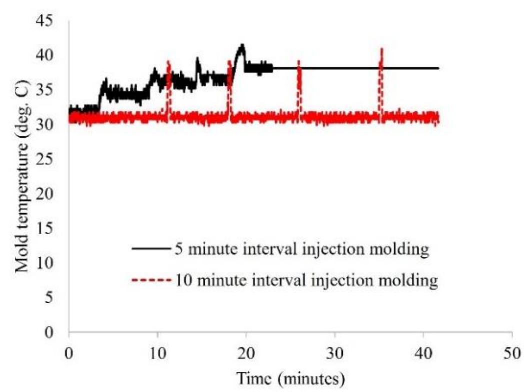

Figure 6 Effect of cycle time on mold temperature distribution.

In order to investigate the effect of cycle time on the mold temperature, several injection molding trials with two different cycle times i.e. 5 minutes and 10 minutes, were carried out. In figure 6, the solid black line refers to injection molding with a 5-minute cycle time and the dotted red line refers to injection molding with a 10-minute cycle time. The sharp temperature spikes on each graph refer to the injection phase of the molding process when the molten ABS plastic is being injected into the mold cavity. In case of a 5-minute cycle time, the mold temperature increased as time required to dissipate heat from mold was relatively short. As a results the mold temperature rises from a room temperature of approximately 30 ºC to 38.02 ºC. On the other hand, for a 10-minute cycle time, the mold temperature rises during the injection molding but it returns to the room temperature as there is now sufficient time available for mold to dissipate heat to the environment.

Figure 7 shows results of a parametric study to evaluate the effect of barrel heating and mold heating on the quality of injection molded ABS product. The Trial sets 1 and 2 refer to the thermal condition when insufficient heat was supplied and such under heating resulted in incomplete products. On the other end, the excessive heating resulted in excessive distortion of the product as represented by the results of Trial set 4. When ABS plastic was heated and injected at the proper barrel and mold temperatures, the product quality was greatly improved as can be seen by the results of Trial set 3. The optimum barral and mold temperatures found to be was 210 ºC and 38.5 ºC.

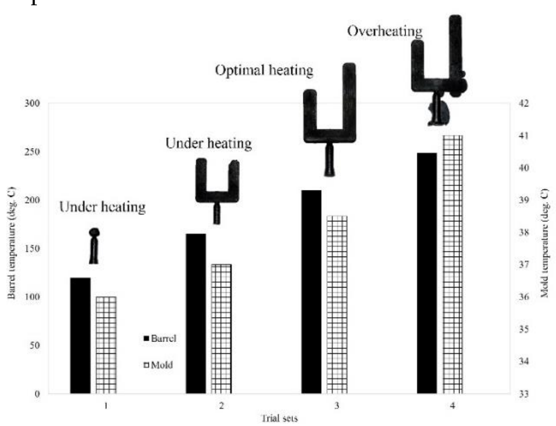

Figure 7. Heating effect on the quality of injection molded product.

V. CONCLUSIONS

Thermal characterization of injection molding process for ABS plastic is carried out using temperature sensors installed at various locations of the barrel of in-house developed injection molding machine and at the product mold. A cost effective data acquisition was built to gather the sensor data using ARUDINO UNO microcontroller and PAQ-DAQ software add-in to Microsoft Excel.

The measured results showed that the barrel of injection molding machine was non-uniformly heated as there exists a thermal gradient along the nozzle length. A uniformly heated barrel may results in a short melting time of ABS plastic, subsequently, leading to lower a cycle time. On the other hand, the sensor data from the mold showed that the mold got uniformed heated when molten plastic was injected to it. Also, when the cycle time was made short, then, the mold temperature started to rise due to lower heat dissipation and vice versa. Lastly, a parametric study was conducted and the optimum temperature for the injection machine barrel and mold were identified to be 210 ºC and 38.5 ºC that provided a dimensionally stable product.

REFERENCES

[1] D. V. Rosato and M. G. Rosato, *Injection molding handbook*, Springer Science & Business Media, 2012.

[2] J. Shoemaker, *Moldflow design guide: a resource for plastics engineers*, vol. 10, Hanser Verlag, 2006.

[3] T. A. Osswald, L.-S. Turng and P. J. Gramann, *Injection molding handbook*, vol. 2, Hanser New York, 2002.

[4] I. I. Rubin and A. A. Rubin, *Injection molding: theory and practice*, Wiley New York, 1972.

[5] C. W. Macosko, RIM, *Fundamentals of reaction injection molding*, Hanser Munich, 1989.

[6] J. P. Beaumont, R. L. Nagel and R. Sherman, *Successful injection molding: process, design, and simulation*, Hanser Publishers New York, 2002.

[7] S. L. Mok, C. K. Kwong and W. S. Lau, "Review of research in the determination of process parameters for plastic injection molding," *Advances in Polymer Technology: Journal of the Polymer Processing Institute*, vol. 18, no. 3, pp. 225-236, 1999.

[8] X.-P. Dang, "General frameworks for optimization of plastic injection molding process parameters," *Simulation Modelling Practice and Theory*, vol. 41, pp. 15-27, 2014.

[9] J. Meckley and R. Edwards, "A study on the design and effectiveness of conformal cooling channels in rapid tooling inserts," *The Technology Interface Journal*, vol. 10, no. 1, pp. 1-28, 2009.

[10] A. B. M. Saifullah, S. H. Masood and I. Sbarski, "New cooling channel design for injection moulding," in *Proceedings of the World Congress on Engineering*, 2009.

[11] M. Konsulova-Bakaloca, "Application of SolidWorks Simulation for Design of Cooling System for Injection Molding," *International Virtual Journal for Science, Techniques and Innovations for the Industry Machines, Technologies, Materials*, pp. 31-34, 2012.

[12] Y. Wang, K.-M. Yu, C. C. L. Wang and Y. Zhang, "Automatic design of conformal cooling circuits for rapid tooling," *Computer-Aided Design*, vol. 43, no. 8, pp. 1001-1010, 2011.

[13] L. A. Wood, "Glass transition temperatures of copolymers," *Journal of Polymer Science*, vol. 28, no. 117, pp. 319-330, 1958.

[14] T. Instruments, "LM35 Precision Centigrade Temperature Sensors," *LM35 datasheet, Aug*, 1999.

[15] Y. A. Badamasi, "The working principle of an Arduino," in *Electronics, computer and computation (icecco), 2014 11th international conference on*, 2014.

[16] R. D. Tipones, K. A. A. Gutierrez and J. P. B. Valencia, "Cost-Effective Microcontroller Material Strength Impact Tester Using PLX-DAQ for Data Acquisition," in *Proceedings of the 8th AUN/SEED-Net RCEEE*, 2015.

[17] S. H. Masood and N. N. Trang, "Thermal analysis of conformal cooling channels in injection moulding," in *Proceedings of the 3rd BSME-ASME International Conference on Thermal Engineering*, 2006.

[18] M. Khan, S. K. Afaq, N. U. Khan and S. Ahmad, "Cycle time reduction in injection molding process by selection of robust cooling channel design," *ISRN Mechanical Engineering*, vol. 2014, 2014.

[19] C. Fernandes, A. J. Pontes, J. C. Viana and A. Gaspar-Cunha, "Modeling and Optimization of the Injection-Molding Process: A Review," *Advances in Polymer Technology*, vol. 37, no. 2, pp. 429-449, 2018.

[20] K.-S. Chin and T. N. Wong, "Knowledge-based evaluation for the conceptual design development of injection molding parts," *Engineering Applications of Artificial Intelligence*, vol. 9, no. 4, pp. 359-376, 1996.

Pakistan Journal of Engineering and Technology, PakJET
Multidisciplinary | Peer Reviewed | Open Access

Volume: 1, Number: 1, Pages: 45- 51, Year: 2018

Analysis and Estimation of Within the Desiccant and Without the Desiccant Dehumidification System Performance

Behzad Rustam*[,1], Ahmad Shafi[1], Atif Ilyas[1] ,Muhammad Usman[1], Tauqeer Ahmed khan[1]

[1]Mechanical Engineering Department, The University of Lahore, 1-KM Raiwind Road, Lahore, 54000, Pakistan
*Corresponding author: Behzad Rustam (email: behzad.rustam@me.uol.edu.pk)

***Abstract*—In this research the heat recovery in the HVAC system of a newly constructed general hospital building was considered for the analysis and estimation of desiccants dehumidification system performance. In the previous two decades, expanded urbanization and industrialization have caused a huge arise of the energy utilization of buildings. Energy utilization via air conditioning represents 1/3 of the aggregate energy utilized by the developed society. Cooling and dehumidifying new ventilation air comprises 20– 40% of the total energy stack for cooling in hot and moisturized areas. Currently, there is developing interest for energy saving advancements in buildings, thus to this, energy efficient technologies are ending up more mainstream among researchers and developers. In this respects, to satisfy energy protection demands, improvement of advance heat or energy recuperation with energy proficient ventilation system has been focused in this study. Hourly Analysis Program (HAP) was used for key features to design HVAC system and to estimate annual energy consumption. Using HAP, annual energy estimation of cooling and heating loads were determined. The energy saved using HRWheel-1800, HRWheel-1700 and HRWheel-2000 was 39%, 28% and 19% respectively. The required air flow rate computed as 9500CFM, 7688CFM, and 7848CFM respectively.**

Index Terms—Desiccant Dehumidification System (DDS); Heating Ventilation and Air Conditioning (HVAC); Hourly Analysis Program (HAP)

I. INTRODUCTION

Pakistan is facing severe energy crises for the last two decades. The major cause for the current shortfall in electricity is increasing human population, modernization and urbanization. Electricity shortfall during 2017-18 in Pakistan, through all sources is expected around 7000 MW. Energy crisis issue will prevail for long years to come if sincere and planed efforts are not initiated promptly and urgently on national bases.

One of the high energy consumption field is the Heating ventilation and air conditioning (HVAC). Desiccant dehumidification is a process of treating the air to maintain the temperature and humidity to a comfort level. To maintain the desired temperature and humidity, a considerable amount of energy is utilized. In the last few years, urbanization and industrialization have increased to a certain extent and due to which energy consumption has risen strangely. Almost one third of society's energy consumption is utilized by air conditioning. More accurately, main portion of energy is consumed to cool and dehumidify fresh air. Hourly analysis program was used to calculate and for estimation of energy of commercial buildings as well as domestic. HAP application is a computer tool which helps engineers in scheming HVAC systems for commercial homes. HAP is a two in one tool, first it is used to comprise the different loads and second is to estimate the building energy. Many researchers have worked on the application of heat recovery wheels to overcome the energy consumption of HVAC system. They have the use of this technique under various weather conditions. Jose Fernandez-Seara et al.[1] performed many tests on the heat exchanger to check out its performance under reference conditions when integrated within the system. Duration of each experiment was four hour. Operation of heat exchanger was unsteady during the first hours but later on it became stable. Efficiency and the heat transfer remain almost constant during the whole period of time. During the experiment, pressure drop rises and this is due to the condensation on the surface of exchanger. After that they carried the number of experiments by varying the outdoor design conditions. They varied the temperature of fresh air, relative humidity of exhaust air and the flow rate at a time by keeping all other variables constant. Heat transfer decreases rapidly while efficiency of the exchanger remains almost same as the inlet temperature increases. Heat transfer and efficiency have no significant effect by the change in relative humidity. Effect on both these two was within 10%. A rapid rise in heat transfer has been seen due to the increase in flow rate but by increasing flow rate, efficiency decreases. C.-A. Roulet et al.[2] pointed that performance of a heat recovery unit can be evaluated from the worldwide effectiveness of HR unit and particular net energy saving or coefficient of performance (COP). We should consider the worldwide effectiveness of the whole framework not the nominal proficiency of the HR unit only. They performed measurements on a number of heat recovery units. They used the technique of tracer gas dilution. During their measurements, they found that SNES may be even negative. In the best case, the value of SNES was 2.7. For those systems having nominal efficiency 70%, global which is the real efficiency reduced to 43%. It's not always fruitful to use the heat recovery unit. During the measurements, they found some systems with efficiency less than 10%. Those systems used more energy than they saved. Efficiency of the system depends on the infiltration, exfiltration, internal and external recirculation rates and on parasitic leakages and shortcuts. Younness EI Fouih et al.[3] considered three different ventilation systems and evaluated their performance in seven different climatic zones in France. For this purpose they considered three different types of buildings. These categories were flat, house and a small office. They suggested that we should consider the total energy consumption consisting of ventilation, cooling and heating consumption for energy comparison. For office, HRV (heat recovery ventilation system) was less proficient than the MEV (mechanical extract ventilation system) for each climatic zone. Performance of HRV was almost same for the flat and the house case. For the flat and house, energy consumption of HRV is less than that of MEV. Energy consumption of HRV was more and less than that of HCV (humidity controlled ventilation) for climatic zones. They showed that system parameters impact the energy based performance of the system. Efficiency of the heat exchanger and the SFP (specific fan power) of the fan have the vital role on the overall energy utilization of the system. Shahram Delfani et al.[4] evaluated experimentally four different combinations of heat recovery with the ventilation system in different climatic regions of Asia. In the two systems, they used 100% fresh air, and in the two they used 30% fresh air. They considered 40 different test points for this purpose. Their experimental setup could vary the outdoor design conditions. Apparatus could calculate the temperature, humidity and velocity at different points in the system. They calculated the energy consumption of each system. Consumption of MHCC (with mixer and heat exchanger) was lowest than any other system in all the systems. Consumption of HCC (with single heat exchanger) was highest in every case of the selected points. They found that by using an extra heat exchanger, we can reduce the consumption of heating, cooling and ventilation system by almost 32%.

Yanming et al.[5] worked on the applicability of the heat recovery unit to reduce energy consumption especially in the winter season in different zones of China. They surveyed for the comfort temperature in super markets with high occupant densities. They suggested that comfort temperature is closely related to the clothing insulation of the occupants. They found that latent recovery is not suitable in winter because values of humidity ratio are much above the critical values. They showed that sensible recovery is suitable and it depends on the outdoor temperature. They divided China into five zones on the climatic basis and into three regions according to the temperature of outdoor climate. They calculated two critical temperatures for heat recovery. If we use a rotational fan with variable speed instead of constant speed, heat recovery has always a positive impact on energy saving except Guangzhou. Mohammad Rasouli et al.[6] studied the uncertainties about the energy and economic performance of an energy recovery unit due to unpredictability in different building related parameters and also due to different HVAC parameters. To carry out their research, they selected an office building in Chicago. After their research, they come to the conclusion that cooling load, heating load and the annual heating energy are more sensitive to ventilation rate. Internal loads have more effect on the annual cooling energy. They suggested that the size of HVAC equipment can be minimized by using energy recovery unit. They considered an ERV with 75% sensible and 60% latent effectiveness. They showed that this ERV can decrease the cooling and heating load by 30% and 18% respectively. This ERV normally has the period of 2 years. Envelope related parameters and internal loads have no significant effect on payback period of ERV. While with increasing ventilation rate, payback period can reduce greatly. Payback period of an ERV is strongly dependent on its own parameters which includes effectiveness, initial cost and on the parameters of HVAC equipment which includes initial cost and the efficiency mainly.

Y.P. Zhou et al.[7] developed the model of energy recovery by using Energy Plus software. They investigated its performance and its availability under different temperatures and also under different weathers. For this purpose, they considered two different cities of China i.e. Shangai and Beijing. Availability of ERV is high enough in both the cities. Its range is between 0.6-0.9 for Shangai as well as Beijing. Performance of ERV is little bit better in Shangai as compared to that in Beijing. Some cooling recovery exists even in winter season. But its value is very small as compared to the heating recovery in winter season. While increasing the set-point, energy recovery performance decreases. In the same manner, if we elevate the set-point, heating recovery also increases and if we raise the set-point, cooling recovery decreases but the change is not significant. Availability of ERV is low in summer as compared to that in winter. There is a significant amount of heating recovery in summer. In summer season, if we increase the set-point, performance of ERV also increases. Performance of ERV is better in Shangai than that in Beijing. If we increase the set-point, cooling recovery decreases and heating recovery rises. Using ERV is not useful in Beijing when set-point is higher than 24 °C. Latent recovery is the main factor for better performance of ERV in Shangai in warmer months. The present study focusses to fulfill energy conservation demands, improvement of advance energy or heat recovery with energy-efficient ventilation systems. This project is essentially an effort to express desiccant dehumidification system behavior.

II. RESEARCHER METHODOLOGY

A. Analysis of Desiccant Dehumidification

Peak cooling coil load, design airflow CFM and the fan motor BHP were calculated for the sizing of the HVAC system. Proceeding further annual energy consumption by cooling, heating, supply fan, lighting and other electrical equipment was determined through simulation tool. Research has been carried out for the weather conditions of Lahore because Typical Metrological Year 2 file was only available for this city of Pakistan. Hourly Analysis Programmed software's was used for research. Hourly analysis application (hap) is a computer tool which helps engineers in scheming HVAC systems for commercial homes. HAP is equipment in a single. Foremost it is a tool for estimating loads and designing structures. Some other, it's far a tool for simulating constructing strength use and calculating strength of the system. In this capacity it's tons useful for plan design and detailed design energy estimations. HAP makes use of the ashrae transfer reason approach for load calculations and precise 8,760 hour-with the aid of-hour model techniques for the power research. This application is unconfined as separate, however like products. The "hap system design load" program can provide system layout and cargo estimating capabilities. The overall "hap" program offers the same system design competencies plus energy research features. Until now calculations were made without using heat recovery. Now we will incorporate heat recovery units into the system. Now all the above mentioned parameters were determined with the inclusion of heat recovery units into the system. Analysis has been carried out by using three different types of Heat Recovery units which are as follows

- HR Wheel-2000-SG-200
- HR Wheel-1700-MS-200
- HR Wheel-1800-MS-270

In the above code, HRW is the abbreviation for Heat Recovery Wheel, figures after HRW e.g. 2000, 1700 are the diameters of wheels. SG denotes for silica gel and MS for Ecosorb 300 (Molecular Sieve 3A). Figures after SG or MS e.g. 200 and 270 are the depths of wheels.

Two different types of desiccants have been used for the analysis:

- First one is the Silica Gel
- Second desiccant is the Ecosorb 300 (Molecular Sieve 3A

i. Analysis without Heat Recovery Wheel

Air system sizing summary for treated fresh unit without heat recovery

Air system information

Air system name ………………. TFU	Number of zones…… 1
Equipment class………………. CW AHU	Floor Area………….. 3484.8 ft^2
Air system Type………………. SZCAV	Location……………. Karachi, Pakistan

Sizing Calculation Information

Zone and Space Sizing Method:	
Zone CFM…… Sum of Space airflow Rates	Calculation Months… Jan to Dec
Space CFM…… Individual peak space load	Sizing Data………..… Calculated

Central Cooling Coil Sizing DATA

Total coil load………………………………… 82.0 Tons	Load Occurs at………… Jun 1500
Total coil load…………………………………982.3 MBH	OA DB/WB…………….…99.0/82.0 F
Sensible Coil load…………………………..… 4822.1 MBH	Entering DB/WB………… 98.2/81.3 F
Coil CFM at Jun 1500…………………………10001 CFM	Leaving DB/WB…………. 55.4/54.9 F
Maximum block CFM……………………….10001 CFM	Coil ADP……………………….45.6 F
Sum of Peak Zone CMF……………………. 10002 CFM	Bypass Factor……….…………..0.110
Sensible Heat Ratio…………………………………. 0.487	Resulting RH…..…………..…….. 52 %
Ft^2/Ton……………………………………………….. 41.9	Design Supply Temp……….…. 56.0 F
BTU/(hr-ft^2) ………………………….………….. 287.5	Zone T- stat check………… 1 of 1 OK
Water flow@ 10.0 F rise……………………… 195.58 gpm	Max zone Temp Deviation…….. 0.0 F

Central Heating Coil Sizing

Max coil load………………………………… 226.8 MBH	Load occurs at………………. Des Htg
Coil CFM at Des Htg………………………… 10002 CFM	BTU/(hr-ft2) …………………… 66.7
Water flow@ 20.0 F rise……………………… 22.59 gpm	Ent. DB/Lvg DB………... 50.4/71.3 F

Table 1 Design Cooling System Data

component	location	dbt (f)	airflow (cfm)	sp. humidity	co_2 level (ppm)	s. heat (btu/hr.)	latent heat (btu/hr.)
air ventilation	inlet	98.0	9501	0.1985	404	255791	475754
vent – return mixing	outlet	99.8	10001	0.01924	400	-	-
supply fan	outlet	97.2	10002	0.01924	400	4548	-
central cooling coil	outlet	54.5	10000	0.00869	405	472085	500271
central heating coil	outlet	55.9	10001	0.00869	404	26445	-
cold supply duct	outlet	58.7	9501	0.00869	405	-	-
return plenum	outlet	77.0	9501	0.00924	478	0	-
duct leakage air	outlet	55.9	501	0.00869	405	-	-
return duct	outlet	74.5	10005	0.00921	405	-	-

Table 2 Design Heating System Data

component	location	dry bulb temp (f)	specific humidity (lb /lb.)	air flow (cfm)	co2 level (ppm)	s. heat (btu/hr.)	latent heat (btu/hr.)
air ventilation	inlet	48.9	0.00365	9501	404	-196168	0
return-vent mixing	outlet	49.9	0.00365	10001	405	-	-
supply fan	outlet	50.5	0.00365	10002	401	4449	-
central cooling coil	outlet	50.6	0.00365	10001	400	0	0
central heating coil	outlet	71.5	0.00365	10002	405	225675	-
cold supply duct	outlet	71.2	0.00366	9501	401	-	-
return plenum	outlet	67.9	0.00365	9501	405	0	-
duct leakage air	outlet	71.5	0.00365	505	405	-	-
return duct	outlet	68.4	0.00366	10001	402	-	-

ii. Analysis with Heat Recovery Wheel

Air system sizing summary for treated fresh unit with heat recovery

Air system information

Air system name ………………. TFU
Equipment class………………. CW AHU
Air system Type………………. SZCAV

Number of zones…… 1
Floor Area………….. 338.8 ft^2
Location……………. Karachi, Pakistan

Sizing Calculation Information

Zone and Space Sizing Method:
Zone CFM…… Sum of Space airflow Rates
Space CFM…… Individual peak space load

Calculation Months… Jan to Dec
Sizing Data……….… Calculated

Central Cooling Coil Sizing DATA

Total coil load………………………………… 46.9 Tons
Total coil load…………………………………972.5 MBH
Sensible Coil load…………………………..… 482.1 MBH
Coil CFM at Jun 1500…………………………10001 CFM
Maximum block CFM……………………….10001 CFM
Sum of Peak Zone CMF……………………. 10001 CFM
Sensible Heat Ratio…………………………………. 0.488
Ft^2/Ton……………………………………………….. 41.9
BTU/(hr-ft^2) ………………………….………….. 287.5
Water flow@ 10.0 F rise……………………… 194.58 gpm

Load Occurs at……………… Jun 1500
OA DB/WB……………..…98.0/82.0 F
Entering DB/WB………… 98.5/81.4 F
Leaving DB/WB…………. 54.5/54.0 F
Coil ADP………………………46.7 F
Bypass Factor……….…………..0.110
Resulting RH….……….….….. 50 %
Design Supply Temp……….…. 55.3 F
Zone T- stat check………… 1 of 1 OK
Max zone Temp Deviation…….. 0.0 F

Central Heating Coil Sizing Data

Max coil load………………………………… 225.8 MBH
Coil CFM at Des Htg………………………… 10001 CFM
Water flow@ 20.0 F rise………………………. 22.59 gpm

Load occurs at………………. Des Htg
BTU/(hr-ft2) …………………… 66.8
Ent. DB/Lvg DB………..... 50.5/71.4 F

Supply Fan Sizing Data

Actual Max CFM ………………...………. 10001 CFM
Standard CFM………………………………. 9995 CFM
Actual Max CFM/ft^2 ……………….…..……. 10002 CFM/ft^2

Fan Motor BHP…..………. 1.76 BHP
Fan Motor BHP…………..… 1.3 KW
Fan Static……………….. 0.61 in wg

a. *Analysis with HRW-2000-SG-200*

Table 3 Design Cooling System Data

component	location	dry bulb temp (f)	specific humidity (lb /lb.)	air flow (cfm)	co2 level (ppm)	s. heat (btu/hr.)	latent heat (btu/hr.)
air ventilation	inlet	82.3	0.01677	7848	400	70414	283239
return- vent mixing	outlet	81.9	0.01639	8261	404	-	-
supply fan	outlet	82.3	0.01639	8261	404	3675	-
central cooling coil	outlet	53.6	0.00861	8261	404	256119	304952
central heating coil	outlet	57.6	0.00861	8261	404	35638	-
cold supply duct	outlet	58.4	0.00861	7848	404	-	-
return plenum	outlet	74.9	.00919	7848	493	0	-
duct leakage air	outlet	57.6	.00861	413	404	-	-
return duct	outlet	74.0	0.00916	8261	488	-	-

Table 4 Design Heating System Data

component	location	dry bulb temp (^{0}f)	specific humidity (lb /lb.)	air flow (cfm)	co2 level (ppm)	s. heat (btu/hr.)	latent heat (btu/hr.)
air ventilation	inlet	68.0	0.00817	7849	401	8472	33675
return-vent mixing	outlet	68.0	.00813	8262	401	-	-
supply fan	outlet	68.4	0.00813	8262	401	385	-
central cooling coil	outlet	50.5	0.00725	8262	401	16949	3456
central heating coil	outlet	68.1	0.00725	8263	402	15734	-

cold supply duct	outlet	68.2	0.00725	7849	401	-	-
return plenum	outlet	68.3	0.00727	7849	402	0	-
duct leakage air	outlet	68.4	0.00725	414	401	-	-
return duct	outlet	68.5	0.00727	8262	405	-	-

b. *Analysis with HRW-1700-MS-200*

Table 5 Design Cooling System Data

component	location	dry bulb temp (f)	specific humidity (lb /lb.)	air flow (cfm)	co_2 level (ppm)	s. heat (btu/hr.)	latent heat (btu/hr.)
air ventilation	inlet	82.5	0.01749	7849	401	70414	309739
return-vent mixing	outlet	81.4	0.01707	8262	402	-	-
supply fan	outlet	82.5	0.01707	8262	403	3675	-
central cooling coil	outlet	53.5	0.00860	8262	405	258775	332155
central heating coil	outlet	57.7	0.00860	8262	405	38297	-
cold supply duct	outlet	58.5	0.00860	7849	404	-	-
return plenum	outlet	74.8	0.00921	7849	495	0	-
duct leakage air	outlet	57.7	0.00858	414	405	-	-
return duct	outlet	74.1	0.00917	8262	488	-	-

Table 6 Design Heating System Data

component	location	dry bulb temp (f)	specific humidity (lb /lb.)	air flow (cfm)	co_2 level (ppm)	s. heat (btu/hr.)	latent heat (btu/hr.)
air ventilation	inlet	69.0	0.00786	7848	400	8472	22373
return-vent mixing	outlet	69.0	.00783	7848	400	-	-
supply fan	outlet	69.4	0.00783	8261	400	3675	-
central cooling coil	outlet	50.0	0.00724	8261	400	168286	22963
central heating coil	outlet	68.0	0.00724	8261	400	156139	-
cold supply duct	outlet	68.0	0.00724	7848	400	-	-
return plenum	outlet	68.0	0.00726	7848	401	0	-
duct leakage air	outlet	68.0	0.00724	413	400	-	-
return duct	outlet	68.0	0.00726	8261	401	-	-

c. *Analysis with HRW-1800-MS-270*

Table 7 Design Cooling System Data

component	location	dry bulb temp (f)	specific humidity (lb /lb.)	air flow (cfm)	co_2 level (ppm)	s. heat (btu/hr.)	latent heat (btu/hr.)
air ventilation	inlet	80.5	0.01550	7688	400	56726	231541
return-vent mixing	outlet	80.5	0.01518	8092	405	-	-
supply fan	outlet	80.5	0.01518	8092	405	3599	-
central cooling coil	outlet	53.90	0.00862	8092	405	235713	252017
central heating coil	outlet	57.6	0.00862	8092	405	32835	-
cold supply duct	outlet	58.5	0.00862	7688	405	-	-
return plenum	outlet	74.8	0.00918	7688	495	0	-
duct leakage air	outlet	57.6	0.00862	405	405	-	-
return duct	outlet	74.0	0.00915	8092	490	-	-

Table 8 Design Heating System Data

component	location	dry bulb temp (f)	specific humidity (lb /lb.)	air flow (cfm)	co_2 level (ppm)	s. heat (btu/hr.)	latent heat (btu/hr.)
air ventilation	inlet	70.9	0.00853	7688	400	24067	46436
return-vent mixing	outlet	70.8	0.00847	8092	400	-	-
supply fan	outlet	71.2	0.00847	8092	400	3599	-
central cooling coil	outlet	50.4	0.00723	8092	400	181690	47688
central heating coil	outlet	68.0	0.00723	8092	400	154024	-
cold supply duct	outlet	68.0	0.00723	7688	400	-	-
return plenum	outlet	68.0	0.00726	7688	401	0	-
duct leakage air	outlet	68.0	0.00723	405	400	-	-
return duct	outlet	68.0	0.00726	8092	401	-	-

III. RESULTS AND DISCUSSIONS

A. Cooling Load

Cooling load of the system without heat recovery was 81 tons as mentioned in research methodology. While inclusion of recovery units into the system, reduces the load of the cooling coil. Cooling load reduces to 49.2 tons by using 1700-MS-200 recovery unit. With the use of 2000-SG-200 unit, cooling load reduces to 46.8 tons. Cooling load reduces to least i.e. 40.6 tons by using 1800-MS-270.

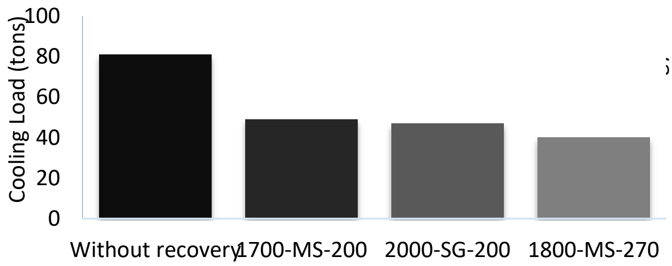

Figure 1 Cooling Load Comparison

B. Design Airflow

Design CFM of air required to maintain a better indoor air quality was 9500 without using recovery unit as shown in the figure 2. If we use recovery unit 1700-MS-200, CFM reduces to 7848. 2000-SG-200 yields the same value. While CFM of required air reduces down to 7688 by the use of 1800-MS-270.

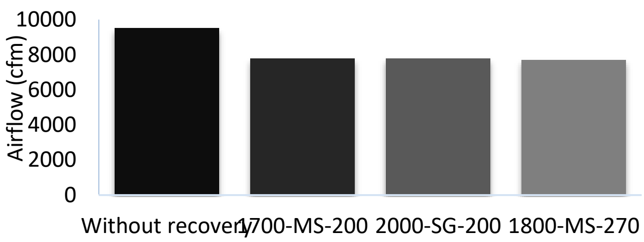

Figure 2 Design Airflow Comparisons

C. Fan Motor Sizing

Fan motor required for the system without recovery unit was of 1.75 BHP as shown in the graph below. Motor size reduces to 1.44 BHP by using 1700-MS-200. When the recovery unit 2000-SG-200 was incorporated into the system, fan motor of same BHP was required. Use of recovery unit 1800-MS-270 gives the minimum value of fan motor BP i.e. 1.41.

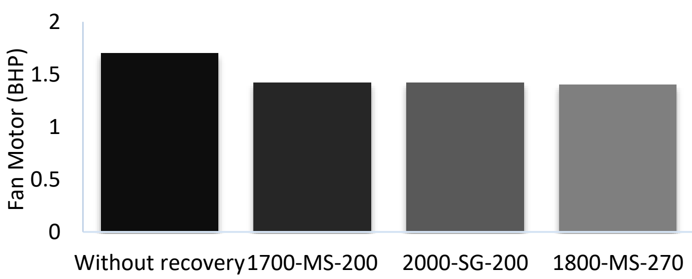

Figure 3 Fan Motor Sizing Comparisons

D. Annual Energy Consumption by Cooling Coil

Energy that will be consumed throughout the year by the cooling coil of the system without heat recovery unit will be 1286.3 MBTU as shown in the figure 4. While annual energy consumption by cooling coil is 1071.4 MBTU by 1700-MS-200 as well as by 2000-SG-200. System using 1800-MS-270 recovery unit gives less energy consumption i.e. 1051 MBTU.

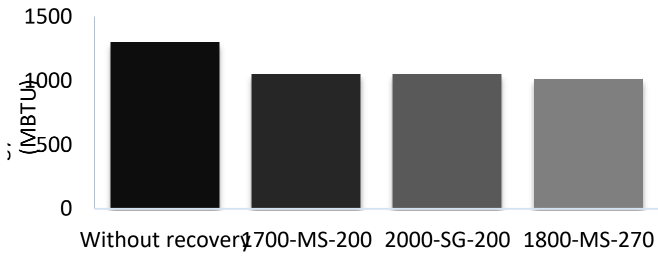

Figure 4 Annual Energy Consumption by Cooling Coil Comparison

E. Annual Energy Consumption by Heating Coil

Energy that will be consumed throughout the year by the heating coil of the system without heat recovery unit will be 184.5 MBTU as shown in the figure 5. While annual energy consumption by heating coil is 115.8 MBTU by 1700-MS-200 as well as by 2000-SG-200. System using 1800-MS-270 recovery unit gives less energy consumption i.e. 108.5 MBTU.

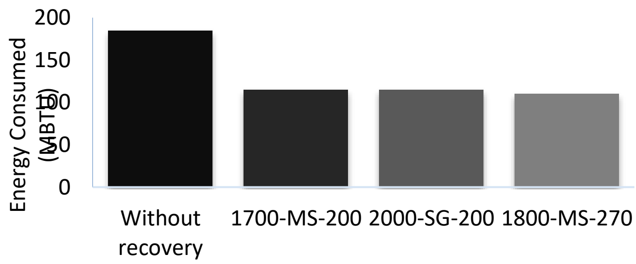

Figure 5 Annual Energy Consumption by Heating Coil Comparison

F. Annual Energy Consumption by Supply Fan

Energy that will be consumed throughout the year by supply fans of the system without heat recovery unit will be 3797 kWh as shown in the figure 6. While annual energy consumption of supply fans is 3163 kWh by 1700-MS-200 as well as by 2000-SG-200. System using 1800-MS-270 recovery unit gives less energy consumption i.e. 3101 kWh.

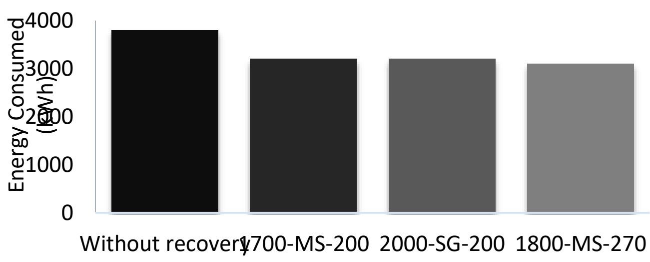

Figure 6 Annual Energy Consumption by Supply Fan Comparison

IV. CONCLUSION

- Maximum heat recovery is possible by using HR Wheel-1800-MS-270
- Cooling load reduces by 39% with the use of HR Wheel-1800-MS-270. While by using
  - HR Wheel-1700-MS-200 cooling load decreases only by 30% and by using
  - HR Wheel-2000-SG-200 cooling load decreases by 33%
- In reduction of designed CFM of airflow, HR Wheel-1800-MS-270 shows the best performance. CFM decreases by 19% by using HR Wheel-1800-MS-270. Both
  - HR Wheel-1700-MS-200 and HRWheel-2000-SG-200 decreases CFM equally by 17%
- BHP of fan motor is decreased by 19% by the use of HRWheel-1800-MS-270. While both
  - HRWheel-1700-MS-200 and HRWheel-2000-SG-200 decreases BHP of fan motor equally by 18%
- HRWheel-1800-MS-270 reduces the annual energy consumption of cooling coil by 18%. Reduction in annual energy consumption is 17% by using either HRWheel-1700-MS-200 or HRWheel-2000-SG-200
- Reduction in annual energy consumption of heating coil is 41% if we incorporate HRWheel-1800-MS-270 into the system. This reduction minimizes to 37% by using HRWheel-1700-MS-200 or HRWheel-2000-SG-200
- HRWheel-1800-MS-270 reduces the annual energy consumption of supply fans by 18%. Annual energy consumption is decreased by 17% by using either HRWheel-1700-MS-200 or HRWheel-2000-SG-200.

V. NOMENCLATURE

BTU British thermal unit
CFM Cubic Feet per Minute
KWh Kilo Watt Hour
TR Ton of Refrigeration
DHRW Desiccant Heat Recovery Wheel
DB Dry Bulb Temperature
WB Wet Bulb Temperature
RH Relative Humidity
1Unit of Energy = 1KWh
TCCL Total Cooling Coil Load
THCL Total Heating Coil Load
DDs Desiccant Dehumidification System
BHP Brake Horse Power
SG Silica Gel
EMS Ecosorb Molecular Sieve

VI. ACKNOWLEDGEMENT

The authors gratefully acknowledge the financial and technical support of the University Of Lahore and Higher Education Commission (HEC) Pakistan.

REFERENCES

[1] J. Fernández-Seara, R. Diz, F. J. Uhía, A. Dopazo, and J. M. Ferro, "Experimental analysis of an air-to-air heat recovery unit for balanced ventilation systems in residential buildings," *Energy conversion and management,* vol. 52, pp. 635-640, 2011.
[2] C.-A. Roulet, F. Heidt, F. Foradini, and M.-C. Pibiri, "Real heat recovery with air handling units," *Energy and Buildings,* vol. 33, pp. 495-502, 2001.
[3] Y. El Fouih, P. Stabat, P. Rivière, P. Hoang, and V. Archambault, "Adequacy of air-to-air heat recovery ventilation system applied in low energy buildings," *Energy and Buildings,* vol. 54, pp. 29-39, 2012.
[4] S. Delfani, H. Pasdarshahri, and M. Karami, "Experimental investigation of heat recovery system for building air conditioning in hot and humid areas," *Energy and Buildings,* vol. 49, pp. 62-68, 2012.
[5] Y. Kang, Y. Wang, K. Zhong, and J. Liu, "Temperature ranges of the application of air-to-air heat recovery ventilator in supermarkets in winter, China," *Energy and Buildings,* vol. 42, pp. 2289-2295, 2010.
[6] M. Rasouli, C. J. Simonson, and R. W. Besant, "Applicability and optimum control strategy of energy recovery ventilators in different climatic conditions," *Energy and Buildings,* vol. 42, pp. 1376-1385, 2010.
[7] Y. Zhou, J. Wu, R. Wang, S. Shiochi, and Y. Li, "Simulation and experimental validation of the variable-refrigerant-volume (VRV) air-conditioning system in EnergyPlus," *Energy and buildings,* vol. 40, pp. 1041-1047, 2008.

Pakistan Journal of Engineering and Technology, PakJET
Multidisciplinary | Peer Reviewed | Open Access

Volume: 1, Number: 1, Pages: 52- 56, Year: 2018

Development of Low Cost Solutions towards Automation of a Typical Wheelchair

Imran Ahmed[*,1], Mohammad Aamir Khan[1], Tauqeer Ahmed Khan[1]

[1]Mechanical Engineering Department, The University of Lahore, 1-KM Thokar Niaz baig, Raiwind Road, Lahore, Pakistan
*Corresponding author: Imran Ahmed (email: imran.ahmed@me.uol.edu.pk)

***Abstract*—This paper is about design, development and kinematic analysis of the wheelchair for disabled persons. Design improvements and suspension incorporation are among various ideas that were investigated and incorporated in the design. The proposed Design solution uses two wiper motors and a mechanical power system with timing belts and pulleys. Wheelchair motion is controlled using android application. Android based Smartphone provide a new technique for interaction between machine and human beings. Wheelchair can move in all four directions left, right, forward, backward and stop. A 3D model of the wheelchair was prepared in CREO. Structural analyses are performed on CREO software and final vehicle was simulated in ADAMS to access stability and ride quality. Motion simulation for the wheelchair is observed in Adams Software package in two cases: First one is traction motion and second is steering motion. Wheelchair stability test was also studied in ADAMS. Results obtained from Adams simulation describe the efficiency of proposed wheelchair driving system. The final outcomes were an economical design which was found penetration in Pakistani market**

***Index Terms*— Automation; Low Cost Solutions; Wheel Chair; Dynamic Analysis; Stability Analysis.**

I. Introduction

We have structured this paper in four sections. In the introduction part literature review of existing design of wheelchair is presented. In the 2nd part design of experimental wheelchair prototype and the design solution for the motion control of the wheelchair is described. Third part presents the kinematics of electric wheelchair by performing wheelchair motion simulation is Adams Software package. In last part dynamic stability analysis of the wheelchair are presented. Physically injured and disables patients with good mental strength try to get through places using manual and conventional wheelchairs. To face this problem an android based automatic wheelchair is used. The available wheelchairs are very expensive so a common person cannot afford. The price for automatic wheelchair is between Rs. 250,000 to Rs. 600,000. [6] The major objective of this project is to design and assemble a very low cost automated wheelchair having a weight upto90kg.The anticipated arrangement of the wheelchair comprises of two wiper motors. These wiper motors are used to drive each rear wheel of the wheelchair and drive train comprising of toothed belts worldly course of action pulleys and distinctive mechanical parts that couples the motors pole to the shaft of driving wheel. Precise Velocity and torsion produced by every wiper motor is control by maintaining the beat measurement. Ordinarily strong state transfers square measure normally is used to switch offer the voltage extremity for the purpose to fluctuate running bearing of PM (permanent magnet) wiper motors [1] [2]. Wheelchair administration module is utilized to change over point information from the humanoid telephone motors control flag. Administration modules square measure microchip based for the most part and has a few flexible values. Control module use input to show whether the motor is reacting legitimately to android application order [7] [8].

II. Design And Control System Development Of Wheelchair

For this reason, desired solution of the wheelchair design is made in CREO Computer software package [10]. Bolstered wheelchair elements computed parameters is built up the required torque and speed of impetus motors. Two wiper motors are connected to each back wheels of the wheelchair. The electric wheelchair is operated on 12V and draw in near 3A when fully loaded. The majority of riggings territory unit metal for duplicated durability and furthermore to solidified yield shaft has 9.5mm breadth. It is upheld

by two metal balls. This can be pre-designed for the 90 (degree) shift of movement, anyway this could be changed by reconfiguring the inserted controller [11]. Update seat drive prepare comprising of toothed belts, toothed pulleys and diverse mechanical parts. This is used to couple motors shaft with the shaft of driving wheel of wheelchair. Wheelchair model developed in CREO Software is shown in Figure 1.

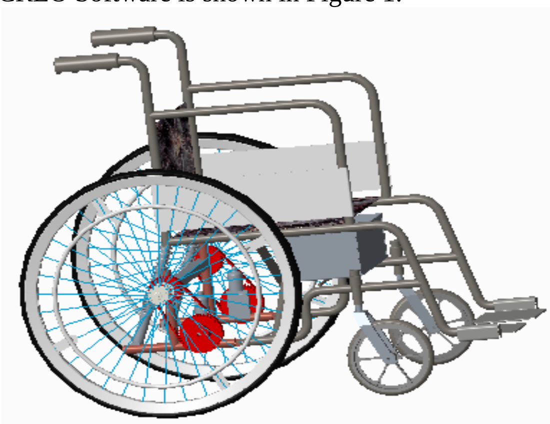

Figure 1 Creo Model of Wheelchair

Model develop in CREO Software is important because we can use it for simulation of wheelchair in Adams Software to study the motion dynamics. This Model is also important for further study in order to do optimization in development to minimize weight and ergonomics. Wheelchair uses the timing bets for motion transmission. Belt transmission system in shown in figure 2.

Figure 2 Wheelchair belt transmission

This experimental model of wheelchair is assembled at Mechanical Engineer Department "The University of Lahore" is shown in Fig. 3 and figure 4. The desired design solution of electric wheelchair use two wiper motors each attached to the rear wheels. Motion is transmitted to the wheels by using timing belts. Belt transmission doubles the motor torque and reduces the angular velocity.

Figure 3 Wheelchair Prototype Front View

Figure 4 Wheelchair Prototype Side View

Control system to be implemented is predicated on L298N H-bridge motor controlling module. H-Bridge's square measure for the most part used in predominant motor speed and course. Relate in Nursing H-Bridge consists of four relays and drive current in either directions. It is controlled with the help of Pulse breadth modulation. Pulse expansiveness Modulation could be an implies that in predominant the time of Associate in nursing electronic pulse breadth. The more drawn out the beats the snappier the wheel can flip and shorter the beats, wheel can flip slowly. Wiper motors can keep going for any longer and be a ton of solid whenever it is control by PWM [13]. Microcontroller used in this project is predicated on Arduino 2560 mega board. It has fifty four input/output pins. It has sixteen simple data sources and four UARTs equipment serial ports and a sixteen (MHz) oscillator. USB connection also available is this Arduino microcontroller. An impact jack to associate in Nursing ICSP header and reset button. [14] [15], see Figure. 5

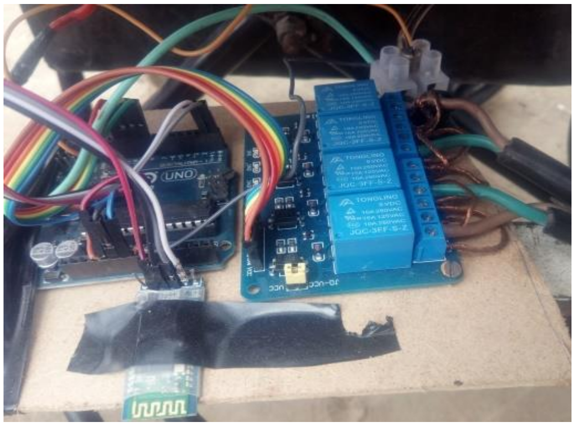

Figure 5 Control System Development of Wheelchair

III. Motion Analysis Of Wheelchair

Movement examination of wheelchair motion is performed in MSC Adams Software package, for this reason, we have imported the model developed in CREO software into Adams software package database. Through a fitting Adams-created method is broke down what's more on the grounds that the wheelchair movement flight and in this manner the movement parameters. First the parts materials assortments unit illustrated, upon the projects that figures the dormancy properties all things considered. Upon this progression, next the turn joints of the wheel's zone unit delineated. Wheelchair front wheels move independently and are fitted on structure of chair by the help of pivotal outspread heading. Kinematics of the model has been developed in Adams is shown in Figure.6

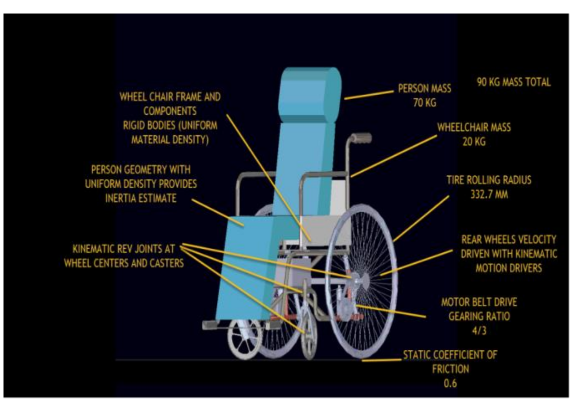

Figure 6 Wheelchair Kinematic Model in ADAMS

The contacts powers between the haggles are typically depicted by the contact mechanism demonstrate that's dictated by mechanical parameters. For example, the firmness, drive type, damping or rubbing coefficients and infiltration profundity. These parameters are characterized by concentrate advance writing [16] [17]. The wheelchair ground contacting parameters are described which are important to specify in order to obtain proper contact between the wheels and the ground. By considering the efficiency and preciseness, impact method is utilized to define wheelchair wheel and ground contact parameters [16] [18].

A. Analysis Parameters

Necessary parameters that are required to perform the motion analysis are studied form the literature and are explain here as: Coefficient of friction between ground and wheels is finalized by studying the literature and is given as

μ=0.4-0.6 this is for old asphalt and concrete type roads.

Stiffness (K) Contacting bodies detail is specified from the literature. The typical values of Poisson ratio and Young modulus for ground are v = 0.16 and E = 2.2×10^{10}(N/m^2) and for wheel v = 0.28 and E = 92 7.3 0 (N/m^2).

Force exponent (e) Value of force exponent is e=1.3. [16] [17].

Damping Coefficient. (C).In this case of simulation value of damping coefficient is used C=100 (Ns/m).
Penetration depth. In many cases reasonable value that is used for this purpose is 0.01mm. In our case we have used the value 0.1mm. Because of numerical convergences in MSc Adams software.

Typical values for dynamic friction and static friction are: μ_d = 0.18, μ_s = 0.2. Values of static and dynamic viscous velocity founded in literature are: v_s = 10mm/s, v_d =100mm/s

The Electric wheelchair movement examination has been performed in Adams software. 1st the primary case for straight line movement, the two motors are set to keep running with same speed. For this reproduction both the motors keep running with 41 (rpm), and the wheelchair movement direction has been appeared in Figure 7, the impetus torque being appeared in Figure 8. Wheelchair mass center velocity is shown in figure 9. We can observe that the Wheelchair motion speed is relatively consistent

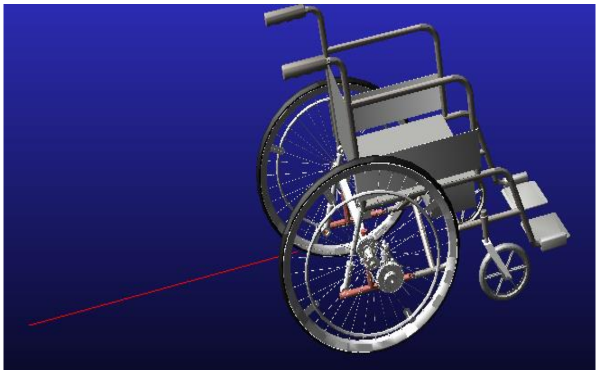

Figure 7 Straight line Motion Trajectory

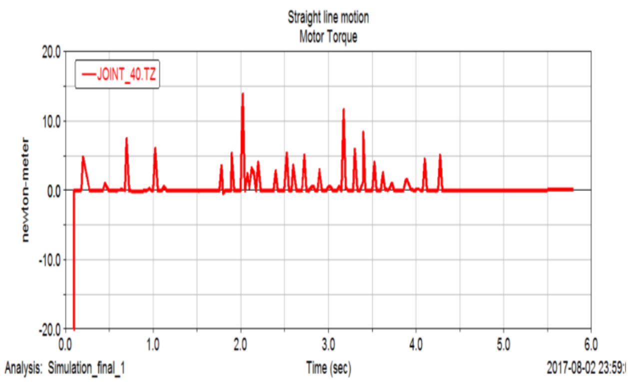

Figure 8 Propulsion Torque for Straight line motion.

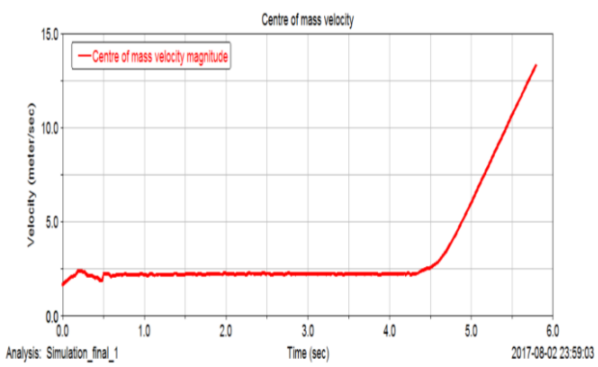

Figure 9 Wheelchair mass center velocity

In 2nd case of motion simulation, right side motor is set to run with 18.15 (rpm) and the left motor runs with 41(rpm). Traced motion trajectory of wheelchair can be observed in figure 10. Right and left motors torque measured in Adams software is given in figure 11 and 12. Wheelchair displacement is shown in figure 13 and mass center velocity in figure 14. We can see clearly that more torque is required for right wheel as compare to the left wheel. The reason is because it will spin at low angular speed.

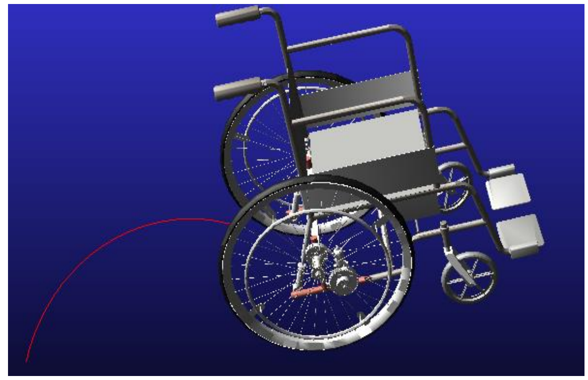

Figure 10 Wheelchair motion trajectory for steering motion

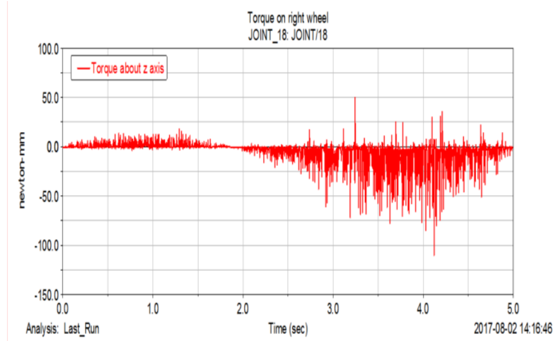

Figure 11 Propulsion torque for right wheel

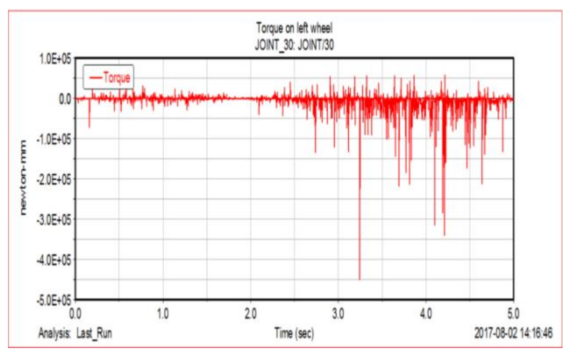

Figure 12 Propulsion torque for left wheel

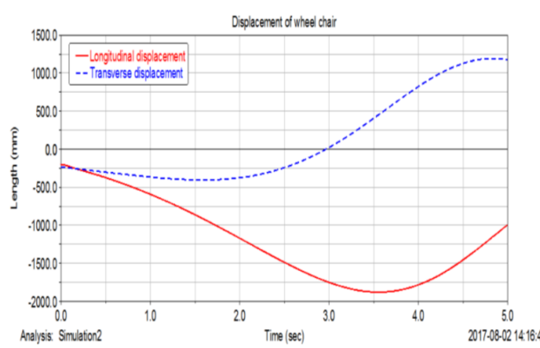

Figure 13 Displacement of wheelchair along longitudinal and transversal axis.

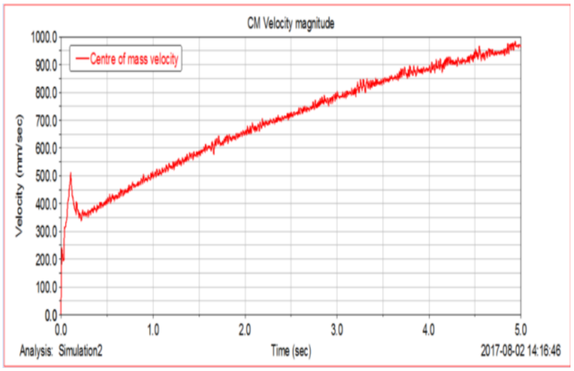

Figure 14 Wheelchair Velocity magnitude.

IV. COST ANALYSIS

This project is aimed to reduce the cost of automated wheelchair and make it available for common people. The total cost of the prototype wheelchair is shown in table 1.

Table 1. Cost Analysis of Wheelchair

Particulars	**Cost (Rupees)**
Wheel chair	4,500
Motors	2,500
Assembling and machining cost	5,000
Pulleys	4,500
Controller System	5,000
Batteries	2,500
Android phone	15,000
Total Cost	39,000

Our project cost 39,000 with a Android phone and market price of the powered wheel chair is 170, 000. [18]

V. CONCLUSIONS

The proposed wheelchair prototype model is successfully designed, implemented and controlled by using an Android application. The new innovative design and expected low cost of the automated wheelchair will make this independent mobility system available to a much broader pool of consumers than the more expensive products with safety and operational deficiencies. In the dynamic analysis on the automated wheelchair we can see that when wheelchair moves on flat type path the values of torque in straight line motion and in steering motion are little low. We can see in the results plots greater value of torque is required when the wheelchair is moving on a bump and pit type surface.

REFERENCES

[1] A. G. Rodriguez, A. G. G. Rodriguez and R. Morales, “Mechanical Synthesis for Easy and Fast Operation in Climbing and Walking Robots, Climbing and Walking Robots” IntechViena, 2010.

[2] R. Gurpude, P. Dhopte, K. Chimote, and A. Bhambulkar, “Design, Synthesis & Simulation of Four Bar Mechanism for Guiding Wheel for Climbing,” *International Journal of Computer Technology and Electronics Engineering (IJCTEE)* Vol. 2, Issue 2, April 2012.

[3] A. B. Hassan, “Design and Fabrication of a Motorized Prototype Tricycle for the Disable Persons,” *IOSR Journal of Engineering*, Vol. 2(5), pp.1071-1074. May 2012.

[4] G. Ionut Daniel, D. Nicolae, and M. Alexandru, “design and structural analysis of a powered wheelchair transmission” *acta universitatis cibiniensis – technical series.* vol. Lxvii 2015.

[5] A. Sutradhar, M. S. H. Sunny, M. Mandal, R. Ahmed, “design and construction of an automatic electric wheelchair,” presented at 3rd international conference on electrical information and communication technology (eict) khulna, bangladesh, 7-9 Dec. 2017.

[6] G. S. Modak, M. M. Bhoomkar, “Evolution of a Stair-Climbing Power Wheelchair,” *IOSR Journal of Mechanical and Civil Engineering (IOSR-JMCE)*, pp. 36-41, 2009.

[7] H. Salmin, H. Rakibul, P. Kumar Kundu, B.M. F. J. Shuvo, “Design and Implementation of an Electric Wheelchair to economize it with respect to Bangladesh,” *International Journal of Multidisciplinary Sciences and Eng*. 2014.

[8] B. James, D.S. Reswick, “Automatic transmission for electric wheelchairs,” *Journal of Rehabilitation Research and Development* Vol. 22 No. 3. June, 2012.

[9] PTC Creo 4.0. Research Software, 2016.

[10] Motor controlling manual, Palolo Simple Motor Controller User's Guide, 2001–2014.

[11] P. Wellman, V. Krovi, V. Kumar, and W. Harwin, “Design of a Wheelchair with Legs for People with Motor Disabilities,” *IEEE Transactions on Rehabilitative Eng*. Vol. 3, pp.343-353, 1995.

[12] Tesla Robotics and Electronics “Arduino Modules - L298N Dual H-Bridge Motor Controller”

[13] Dr. Subhi, R. M. Zeebaree, and H. M. Yasin, “Arduino Based Remote Controlling for Home: Power Saving, Security and Protection,” 2013.

[14] R.F. Edlich, K.P. Nelson, M.L. Foley, R.M. Buschbacher, W.B. Long and E.K. Ma, “Technological advances in powered wheelchairs,” J. Long. Term. Eff. Med. Implants, vol. 14, pp.107.130, 2004.

[15] D. Kong, J.M. Meagher, C. Xu, X. Wu, Y. Wu, “Nonlinear Contact Analysis of Gear Teeth for Malfunction Diagnostics,” presented at 5th Conference and Exposition on Structural Dynamics, 2008.

[16] MSC Adams reference manual. ISI research software, 2013

[17] K. Vernekar, and H. Kumar, “Computational and Experimental Approach for Fault Detection of Gears” *Columbia International Publishing Journal of Vibration Analysis, Measurement, and Control* Vol. 2 No. 1 pp. 16-29. 2014.

[18] V. Kaundal, R. Singh, “Low Cost Robotic Wheel Chair for Disabled People in Developing Countries” presented at Conference on Advances in Communication and Control Systems. *(CAC2S 2013)*. 2013.

Pakistan Journal of Engineering and Technology, PakJET
Multidisciplinary | Peer Reviewed | Open Access

Volume: 1, Number: 1, Pages: 57- 65, Year: 2018

Re-Strengthening/Retrofitting of Concrete Columns at Laboratory Scale Level

Dr. Abdul Ghaffar[1, *], Dr. M Burhan Sharif[2], Dr. Zia ur Rehman[2]

[1]Quaid-e-Azam College of Engg. and Tech. Sahiwal, [2]University of Engineering and technology, Lahore
*Corresponding author: Dr. Abdul Ghaffar (email: abdulpk@yahoo.com,)

Abstract*— *Natural disasters like Earthquakes, Tsunamis, Sea and Wind Storms are common in the world. Their intensity and location are unpredictable. Major effects of these natural forces are the loss of human life and property. The damage to the property is different for different locations and for different types of structures. Extensive damage requires demolishing of structures. But moderate to medium level damage to the structures can be compensated by using the re-strengthening / retrofitting techniques. Re-strengthening / retrofitting is not a latest technique used for reinforcing the structure. It is as old as humanity. Usually everyone wants to restore their property with minimum cost. These days the framed structures are very common. Moderate level damages to these structures includes plastic hinge formation at the beam column joints, spalling and partial crushing of concrete, etc. The structures which have failed to such extent but are staying at their position can be restored by retrofitting. Generally, the member dimensions are increased and a bond is created between the new material and the old material so that they both contribute against loads. In this laboratory scale level study columns are prepared and loaded to the certain damage level. After that columns are re-strengthened/retrofitted by reinforced concrete jacketing and their behavior is studied after jacketing. Testing results show that load carrying capacity of the columns is increased and columns are still useable. In this way huge cost required for demolition and rebuilding can be saved.

Index Terms*— *Re-strengthening, Retrofitting, Concrete jacketing, Reinforced concrete.

I. INTRODUCTION

If we modify the structural members in order to increase their seismic resistance, or to bear excessive ground motions and ground failures during earthquakes, such modifications are called retrofitting. As understanding of seismic behavior / demand of structures is improving day by day, and also keeping in view the lessons learnt from the recent earthquakes near and around urban areas, the requirement of retrofitting is constantly increasing.

Before the development of seismic codes, structures were used to be designed without reinforcement detailing required for protection against seismic activity, and this was done in developed countries like Japan and US till 1960s and in countries like China and Turkey till 1970s [1]. Many research organizations realized this problem, and some state of the art reports and guidelines are published to assess the seismic damage etc. and to judge the quantum of rehabilitation and retrofit requirements. i,e. ASCE-SEI 41(American Society of Civil Engineers) [2] and NZSEE's guidelines (New Zealand Society for Earthquake Engineering) [3].

Although the usual techniques available for retrofit are equally applicable to natural hazards like tornados, thunderstorms, tropical cyclones and severe-winds, however the current focus of retrofitting is primarily for improving structural performance to reduce the seismic hazards. It must be kept in mind that there is nothing like earthquake-proof structure. However, by using proper design practices or subsequently carrying out adequate retrofits, structural performance during seismic activity can be enhanced up-to a great extent [1].

Some practical applications like strengthening and seismic retrofitting have been studied in the past. These applications include the use of braces, infills or jacketing. More recently, applications like supplemental damping devices, base isolations or advanced materials including SMA (Shape Memory Alloys) or FRPs (Fiber Reinforced Polymers) are used. Most of the above-mentioned techniques are developed through research and upgrades, but issues like invasiveness, cost effectiveness and practical implementation of these techniques are still posing challenges to the researchers [3].

During an earthquake, damages of columns are more detrimental as compared to other structural parts. If severe damage occurs then there is no option except to demolish the structure and to rebuild it with seismic design provisions. If damage is small, these columns can be reused after re-strengthening / retrofitting. Among the available techniques RC jacketing is the easiest to carry out in the field. To check the effectiveness of RC jacketing a small laboratory scale study is planned, details of which are presented in the following sections.

II. LITERATURE REVIEW

Repair of a deteriorated structure or rehabilitation of damaged concrete is a science as well as an art. For repair purposes, many techniques are available out of which a suitable and adequate technique is selected for a certain work site. The basic aims of rehabilitation and repair of concrete include improving the following [4]:

1. The integrity of a structure.
2. Appearance of a structure.
3. Durability of a structure.
4. Functional performance of a structure.
5. Water-tightness of a structure.

Concrete is not only damaged by earthquakes but there are many other processes which also damage the concrete and hence reduce its load carrying capacity and its useful life. By strengthening concrete, its service life can be considerably enhanced. Defects and damages in concrete may be due to: impact or earthquake loading (called accidental loading), attacks and reactions like acid, alkali-silica, aggressive-water, alkali-carbonate, sulfates, other chemical reactions and corrosion of embedded-metals (called chemical reactions), poor-design-details or inadequate design or structural errors (called errors), cavitation and abrasion (called erosions), settlements, freezing and thawing (called movements), drying and plastic shrinkages, fire damages, weathering and internal/external temperature changes etc.[4].

Strengthening of reinforced concrete structures may be required to increase their load carrying capacities. In such situations either additional concrete elements are required or whole structure needs to be retrofitted, repaired or strengthened. For strengthening of columns commonly used methods include FRPs (fiber reinforced polymers) jacketing, steel jacketing or reinforced concrete jacketing. All above mentioned jacketing techniques are proven to effectively enhance load carrying capacities of the columns [5].

Julio Garzón-Rocaet et al. [6] conducted a series of experiments on prototype columns with steel caging, using beam-column joint simulations under axial and bending load combinations. To monolith the beam-column joints with the caging, column capitals are provided either with steel bars or chemical anchors. After experimentation it was learnt that steel caging enhanced both the ductility and failure loads of the strengthened columns.

Khair Al-DeenIsamBsisu [7] conducted theoretical as well as experimental study on twenty different RCC columns, which were retrofitted using steel-jacketing technique. Concentric axial loads were used to test all these twenty columns. According to his conclusions retrofitted square RC columns using full steel jackets, enhancement in compressive strength is more than 100% above the strength of originally un-retrofitted column. The confinement provided by the steel jacketing has also improved the ductility of the column.

Pasala Nagaprasad et al. [8], suggested a rationalized design approach for concrete columns for proportioning the steel cage depending upon its confinement effects, and to validate the suitability of proposed design approach and steel cage detailing in the vicinity of regions of expected plastic hinges. From his study he concluded that RC columns found deficient under combined axial and cyclic lateral loading, their performance can be improved using steel caging technique, even without use of binding materials in the gaps existing between steel angles and the concrete. Encouraging results are obtained from the study and the proposed design approach was found to be reasonably accurate. Detailing of end battens of the steel cage located in the potential plastic hinge region played an important role in improving the column’s overall behavior under lateral loads. By increasing the width of the end-battens, plastic rotational capacity is increased as well, while improving the lateral load resistance. However, a minor overall effect on energy dissipation was observed.

Rosario Montuori et al. [9], tested thirteen different specimens under axial load. He suggested a theoretical model for prediction of moment-curvature behavior of reinforced concrete columns which are confined using angles and battens. According to authors proposed theoretical model proved its ability for predicting the performance of strengthened columns with angles and battens.

This present study is conducted to evaluate effect of RC jacketing on the behavior of damaged RC columns. A comparison is made between the capacities of original column without jacketing and damaged column with jacketing.

III. EXPERIMENTATION

For the purpose of this research, columns of 6-inch x 6-inch x 36-inch (152 mm x 152 mm x 914 mm) were casted. Number of columns was three designated as C-1, C-2 and C-3 with varying concrete strengths. These columns were reinforced with 4 - # 3 (9.5 mm) bars. Stirrups of # 2 (6.4 mm) size were provided at 4-inch (100 mm) c/c. Four cubes are casted from the mix of each column and tested at the ages of 7 and 28 days. The observed concrete strengths are given in the Table 1, whereas columns casted in lab. and reinforcement details are given in Figure: 1.

Table 1 Strength of concrete used for casting columns.

Column	Type of Specimen	7 days strength			28 days strength		
		Load (tonns)	(psi)	Average	Load (tonns)	(psi)	Average
C-1	Cylinder	21.25	1684	**1654 Psi (11.4 MPa)**	26.6	2107	**2064 psi (14.23 MPa)**
	Cylinder	20.50	1624		25.5	2020	
C-2	Cylinder	24	1901	**2060 Psi (14.2 MPa)**	39	3090	**2733 psi (18.85 MPa)**
	Cylinder	28	2218		30	2377	
C-3	Cylinder	37	2931	**3010 Psi (20.76 MPa)**	52	4120	**3882 psi (26.77 MPa)**
	Cylinder	39	3090		46	3644	

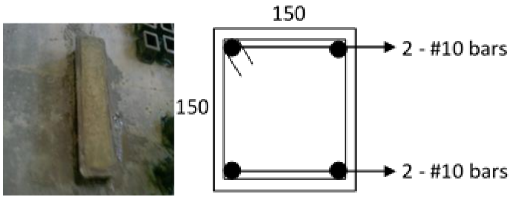

Figure 1 Casting of columns in the laboratory and reinforcement details.

After 28 days of curing, columns were tested using universal testing machine. Axial loads as well as deformation in all three axes were noted. Longitudinal axis was designated as z-axis whereas cross-sectional axes were designated as x and y axis. Deformations in all three axes were noted with the help of dial gauges and are reported in the following sections. Columns were loaded up to failure and failure load was recorded from the display of UTM. Different staged of testing and failure are shown in Figure: 2.

Stage 1

Stage 2

Stage 3

Stage 4

Stage 5

Stage 6

Figure 2 Different stages of experimentation.

After complete failure, columns were retrofitted by jacketing RCC around the failed columns. Thickness of jacketing was 1.5" (38 mm), hence column dimensions were 9" x 9" x 36" (228 x 228 x 914 mm) after jacketing. Column was reinforced with 4 - # 3 (9.5 mm) bars and stirrups of # 2 (6.4 mm) bars. Reinforcement bars of jacket were attached to dowels drilled in the failed columns. Process of jacketing and final cross-section of retrofitted column is shown in Figure: 3.

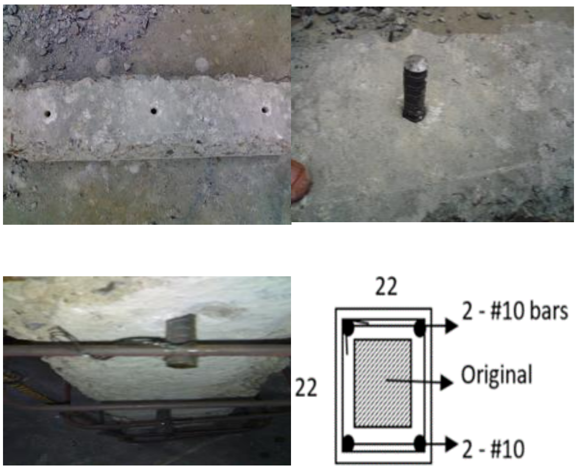

Figure 3 Reinforcement details of retrofitted column.

IV. EXPERIMENTAL RESULTS AND DISCUSSION

Columns are tested using Universal Testing Machine installed in the Test Floor lab of UET, Lahore. Longitudinal axis is designated as z-axis whereas cross-sectional axes are designated as x and y axis. Deformations in all three axes are noted with the help of dial gauges and are reported in the following sections. Results obtained for column C-1 Before and after retrofitting are shown in tables 2. Whereas load deformation curves for column C-1 before and after retrofitting are shown in Figures 4 and 5.

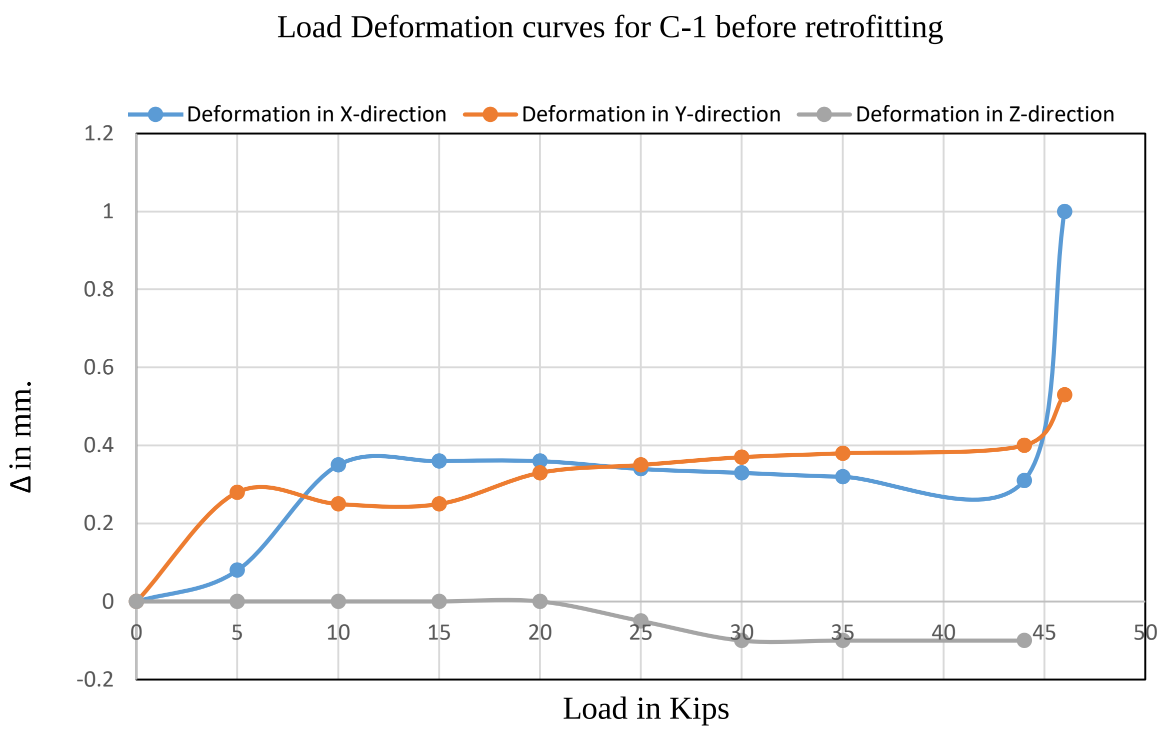

Figure 4 Load deformation curves of column C-1 before retrofitting.

Table 2 Performance of column C-1 before and after retrofitting.
Δ_x, Δ_y and Δ_z represent the deformations in x, y and z directions.

Sr. No.	**Performance Before Retrofitting**					**Performance After Retrofitting**			
	LOAD	Δ_x	Δ_y	Δ_z	**REM.**	Δ_x	Δ_y	Δ_z	**REM.**
	(Kips)	**mm.**	**mm.**	**mm.**		**mm.**	**mm.**	**mm.**	
1	0	0	0	0		0	0	0	
2	5	0.08	0.28	0		0.05	0	-0.1	
3	10	0.35	0.25	0		0.15	0.05	-0.1	
4	15	0.36	0.25	0		0.22	0.07	-0.1	
5	20	0.36	0.33	0		0.3	0.07	-0.2	
6	25	0.34	0.35	-0.05		0.33	0.1	-0.2	
7	30	0.33	0.37	-0.1		0.38	0.1	-0.2	
8	35	0.32	0.38	-0.1		0.4	0.1	-0.3	
9	40	0.31	0.39	-0.1		0.4	0.1	-0.3	
10	44	0.31	0.4	-0.1	major cracks appeared				
11	45					0.4	0.1	-0.3	
12	46	1	0.53		Failure	0.4	0.1	-0.3	
13	47.4					0.43	0.13	-0.4	major cracks appeared
14	50					0.45	0.2	-0.4	
15	55					0.45	0.1	-0.5	
16	69								Failure

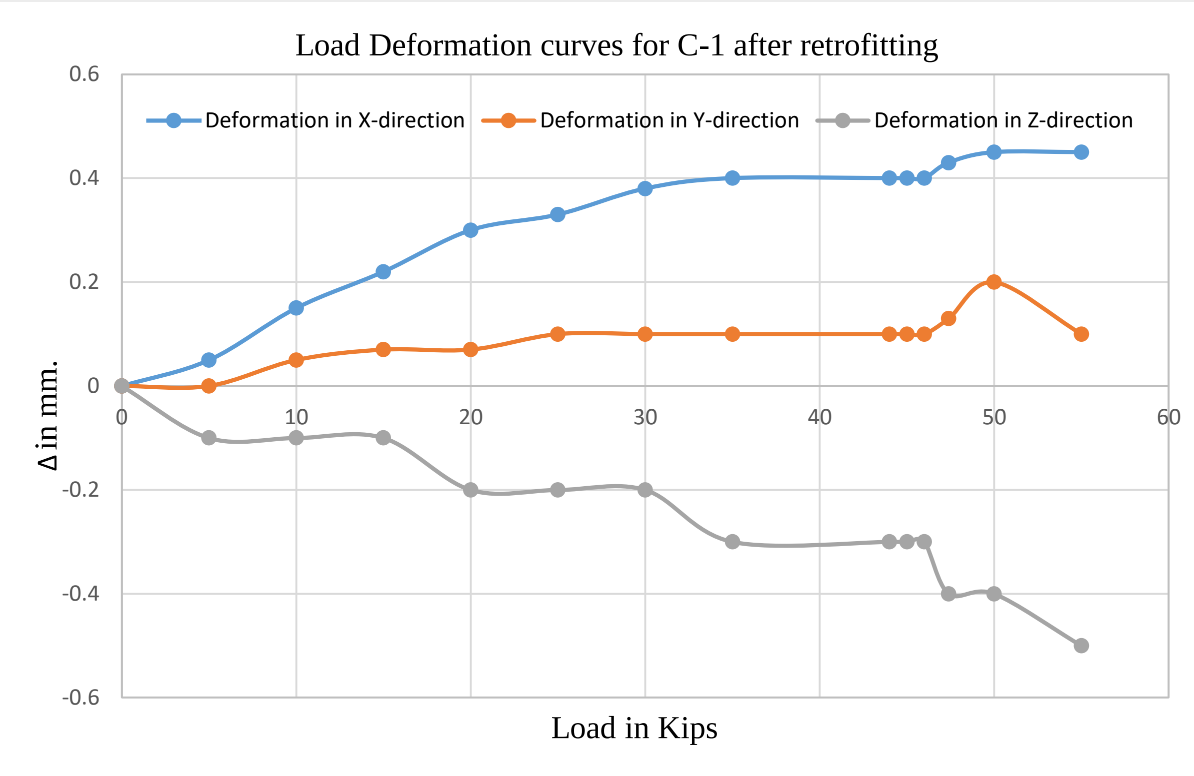

Figure 5 Load deformation curves of column C-1 after retrofitting.

Columns C-2 and C-3 are tested in the same manner. Results obtained for column C-2 and C-3 before and after retrofitting are shown in tables 3and 4 respectively. Whereas load deformation curves for columns C-2 and C-3 before and after retrofitting are shown in Figs 6 to 9.

Table 3 Performance of column C-2 before and after retrofitting.
Δ_x, Δ_y and Δ_z represent the deformations in x, y and z directions.

Sr. No.	**Performance Before Retrofitting**					**Performance After Retrofitting**			
	LOAD	**Δ_x**	**Δ_y**	**Δ_z**	**REM.**	**Δ_x**	**Δ_y**	**Δ_z**	**REM.**
	(Kips)	**mm.**	**mm.**	**mm.**		**mm.**	**mm.**	**mm.**	
1	0	0	0	0		0	0	0	
2	5	0	0.1	-0.1		0.23	0	0	
3	10	0.08	0.2	-0.2		0.23	0.03	-0.2	
4	15	0.13	0.25	-0.3		0.26	0.11	-0.5	
5	20	0.15	0.31	-0.3		0.64	0.59	-0.6	
6	25	0.16	0.36	-0.3		0.69	0.74	-0.7	
7	30	0.17	0.43	-0.4		0.76	0.89	-0.7	
8	35	0.18	0.5	-0.4		0.79	0.91	-0.7	
9	44	0.19	0.58	-0.5		0.84	0.94	-0.7	
10	45	0.25		-0.6	major cracks appeared	0.89	0.97	-0.8	
11	49	0.5			Failure				
12	50					0.89	0.97	-0.8	
13	55					0.89	0.97	-0.8	
14	60					0.89	1.05	-0.8	
15	67					0.89	1.27	-0.8	major cracks appeared
16	72					0.89	1.48	-0.8	
17	73					0.89	1.55		Failure

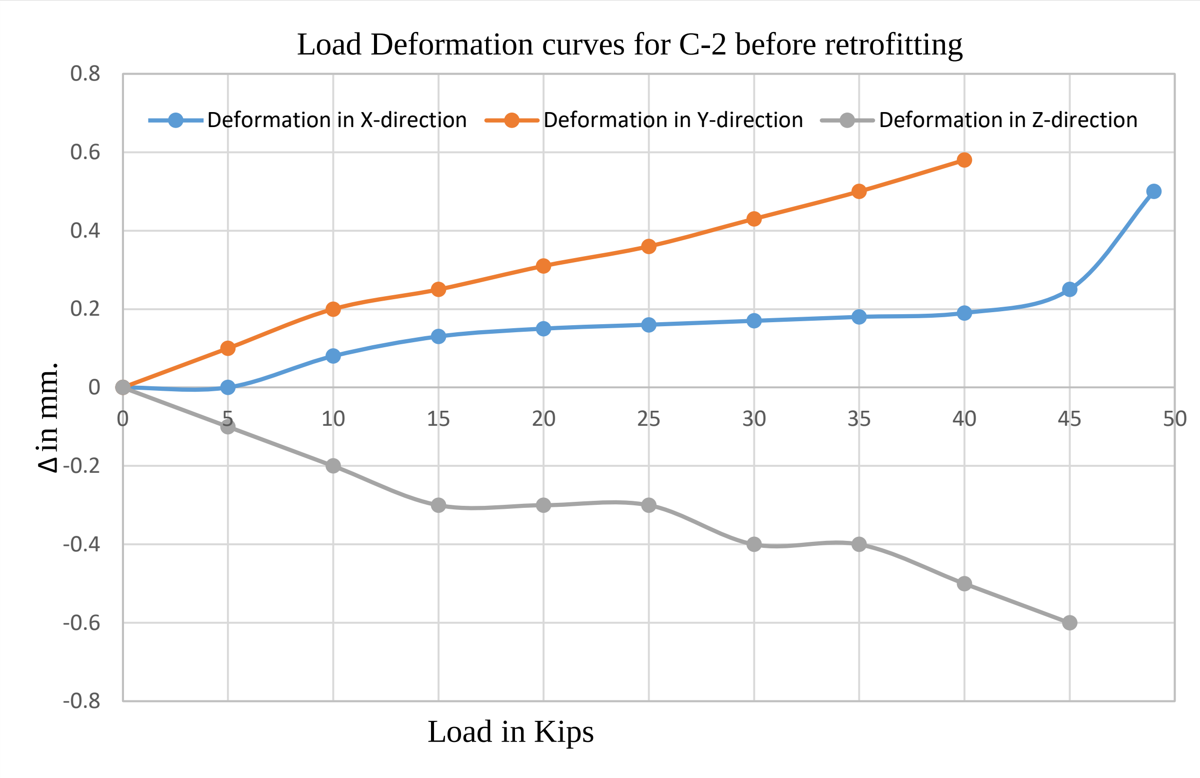

Figure 6 Load deformation curves of column C-2 before retrofitting.

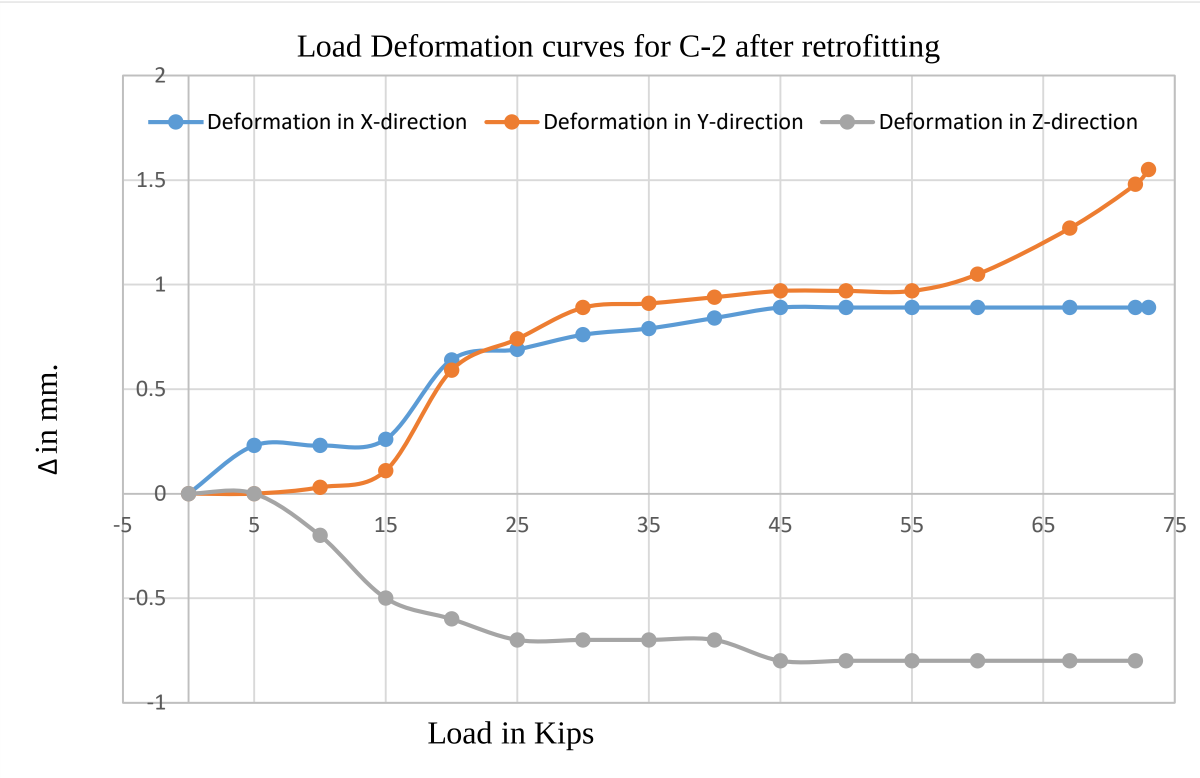

Figure 7 Load deformation curves of column C-2 after retrofitting.

Table 4 Performance of column C-3 before and after retrofitting.
Δ_x, Δ_y and Δ_z represent the deformations in x, y and z directions.

Sr. No.	Performance Before Retrofitting					Performance After Retrofitting			
	LOAD	Δ_x	Δ_y	Δ_z	REM.	Δ_x	Δ_y	Δ_z	REM.
	(Kips)	mm.	mm.	mm.		mm.	mm.	mm.	
1	0	0	0	0		0	0	0	
2	5	0.2	0.05	-0.1		0.06	0	-0.1	
3	10	0.25	0.05	-0.1		0.15	0.03	-0.2	
4	15	0.29	0.06	-0.1		0.46	0.23	-0.4	
5	20	0.32	0.08	-0.2		0.64	0.58	-0.6	
6	25	0.35	0.1	-0.2		0.71	0.7	-0.6	
7	30	0.37	0.11	-0.2		0.79	0.89	-0.7	
8	35	0.38	0.13	-0.3		0.81	0.91	-0.7	
9	44	0.38	0.13	-0.3		0.84	0.94	-0.7	
10	45	0.38	0.13	-0.3		1.31	0.94	-0.7	
11	50	0.38	0.13	-0.3		0.89	0.96	-0.8	
12	55	0.38	0.13	-0.4	major cracks appeared	0.89	0.99	-0.8	
13	59				Failure				
14	60					0.89	1.04	-0.8	
15	65					0.89	1.14	-0.8	
16	70					0.89	1.47	-0.8	
17	75					0.93	1.62	-0.9	
18	80					0.99	1.73	-1	
19	85					1.17	1.93	-1	major cracks appeared
20	87								Failure

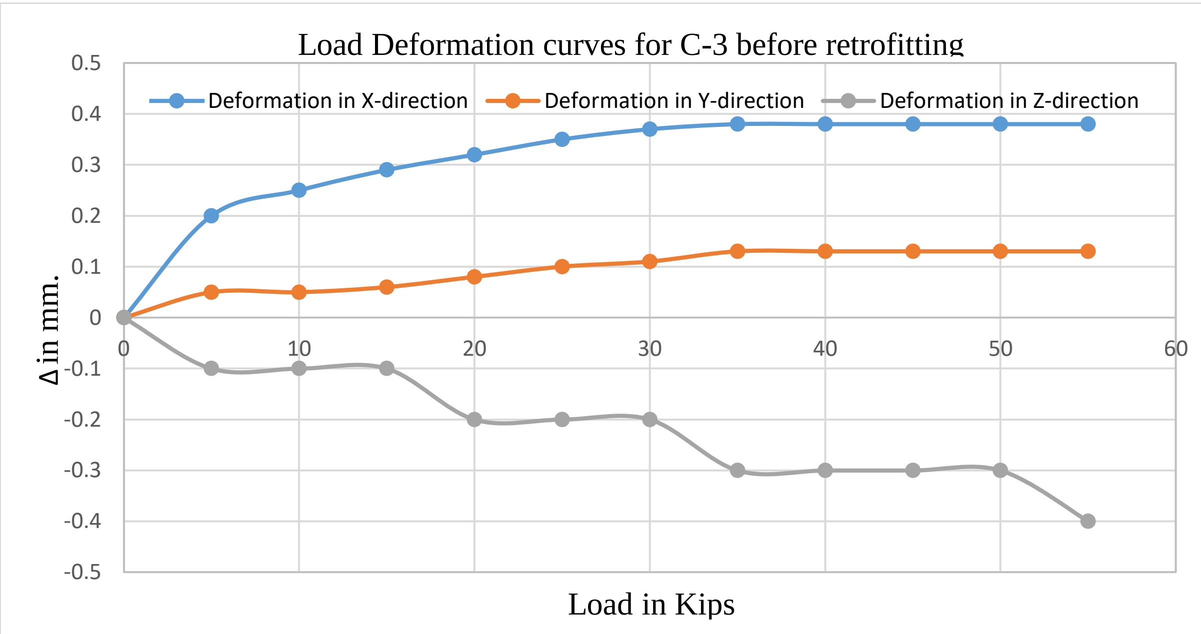

Figure 8 Load deformation curves of column C-3 before retrofitting.

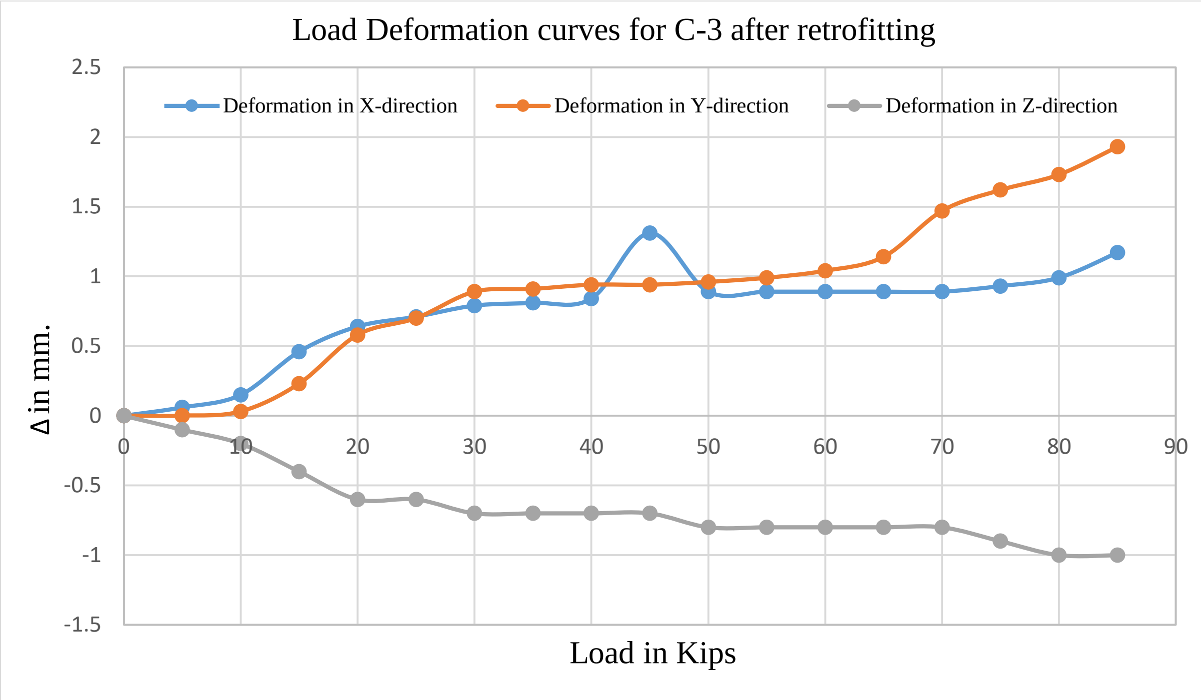

Figure 9 Load deformation curves of column C-3 after retrofitting.

Table 5 Over all summary of test results.

	Column C-1	Column C-2	Column C-3
Concrete Strength before Retrofitting	44000	49000	59000
Concrete Strength after Retrofitting	69000	73000	87000
Increase	56.82 %	48.98%	47.46%
Max. Deformation before Retrofitting	0.4	0.6	0.6
Max. Deformation after Retrofitting	1.17	1.93	1.0
Increase	179.3%	221.7%	66.7%

V. CONCLUSIONS

From the observations of the above study, it is evident that retrofitting by RC jacketing is an easy and viable method for re-strengthening of the damaged concrete columns. It is very simple and no precise and expensive equipment is needed for this purpose. Moreover, this kind of strengthening can be performed for any type of concrete column. On the basis of the experimentations following conclusions are drawn from the study:

1. Observed load capacity of the retrofitted columns increased upto 47.46 to 56.82 %.
2. Area of concrete is 36 in^2 (23104 mm^2) before retrofitting and 45 in^2 (29032 mm^2) after retrofitting. It means area of concrete increased by 25 %, whereas load carrying capacity increased upto 56.82 %. This extra benefit comes from decrease in slenderness ratio of the column.
3. Retrofitted columns show reduction in load capacity with increase in concrete strength.
4. Deformations of retrofitted columns are also increased upto 221.7 %. It means retrofitting also increase the ductility of concrete columns.

REFERENCES

[1] https://en.wikipedia.org/wiki/Seismic_retrofit, accessed On October 21, 2017.
[2] P. Ricci; G. M. Verderame; and G. Manfredi; "ASCE/SEI 41 Provisions on Deformation Capacity of Older-Type Reinforced Concrete columns with Plain Bars" Journal of Structural Engineering, Volume 139 Issue 12 - December 2013
[3] S. Pampanin, Controversial aspects in seismic assessment and retrofit of structures in modern times: understanding and implementing lessons from ancient heritage, bulletin of the new zealand society for earthquake engineering, Vol. 39, No. 2, June 2006.
[4] K. Soudki; Concrete Problems and Repair Techniques https://www.sefindia.org/forum/download.php?id=11783&sid., accessed on October 21, 2017.

[5] M. F. Belal; H. M. Mohamed; S.A., Morad; Behavior of reinforced concrete columns Strengthened by steel jacket, Housing and Building National Research Center Journal 11, 201–212, 2015.
[6] R. Julio, P. Joaquı´n, A. Jose, C. Pedro. An experimental study onsteel-caged RC columns subjected to axial force and bendingmoment, Eng. Struct. J. 33, 580–590, 2010.
[7] B. Khair, Retrofitting of Square Reinforced Concrete Columns Subjected to Concentric Axial Loading with Steel Jackets, The Third Engineering Consultant work conference, Palestine, 2009.
[8] N. Pasala, S. Dipti, R. Durgesh, Seismic strengthening of RC columns using external steel cage, Earthquake Eng. Struct. Dyn.J. 38,1563–1586, 2009.
[9] M. Rosario, P. Vincenzo. Reinforced concrete columns strengthened with angles and battens subjected to eccentric load, Eng. Struct.31, 539–550, 2008

Pakistan Journal of Engineering and Technology, PakJET
Multidisciplinary | Peer Reviewed | Open Access

Volume: 1, Number: 1, Pages: 66- 70, Year: 2018

Assessment of Bond Strength between Concrete and Repairing Cementitious Concrete in Tension and Shear

Imran Nazir[1], Khuram Rashid[2,*]

[1]Department of Architectural Engineering and Design, University of Engineering and Technology;
[2]Department of Architecture, University of Lahore
*Corresponding author: Khuram Rashid (email: khuram_ae@uet.edu.pk)

***Abstract*—To evaluate the bond strength, an experimental work was performed in tension and shear between old concrete and new repairing concrete. Various adhesives, epoxies and fiber reinforced polymer sheet were used at interface on the roughened substrate surface to increase the bond strength. Steel wire brush was used for roughening of substrate surface. Bi-surface shear test and Split tensile test were performed on 150 mm cube to quantify the bond strength in shear and tension, respectively, of composite specimens. The solid specimen is referred to as bulk specimen compared with the composite specimen. Bulk specimen's tensile strength and shear strength were also assessed and it was observed that bond strengths is less than the bulk specimen strengths of both types, that is, tensile and shear. In composite specimens adhesive mode of failure was observed that verify the weakness of interfacial zone. Some improvement in bond strength was also observed with the application of different materials at interface.**

***Index Terms*—Bond strength, Concrete, Repair, Rehabilitation, Silica fume, Strengthening.**

I. INTRODUCTION

Concrete is the cast-in-place, economic and readily available construction material. The regular concrete can be used a s repair material or various other materials may be added to enhance its properties as a repair material. Concrete may be used for a wide variety of structures that include highway bridges, high-rise buildings, tunnels, offshore structures, dams and parking structures. One of the major problems impacting the long-term performance of concrete repairs and bonded overlays is cracking or fracture and their debonding from the concrete substrate. It is a fact that most of the structures built during rapid urbanization of last six or seven decades have either passed their service life or their load rating does not match with the current needs. Rehabilitation and strengthening of this infrastructure is a need of the hour. Special techniques using well developed materials may be employed to not only repair and rehabilitate the structures but also to strengthen the existing structures for the present day loadings and other needs. This can prolong the useful service life of the structures and can increase their stiffness for reduced deflections and vibrations. A monolithic action between the substrate concrete and repairing concrete is essential for the repair to be successful. For this monolithic action, a suitably strong and durable bond between the existing concrete and the repair material is required. There are many materials and admixtures available in construction industry to improve the strength and durability of repairing concrete. Silica fume is one of them which is used as partial replacement of cement in the concrete.

Significant research literature is available regarding the mechanisms, limitations and improvements of bond between existing concrete and repair materials. However, the guidance available in the codes and specifications for keeping an eye on the bond behavior of the repair is limited. There are a large number of factors and practical issues related with the short term and long term performance of the bond strength of the repair materials. One of the major factors affecting this behavior is surface preparation of concrete substrate. A sufficiently clean, lightly rough and stable base material is required to improve the bond strength. It is to be noted that the debonding shear failure may only occur at the interface of the two materials but also just below the interface within the existing concrete surface. The selection of the bonding material itself for a particular application is also an important parameter.

II. LITERATURE REVIEW

Concrete jacketing is most commonly used strengthening technique for structural elements. The concrete surface preparation is equally important for this type of repair. Sometimes, steel dowels are also introduced to strengthening the bond between the existing and the new concretes. Julio, Bronco and Silva and Bett [3], Klinger and Jirsa [4] experimentally studied the behavior of RC columns that were strengthened by jacketing. Surface cleaning and roughening were carried out by using sand blasting. Alcocer and Jirsa [5] worked on the behavior of deficient RC connections overlaid by jacketing. The concrete cover was removed to expose the outermost concrete aggregate by chisel and hammer. Subsequently, Alcocer [6] extended the experimental program by modifying the surface preparation technique. Surface was first prepared as in the original research but thick brush and vacuum cleaner were used in the second step to further clean the surface. Ramirez et al. [7] repaired partially damaged RC columns that were then tested to observe their behavior. The exposed concrete surface and reinforcing bars of all the columns to be repaired were thoroughly cleaned by brushing with a hard wire brush. The research work of Rodriguez and Park [8] consisted of experimentally studying the behavior of strengthened RC columns against simulated seismic loading. Concrete jacketing was used for the strengthening and chipping was employed to prepare the surface of the columns. Stoppenhagen et al. [9] also used jacketing technique to strengthen severely damaged concrete frames. These frames were then tested to evaluate their response against applied loading. An electric chipping hammer was used to roughen the concrete substrate. Influence of the roughness of the substrate surface for the concrete to concrete bond was studied by Julio et. al. [10]. They found that sand blasting is the best technique for roughening the substrate surface to get best bond strength in tension and shear.

All the above mentioned research points towards the importance of getting better bond strength between the original concrete and the concrete of the jacketing. However, the research on directly evaluating this bond strength is still limited. The bond at the interface between two concretes can be experimentally verified by performing either splitting tensile test or by direct shear test. Composite samples can be prepared by joining two pieces of concrete employing selected surface preparation method and bonding technique. Solid monolithic samples may be prepared for the required comparison. These samples are referred to as the “bulk” samples in this research work.

III. METHODOLOGY

Split tensile and Bi-Surface shear tests were performed on three cubical specimens of size 150 mm for bulk and composite specimens to assess the bond strength in tension and shear between concrete and repairing cementitious concrete respectively. Number of specimens for each case is mentioned in Table-1.

Compressive strength

Three cubical bulk specimens of 150 mm size for cement concrete and repairing cementitious concrete were tested to evaluate compressive strength of each material as shown in Fig.2. It was preferred that repairing concrete should have more compressive strength than substrate cement concrete.

Split tensile strength test

As shown in Fig.1(a & b), bond strength in tension between old concrete and new repairing concrete composite specimens were evaluated by performing split tensile test according to ASTM C496 [1]. Bond strength in tension at the interface of two materials in the composite samples of was evaluated by using eq. (1). The same equation was also used for the bulk specimen. The average ultimate load was taken from the experimental data presented in Tables 2 and 3.

$$f_t = \frac{2P_{ut}}{\pi A_t} \tag{1}$$

Where, f_t = Bond strength in tension (MPa); P_{ut} = Average ultimate load (N); A_t = Area of interface (mm^2).

Bi-Surface shear strength test

As shown in Fig.1(c & d), bond strength in shear between old concrete and new repairing concrete composite specimens were evaluated by performing bi-surface shear test. The test details as used by Momayez et. al. [2] were used for the present work. Bond strength in shear of bulk and composite specimens was evaluated by using eq. (2) from average ultimate load of three specimens (Table 2 and 3).

$$f_t = \frac{P_{uv}}{2A_v} \tag{2}$$

where, τ_v = Interfacial bond strength in shear (MPa); P_{uv} = Average ultimate load (N); A_v = Area of interface in shear (mm^2).

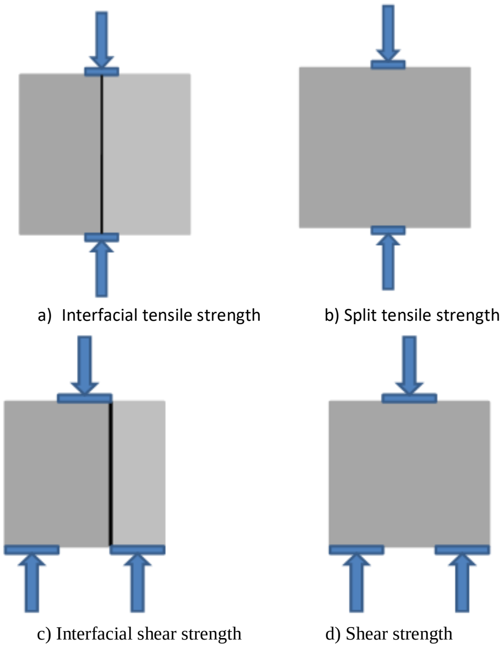

Figure 1 Split and shear bond strength determination.

Various adhesives, epoxies and fiber reinforced polymer sheet were used at interface on the roughened substrate surface to increase the bond strength. Steel wire brush was used for roughening of substrate surface to get better bond offered by friction.

Materials

M-25 concrete (1:1:2) was prepared with water cement ratio (W/C) as 0.45 while repairing cementitious concrete was also prepared with the same mix and water cement ratio but 10% cement was replaced with silica fume. Four types of surface treatments; i) cement paste, ii) epoxy, iii) bonding adhesive and iv) fiber reinforced polymer sheet, were used to prepare the substrate surface and to test which type of chemical is most effective to improve the bond strength in tension and shear.

Specimen preparation

At 1st stage, 150 x 150 x 75 mm (6 x 6 x 3 in.) and 150 x 150 x 100 mm (6 x 6 x 4 in.) specimens were casted for composite specimens using cement concrete for split tensile strength and bi-surface shear strength test respectively. At the same time, bulk specimens of 150 x 150 x 150 mm (6 x 6 x 6 in.) size were also prepared using cement and silica fume in concrete. Wooden molds were prepared to cast these specimens. After 28 days of wet curing in water tank, specimens were taken out and were surface dried [Fig. 2]. Then, its surface having 150 x 150 = 22,500 sq.mm (36 sq.in.) area was roughened by using steel wire brush applied mechanically to get better roughened surface.

Figure 2 Preparation of concrete specimens

Table 1 Number of specimens and types of tests performed to evaluate bond strength.

Test	Strength		
	Compressive	Tensile	Shear
Substrate concrete	3	3	3
Repairing concrete	3	3	3
[1]Comp-CP	---	3	3
[2]Comp-C32	---	3	3
[3]Comp-SBR	---	3	3
[4]Comp-FRP	---	3	3

[1]Composite specimens with cement paste at interface.
[2] Composite specimens with epoxy C32 at interface.
[3] Composite specimens with SBR at interface.
[4] Composite specimens with FRP at interface.

At 2nd stage, epoxy, adhesive, cement paste and fiber reinforced polymer sheet were applied, as per guidelines of vendor, on roughened substrate surface and remaining part of cubes were casted with cementitious concrete to form a complete 150 x 150 x 150 mm (6 x 6 x 6 in.) composite cube. After final setting time, specimens were de-molded and placed in water tank for 28 days curing.

After 28 days of curing, specimens were taken out. Cutting and grinding was performed on sides of the specimens whose surfaces were not proper, so that load can be transferred correctly.

(a) old treated substrate

(b) Pouring of repairing concrete

Figure 3 Preparation of composite specimens.

IV. RESULTS AND DATA DISCUSSION

Replacement of cement with silica fume increases the density of concrete which ultimately results in more strength for repairing concrete (Table-II). Results also prove that shear strength of ordinary concrete or repairing concrete is more than tensile strength. 10% silica fume replacement gives better tensile and shearing strength than cement concrete without silica fume.

Table 2 Test results of bulk specimens.

Test	Strength		
	Compressive	Tensile	Shear
Substrate concrete	30.31	3.69	6.03
Repairing concrete	43.42	4.85	7.87

Table 3 Test results of composite specimens.

Specimen	Tensile (MPa)	Shear (MPa)
Cement paste at interface	0.312	0.770
Epoxy C32 at interface	0.384	0.350
SBR at interface	0.462	0.530
FRP at interface	0.569	0.820

Bond strength in tension

Results dictate (Table-III) that fiber reinforced polymer is best surface treatment for bond strength in tension while at second, SBR latex gives better results. Epoxy stands at third number as its bond strength in tension is the lowest in chemicals. Cement paste as used locally in our country to bond old and new concrete is poor in tensile strength of bond. The results are graphically shown in Fig. 3.

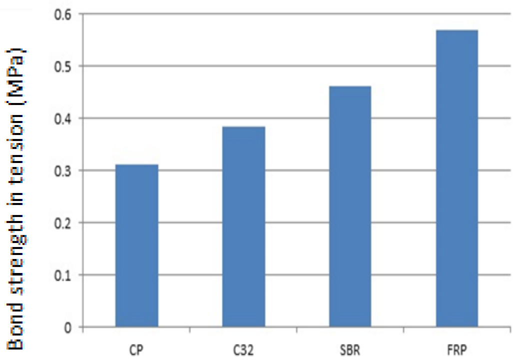

Figure 3 Bond strength in tension using different substrate surface treatments

Bond strength in shear

In case of shearing strength of bond between concrete and repairing concrete, FRP gives best results while cement paste is very close to FRP and was considered as best in shear too. Epoxy gives poor results. The results are graphically displayed in Fig. 4.

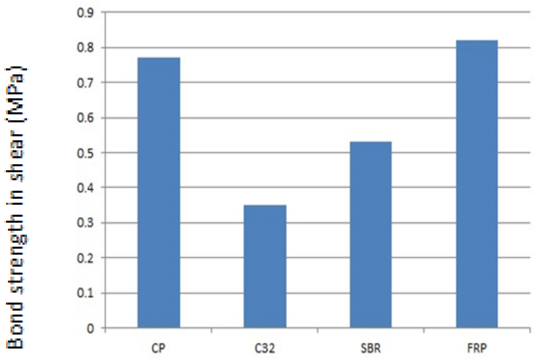

Figure 4 Bond strength in shear using different substrate surface treatments

V. ACKNOWLEDGMENT

The author is grateful to Imporient Chemicals Pvt. Ltd. (ICPL) for providing epoxy, SBR latex and fiber reinforced polymer sheet. The author is very thankful to University of Engineering and Technology, Lahore and Techno Times Construction Company for assistance in casting and testing.

REFERENCES

[1] ASTM C 496-04, Standard test method for splitting Tensile strength of cylindrical concrete specimens, *ASTM International, USA*, 2004.

[2] A. Momayez, M. Ehsani, A. Ramezanianpour, H. Rajaie. Comparison of methods for evaluating bond strength between concrete substrate and repair materials, *Cem. Concr. Res. 35* (4) 748-757, 2005.

[3] ES. Julio, F. Branco, VD. Silva. Structural rehabilitation of columns using reinforced concrete jacketing. *Prog Struct Eng Mater* 5:29–37, 2003.

[4] BJ. Bett, RE. Klingner, JO. Jirsa. Lateral load response of strengthened and repaired reinforced concrete columns. *ACI Struct J;85*(5):499–508, 1988.

[5] S. Alocer, J. Jirsa. Assessment of the response of reinforced concrete frame connections redesigned by jacketing. In: Proceedings of the *Fourth US National Conference on Earthquake Engineering.* vol. 3. May; p. 295–304, 1990.

[6] JL. Ram_ırez, JM B_arcena, JI Urreta, e JA S_anchez. Repair of concrete columns with partial localized damages. *Report T 2.1 and 2.2 BREU–0186*–C, April 1991.

[7] SM. Alcocer. RC frame connections rehabilitated by jacketing. *J Struct Eng;119*(5): 1413–31, 1993.

[8] M. Rodriguez, R. Park. Seismic load tests on reinforced concrete columns strengthened by jacketing. *ACI Struct J* March–April:150–9, 1994.

[9] Dr. Stoppenhagen, JO. Jirsa, LA. Wyllie Jr. Seismic repair and strengthening of a severely damaged concrete frame. *ACI Struct J*; March–April:177–87, 1995.

[10]E.N.B.S. Julio, F. A.B. Branco, V. D. Silva. Concrete to concrete bond strength. Influence of the roughness of the substrate surface. *Cons. Buil. Mate.* 18 675-681, 2004.

Pakistan Journal of Engineering and Technology, PakJET
Multidisciplinary | Peer Reviewed | Open Access

Volume: 1, Number: 1, Pages: 71- 78, Year: 2018

Analysis, Field Testing and Evaluation of Fatigue Life of Plate Girder Railway Bridge at Ravi River

Dr. Mahboob Ali Ch.[1,*], Dr. Zahid A. Saddiqi[2], M. Shoaib Sarwar[2]

[1]Department of Civil Engineering, The University of Lahore, [2]Unit Manager, Fatima Energy
*Corresponding author: Dr. Mahboob Ali Ch. (email: drmahboob@ce.uol.edu.pk)

***Abstract*— Natural disasters like Earthquakes, Tsunamis, Sea and Wind Storms are common in the world. Their intensity and location are unpredictable. Major effects of these natural forces are the loss of human life and property. The damage to the property is different for different locations and for different types of structures. Extensive damage requires demolishing of structures. But moderate to medium level damage to the structures can be compensated by using the re-strengthening / retrofitting techniques. Re-strengthening / retrofitting is not a latest technique used for reinforcing the structure. It is as old as humanity. Usually everyone wants to restore their property with minimum cost. These days the framed structures are very common. Moderate level damages to these structures includes plastic hinge formation at the beam column joints, spalling and partial crushing of concrete, etc. The structures which have failed to such extent but are staying at their position can be restored by retrofitting. Generally, the member dimensions are increased and a bond is created between the new material and the old material so that they both contribute against loads. In this laboratory scale level study columns are prepared and loaded to the certain damage level. After that columns are re-strengthened/retrofitted by reinforced concrete jacketing and their behavior is studied after jacketing. Testing results show that load carrying capacity of the columns is increased and columns are still useable. In this way huge cost required for demolition and rebuilding can be saved.**

Index Terms*— *Re-strengthening, Retrofitting, Concrete jacketing, Reinforced concrete.

I. INTRODUCTION

Most of Pakistan Railways bridges had been put in service more than 100 years ago. Nothing has been done on analysis of these bridges. However routine preventive maintenance and inspections are carried out by Railways. Similarly, Ravi Railway bridge has never been studied under modern loading and traffic requirements and neither has been rehabilitated or strengthened. Nevertheless, bridge piers have been reported to be repaired along with the routine maintenance involving painting of steel elements.

It has become a crucial requirement to work out remaining serviceable life of the railway bridge. Also with the transformation of Pakistan Railways on advanced model trains network with the use of latest and modern locomotives of high speed, it is a requirement of time to check the adequacy of existing old bridges. And as a result a rehabilitation and strengthening program is worked out.

The bridge under study links the towns of Badami Bagh and Shahdara and crosses over River Ravi. Up line has been supported on a deck bridge which is a riveted connected structure. The line was set up for traffic in April 12th, 1875. Down Line bridge has been supported on a truss deck structure that is with riveted connection too. This line was opened for traffic on January 10th, 1913. The railway bridge consists of 15 (fifteen) simply supported spans. Each span is of 94'-6". Up Line Track has been placed on top flange of the steel girder whereas Down line track has been fixed on top members of the steel truss.

In developing this paper, the basic and advanced concepts of fatigue have been taken from ESDEP (European Steel Design Education Program) lectures on Fatigue. These lectures at Ref-2 & 3 below introduce the main concepts and definitions regarding the fatigue process and the main factors that influence the fatigue performance of materials, components and structures.

Another research (Ref-6) describes the result of a study conducted on detailed examination of fatigue test data, other data from studies elsewhere in the world and the results of 14 fatigue and fracture tests on full scale members removed from bridges.

The paper by P. Kunz and M. A. Hirt(Ref-7) presented at Third International Workshop on Bridge Rehabilitation, Technical University, Damstadt, presents a method for evaluation of the failure probability of construction details. This probability has been recommended to be considered during decisions on maintenance and in particular for the selection of supervision and inspection intervals.

Another research paper at Ref-8 by R.K Goel presents a study of existing provisions of Indian Railway Standard Steel Bridge Code and the BS-5400 in respect of fatigue design of Railway Bridges.

II. METHODOLOGY

The prime objective of this study was to calculate the lapsed and balance fatigue life of Ravi Bridge. For this purpose, theoretical analysis as well as actual field testing have been carried out on the bridge. Theoretical values have been interpolated after comparing these with actual readings.

Pakistan Railways have been contacted to share the historical record of rail traffic passed over the bridge and the same have been considered to evaluate fatigue strength. With this analysis, stress ranges and corresponding stress cycles have been worked out that are supposed to be induced in the bridge with the passage of trains to date.

These values have then been plotted on Wohler Curve and fatigue life has been worked out.

III. FATIGUE

Fatigue is the wear and tear caused by repeated (cyclic) application of stresses. Normally these stresses are quite lower than the ones the structure can resist in static condition. Areas and regions experiencing tensile stresses starts becoming weaker and ultimately the failure of the material takes place when the material and its cross section becomes too weak to withstand the stresses. Initiation of cracks and their subsequent propagation is the basic mechanism of failures subject to fatigue. Finally, a Ductile or a brittle failure takes place once the propagating crack reaches its critical length. In the figures below, fatigue crack propagation is shown along with the beach marks (curvy parallel lines). The crack initiates at the edge and propagates perpendicular to the beach lines.

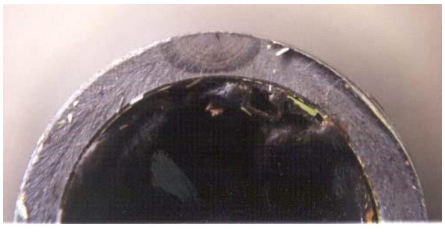

Figure 1 Propagation of fatigue crack initiating from origin along with failure surface. Crack and the beach lines are visible.

Fatigue in structures or in connections can result in failure caused by cyclic application of stresses that are even lesser in magnitude than the ones structure can resist if applied once and not in repetitions. When locomotives and trains pass over a railway bridge, they develop repeated application of stresses due to their movement. With the development of heavy locomotives and carriage cars in railways, the fatigue conditions of older bridges still in service have been put to serious concerns. A bridge might have been carrying a huge number of trains over passed many years and experiencing cyclic stress applications. Such a scenario is highly prone to undergo a fatigue stress and eventually could become a victim of the same.

Fatigue cracks propagates easily in the regions of stress concentration like an abrupt change in geometry such as notches, holes, re-entrant cuts, or any other sudden changes in stiffness.

In a bridge structure all the members are not likely to become a victim of fatigue. All such members which experience compressive stresses under the application of live and dead loading never fail by fatigue. Top chords and end posts of truss structures top flanges of girders and beams are the examples of members never exhibit compression. However, the members experience tensile stresses under dead and live loading like bottom chords and diagonal chords are more prone to fatigue failure.

Stress pattern and cycles under service conditions of rail road loading are not simple enough. It is because of the fact that more than one repetition of stresses may be obtained under certain conditions against a single pass of train. Also there may be some members that undergo only one stress cycle for each pass of train. For the first case the number of stress cycles is the same as the number of axles in a train, but in the second case only one stress cycle is developed for a complete train pass. Hence, the number of stress cycles is a function of spacing and number of the axles of the vehicle, span dimension of the member and the whole structure, and the location of the member in the bridge.

IV. FIELD TESTING OF BRIDGE

Pakistan Railways had arranged the physical testing of Ravi Bridge On Up-line in 2006. During the testing of bridge, 40 (channels) strain gages were fixed at predefined positions on girders and rails. Out of total number of channels, 38 channels were used for installing strain gages and 2 were used to record the LVDTs (Linear Variable Differential Transducers). A control software named STRAIN SMART had been used to process data from strain gages.

The strain gages were fixed to record the readings at predefined location that undergo maximum bending moment, maximum shear forces, and maximum deflections. To monitor the maximum flexural stresses, the gages were installed at mid span of girders situated at top and bottom flanges. Similarly, gages were installed at webs of both girders for monitoring the maximum shear stresses. These were placed at a distance of 3 feet from either supports. Maximum deflection was likely to occur at mid span so (LVDT, Linear Variable Differential Transducers) had been installed at mid span on the flanges of each girder.

Some of the gages had also been installed at rails-Their purpose was to calculate the actual value of wheel loads for each pass of the train at different velocities.

Following figures show the installation of strain gauges at various parts of the bridge.

Visual inspection showed some minor irregularities on few structural parts. A similar buckled lower flange of the girder is shown in fig-2.

Figure 2 Deformed/buckled parts of the girder near the support.

Strain gauges for recording maximum flexural tensile stresses had been installed at the bottom of lower flange of girders. Fig-3 shows installation of same strain gauge.

Figure 3 Strain gauge at bottom of main girder.

A computerized arrangement of interconnection of all gauges had been set up at site for recording their readings against all scan sessions during testing. Figure-4 shows the arrangement set up at site.

Figure 4 Data acquisition and recording systems.

For recording maximum shear stresses, the strain gages had been installed at middle height of the girder at the support. Such a strain gage has been shown in fig-5.

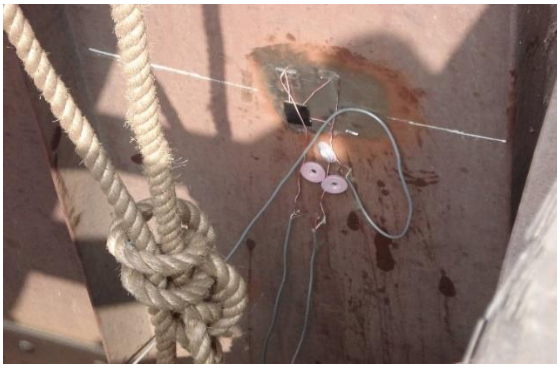

Figure 5 Strain gauge installed at middle height of girder at the support for recording maximum shear stresses.

Some of the strain gauges had also been installed directly at the rails. These were intended to work out the impact value with varying speed of test train. Such gauges have been shown in fig-6 below.

Figure 6 Strain gauge installed at rail for wheel load impact calculations.

Maximum deflections always occur at mid span on a simply supported girder. A system of LVDTs had been installed at the soffit of girders at mid span. The LVDTs are shown in fig-7 below.

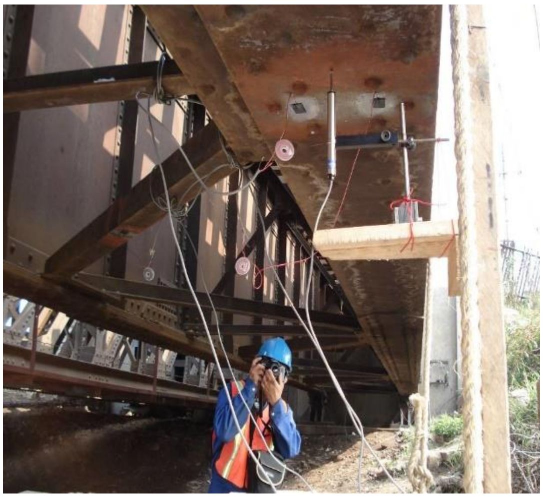

Figure 7 LVDTs installed at girder for max deflection.

Pakistan Railways had arranged a specially assembled TEST TRAIN for physical testing of Ravi Bridge. The TEST TRAIN passed over the bridge on both UP and DOWN directions at different predefined speeds, called SCAN SESSIONS. The schematic diagram of wheels, their spacing and loads acting on each wheel of test train is shown in fig-8.

The installed strain gages recorded and stored the readings against each of 24 train passes. The speed of the Test Train ran over bridge varied between 3.5 km/h and 90 km/h. All the data recorded during testing of bridge under test train, had been processed through STRAIN SMART software. As a result, the strains and deflections and subsequent stresses have been worked out.

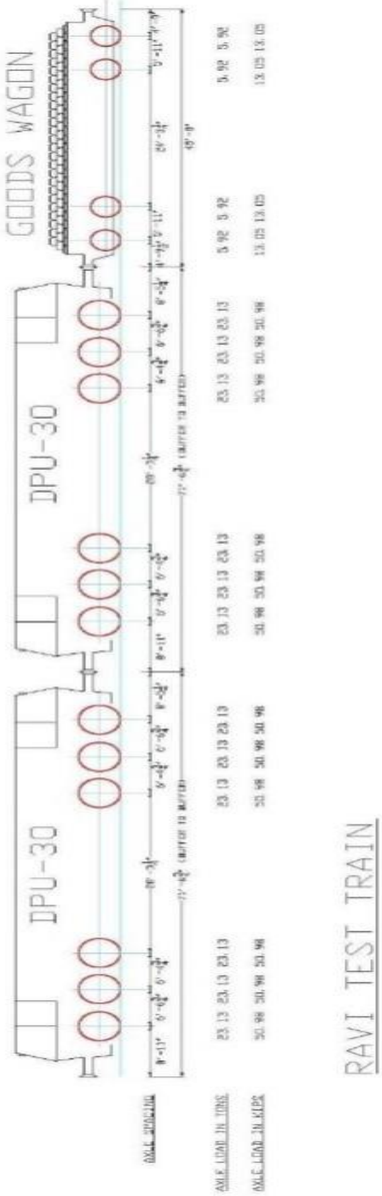

Figure 8 Details of the test train.

Shear Stresses had been worked out for both the girders at their either end. These are tabulated below:-

Shear stress in South Girder East End = 11.51 ~ 14.69 MPa.
Shear stress in South Girder West End = 12.27 ~ 14.13MPa.
Shear stress in North Girder East End = 10.82 ~ 13.72MPa.
Shear stress North Girder West End = 13.38 ~ 15.17MPa.

Flexural tensile and compressive stresses had been worked for both the girders and their values are shown below: -

Flexural Compressive Stress South Girder = 41.51~49.99MPa.
Flexural Tensile Stress South Girder = 35.99~41.16MPa.
Flexural Compressive StressNorth Girder = 42.26~44.81MPa.
Flexural Tensile Stress North Girder = 35.71~ 42.26MPa.

Mid span deflections had been computed from the gauges installed at bottom of both the girders at mid length. Their values are shown below: -

Maximum mid span deflection South Girder = 15.62 mm.
Maximum mid span deflection North Girder = 15.82 mm.

V. THEORATICAL ANALYSIS OF BRIDGE AGAINST TEST TRAIN

The Up-line Bridge has been modeled and analyzed in STAAD PRO 2005. The test train of figure 8 had been modeled in STAAD PRO. Moving load command had been used in STAAD PRO to apply the test train loading in moving pattern. The result of analysis in terms of resulting stresses and strains have been worked out in software and the critical ones are listed in Table 1.

Table 1 Comparison of maximum theoretical and experimental results for the test train

COMPARISON OF MAXIMUM THEORATICAL & EXPERIMENTAL RESULTS												
Sr #	LOCATION OF GAGE	COMPUTER ANALYSIS (TEST TRAIN WADING) Stresses (MPa)		EXPERIMENTAL RESULTS OBTAINED FROM STRAIN GAGES								
		PLANE FRAME MODEL	SPACE FRAME MODEL	3.5 KM/ H	10 KM/ H	*20* KM/ H	30 KM/ H	*40* KM/ H	*50* KM/ H	60 KM/ H	75 KM/ H	*90* KM/ H
1	Shear Stresses-East end of south Girder	26.20 *	26.20 *	11 58 *	11.86 *	13.51.	14.41 *	13.51 *	12.34 *	11.79 *	11.79 *	12.20 *
2	Shear Stresses-East end of north Girder	26.20 *	26.20 *	26.89 *	12.27 *	12.07 "	12.55 *	12.20 *	12.27 *	11.86 *	11.58 *	11.93 *
3	Flexural Compressive Stresses-South Girder	*-76.04 **	-63.71 *	-45.78 *	-41.92 *	-42.75 *	-43.78 *	-44.06 *	-42.51 *	-43.30 *	-44.47 *	-43.71 *
4	Flexural Tensile Stresses-South Girder	*76.04 **	63.55 *	36.54 *	36.89 *	38.27 "	41.02 *	40.39 *	36.61 *	37.78 *	36.61 *	37.09 *
5	Flexural Compressive Stresses-North Girder	*-76.04 **	-62.86 *	-42.82 *	-42.95 *	-43.02 *	-44.13 *	-44.20 *	-43.44 *	-45.09 *	-44.40 *	-43.71 *
6	Flexural Tensile Stresses-North Girder	*76.04 **	63.5 *	36.06 *	36.54 *	38.20 *	41.44 *	39.99 *	38.40 *	39.09 *	39.09 *	38.27 *
7	Shear Stresses-West End of South Girder	26.20 *	26.20 *	13 10 *	13.24 *	13.03 *	13.51 *	13.72 *	13.51 *	13.51 *	12..27 *	14.13 *
8	Shear Stresses-West End of North Girder	26.20 *	26.20 *	14.27 *	14.41 *	14.48 *	14.48 *	14.62 *	14.48 *	14.48 *	14.07 *	13.72 *
´-SHEAR STRESSES, NOTE:COMPUTER ANALYSISINCWOES THEIMPACT VALUEAS PER PAKJSTAN Railways "BRIDGE RULES" ´´. - COMMRESSJVE FLEXURAL STRESSES												

The prime objective here is to calculate the lapsed and balance fatigue life of Ravi Bridge. For this purpose, theoretical analysis as well as actual field testing has been done on the bridge. Theoretical values have been interpolated after comparing these with actual readings.

VI. THEORATICAL ANALYSIS OF BRIDGE UNDER VARIOUS GROUPS OF LOCOMOTIVES

Analysis of the same Railway Bridge has also been done for various groups of locomotives. These locomotives have been reported to pass over the bridge throughout their life. Computer analysis models using STAAD software were prepared for each group loading and the resulting stresses were calculated. The maximum stresses obtained from these results are shown in Table 2.

Table 2 Analysis results for various trains.

Stress Type	Shear Stress. LHR End (MPa)	Shear Stress. SHAHDRA End (MPa)	Flex. Tensile Stress (MPa)	Flex. Comp. Stress (MPa)
ML Load. 1926	31.71	31.71	100.59	100.59
Gr-1 Loco.	24.82	24.82	74.12	74.12
Gr-2 Loco.	24.13	24.13	75.29	75.29
Gr-3 Loco.	22.06	22.06	70.81	70.81
Gr-4 Loco.	20.00	20.00	64.47	64.47
Gr-5 Loco.	17.24	17.24	58.47	58.47

VII. LOAD SPECTRUM FOR FATIGUE ANALYSIS

For the fatigue evaluation, loading is converted into load spectrums. The load spectrums consist of bars representing constant load levels, and the frequency of occurrence of each level. The stress ranges can be taken from the single application of the load from the structural analysis and the corresponding number of stress cycles can obtain from the number of cycles produced by one passage of train multiplied with train traffic record of the controlling authority.

For preparation of load spectrum of the bridge under consideration, stress ranges for each locomotive group train have been worked out in this study. The railway traffic history defining the groups of locomotives has been acquired through Railway Authorities. Table 3 shows the stress ranges and their corresponding with the number of cycles corresponding to each stress range.

Table 3 Groups of locomotives trains Stress ranges and corresponding number of cycles.

Sr #	GROUP ID	STRESS RANGE (MPa)	Δσ (MPa)	NO. OF CYCLES (n)
1	Group-1 Trains	0 ~ 74.12	74.12	225892
2	Group-2 Trains	0 ~ 75.29	75.29	14157
3	Group-3 Trains	0 ~ 70.81	70.81	801214
4	Group-4 Trains	0 ~ 64.47	64.47	112946
5	Group-5 Trains	0 ~ 58.47	58.47	734147

The above mentioned data can also be transformed in form of a traffic histogram and load spectrum as below. The same shall be utilized for the calculation of fatigue life of the bridge.

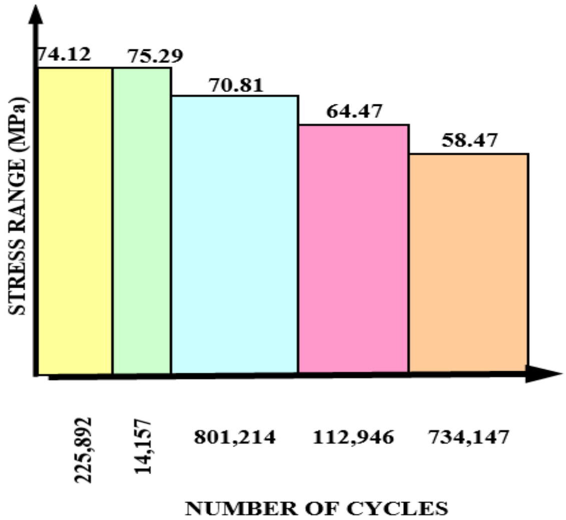

Figure 9 Loading spectrum for service life of Ravi Bridge.

VIII. Α - VALUE

The theoretically computed stress ranges vary from the stresses actually induced in the structural members during testing. This difference is related in form of a ratio of measured stresses to those values computed theoretically and is termed as α –Value.

α-Value for Ravi bridge has been worked out as follows using the results of test train and computer analysis for same loading: -

α – Value (Actual Stress/Theoretical Stress) =38.26/76.04 = **0.503**

The theoretically calculated stresses have been corrected with α –Value, and are given in Table 4.

Table 4 Corrected stress range for groups of locomotive Trains.

Sr #	GROUP ID	STRESS RANGE (MPa)	NO OF CYCLES	CORRECTED STRESS RANGE (MPa)
1	Group-1 Trains	0 ~ 74.12	225892	**0 ~ 37.30**
2	Group-2 Trains	0 ~ 75.29	14157	**0 ~ 37.85**
3	Group-3 Trains	0 ~ 70.81	801214	**0 ~ 35.58**
4	Group-4 Trains	0 ~ 64.47	112946	**0 ~ 32.41**
5	Group-5 Trains	0 ~ 58.47	734147	**0 ~ 29.44**

IX. WOHLER CURVE

WÖHLER was the first one to conduct systematic studies on fatigue of materials. He graphically presented his results in the form of an S-N Curve or Wöhler Curve. These curves are drawn going through a large number of tests. The number of stress cycles is shown on x-axis using logarithmic scale, while the algebraic difference between the two extremes of a stress cycle, called the stress range ($\sigma_{max} - \sigma_{min}$), is taken on the y-axis. A series of Wöhler Curves are plotted for a number of typical welded or bolted connection details showing the relationship between the stress range and the logarithm of the number of cycles.

AREMA (2000) specifications classify various structural members based on the possibility of stress concentration for various types of connection details. The seven stress concentrations categories are named A, B, C, D, E, E/, and F (Fig-9.7.3.4.2A of AREMA 2000). These S-N curves for each category are developed for 95% confidence limit using the available test data. These S-N Curves are reproduced in figure 10.

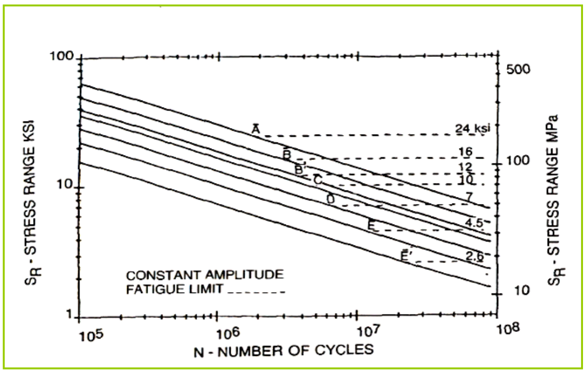

Figure 10 S-N Curve for different categories of structural members.

The above mentioned data is transformed into a constant-amplitude stress range from variable-amplitude stress spectrum for different groups of trains and is used for fatigue life evaluation. AREMA RMC relationship (Art. 15-9-34) has been used to transformation a variable-amplitude stress ranges into an equivalent constant-amplitude stress range: -

$$S_{re} = \alpha\,(\Sigma\, \gamma_i \times SR_i^3)^{1/3}$$

Where:

S_{re} = Effective stress range for total number of variable stress cycles, N_v.

γ_i = Ratio of the number of occurrences of SRi to the total number of variable stress cycles N_v.

SR_i = Stress range of cyclic stress corresponding to the number of occurrences n_i.

α = Actual stress / theoretical stress.

N_v = Total number of loading cycles.

For a given resulting applied stress parameter "S_{re}", a horizontal line is drawn on the fatigue strength (S-N) curve to reach the curve corresponding to the selected connection detail. A vertical line is then drawn to read the fatigue life. If the number of loading cycles that has actually taken place is less than the loading cycles given by the curve, the structure has not passes its fatigue life. Further, the remaining service life of the structure may also be estimated.

It is to be noted that if the "S_{re}" is less than the constant amplitude fatigue limit or if loading cycles are in compression, the fatigue life is infinite.

If the calculated "Sre" value lies over the S-N curve or the horizontal line through the stress range cannot intersect any curve, it means that the member is already over-loaded and proper attention is required to prevent any damage and to continue the service life.

X. RESULTS

Total number of loading cycles "N_v = 1888356 cycles" and effective stress range "S_{re}=33.58MPa as calculated using AREMA RMC relationship (Art. 15-9-34)" when plotted on Wöhler Curve (S-N Curve) and observing the fatigue life against fatigue category "D, riveted structure", the elapsed and balance fatigue life for the bridge are shown in figure 11.

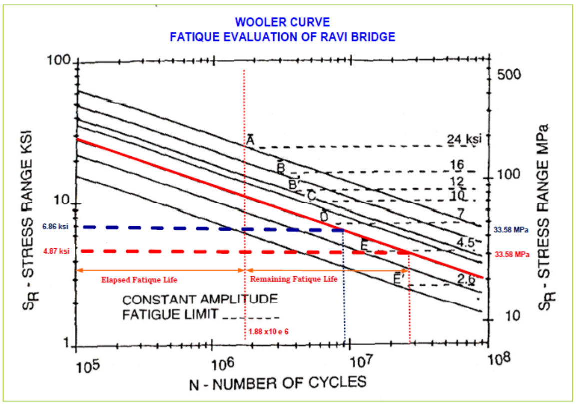

Figure 11 S-N Curve for Ravi Bridge showing elapsed and balance fatigue lives.

The S-N Curve for Ravi Bridge shows that so far the bridge has consumed only approximately 6.7 % of its fatigue life [1.88 x 106 / 2.8 x 107 x 100 = 6.7 %]. The values correspond to red dashed line in figure-11 above.

XI. BRIEF DISCUSSION ON RESULTS

The elapsed fatigue life of the bridge comes out to be just 6.7 % which is a very small figure. This might be due to the combined or individual effect of following reasons: -

- Loading cycles obtained from Pakistan Railways history might be at a lower side. The under consideration bridge was constructed in 1910. And the traffic history record may have a chance of showing lesser number of train passes.
- The bridge girder is supported on a pin support at one end and a roller support on other. Practically there is neither perfect pin nor a roller. Moreover, with this much time elapsed, the behavior of pin and roller might get farther away from true sense of roller and pin.
- □–Value for Ravi Bridge has been worked out as 0.503. Usually this value should range from 0.70 to 0.85. Nevertheless, assuming a value of 0.85 gives a stress range of 47.32 MPa (6.86 ksi). This value is also plotted with blue color dashed line in figure-11 above. Which also results into a 20% elapsed fatigue life.
- The bridge was tested in year 2006 and as such 11 more years of service have already passed.

REFERENCES

[1] AREA “American Railway Engineering Association, (2000)”, Specifications.

[2] “Advanced Introduction to Fatigue (2006)”- Lecture 12.2 ESDEP WG 12.

[3] “Basic Introduction to Fatigue (2005)”- Lecture 12.1 ESDEP WG 12.

[4] E. Bruhwiler and P. Kunz (1993), “Remaining service life of a riveted railway bridge”- Paper Presented at IABSE Colloquium, Copenhagen, Denmark.

[5] “Fatigue design of steel structures (2004)”, STEEL CONSTRUCTION- Journal of the Australian Steel Institute, Vol. 38.

[6] J.W. Fisher, B. T. Yen, D. Wang and J. E. Mann (1987), Lehigh University, Pennsylvania, “Fatigue and fracture evaluation for rating riveted bridges”. Research Paper presented in December 1987.

[7] P. Kunz and M. A. Hirt (June 14, 1992). “Reliability of railway bridges under fatigue loading”- Paper Presented at Third International Workshop on Bridge Rehabilitation, Technical University, Damstadt.

[8] R. K. Goel (2005), “Fatigue life assessment of steel bridges”. Research Paper.

[9] “Structural Fatigue”- A report of Seminar held in Chicago on September 29, 2000, sponsored by AREA Committee 15.

[10] “Traditional Residual Life Assessment for Bridges (2005)”- Lecture 16.4 ESDEP WG 16.